63-3-6

406 073

406073

PRINCETON UNIVERSITY

DEPARTMENT OF AERONAUTICAL ENGINEERING

DDC
JUN 11 1963
TISIA D

#4.

Best
Available
Copy

THE TWO-DIMENSIONAL, TURBULENT WALL JET WITH AND WITHOUT AN EXTERNAL FREE STREAM

by

A. Verhoff

Report No. 626 May 1963

Office of Naval Research Department of the
Navy Contract Nonr 1858(14) in Co-operation
with Bureau of Naval Weapons

"Reproduction, translation, publication, use and disposal in whole or in part by or for the United States Government is permitted."

BIBLIOGRAPHICAL CONTROL SHEET

1. Originating agency and monitoring agency:

O. A.: Princeton University, Princeton, New Jersey
M. A.: Office of Naval Research, Air Branch (Code 461), Washington, D. C.

2. Originating agency report number: Aeronautical Engineering Department Report No. 626

3. Title and classification of title: The Two-Dimensional, Turbulent Wall Jet with and without an External Free Stream (Unclassified)

4. Personal Author: Verhoff, August

5. Date of report: May 1963

6. Pages: 49

7. Illustrative material: 59 figures

8. Prepared for Contract No.: Nonr 1858(14)

9. Prepared for Project No.: NR 212-000

10. Security classification: Unclassified

11. Distribution limitation: Specified by ONR ltr (461:TLW:eew) of April 19, 1963

12. Abstract:

A theoretical as well as an experimental investigation of a plane, two-dimensional, turbulent wall jet is presented. The velocity profiles are described by means of an asymptotic expansion and the growth of the jet and decay of maximum velocity are also predicted.

TABLE OF CONTENTS

SUMMARY i

NOMENCLATURE ii

I INTRODUCTION 1

II THEORETICAL ANALYSIS 4

Part 1: Plane Turbulent Wall Jet 4

- A. Equations of Motion 4
- B. Similar Velocity Profiles 5
- C. Shear Similarity 7
- D. Similarity Function 10
- E. Variation of Velocity and Length Scales 14
- F. Comparison With Glauert's Theory 18

Part 2: Turbulent Wall Jet Beneath a Uniform Free Stream 20

- A. Similar Solution 20
- B. Shear Similarity 21
- C. Similarity Functions 25
- D. Variation of Velocity and Length Scales 29

III EXPERIMENTAL INVESTIGATION 33

IV DISCUSSION 36

- A. Comparison of Experimental Results with Theory 36
  - 1. Plane Turbulent Wall Jet 36
  - 2. Turbulent Wall Jet Beneath a Uniform Free Stream 38
- B. Jet Outlet Conditions 41

V CONCLUSIONS 44

VI REFERENCES 46

TABLE OF CONTENTS
(Continued)

VII APPENDIX 48

VIII TABLES

IX FIGURES

SUMMARY

A theoretical as well as an experimental investigation of a plane, two-dimensional, turbulent wall jet and a turbulent wall jet beneath a secondary uniform stream is presented.

For the case of the plane turbulent wall jet, the growth of the jet as well as the maximum velocity decay are predicted based on the assumption that the shear stress distribution as well as the velocity distribution across the jet remain similar over the useful range of downstream positions. A suggested form for the velocity distribution is compared with the experimental results of this investigation as well as with the results of several previous investigators.

The approach used in the analysis of the plane turbulent wall jet is then extended to the more general case of a turbulent wall jet beneath a secondary uniform stream. The velocity distribution and shear stress distribution are expressed in terms of a number of similarity functions and the ratio of the free stream velocity to the maximum velocity in the jet profile. Forms for these similarity functions are also suggested. The growth of the jet and decay of maximum velocity are again predicted based on the results obtained from the plane turbulent wall jet analysis. The experimental results of this investigation and the results of previous investigators are compared with the velocity profiles as predicted by this analysis.

NOMENCLATURE

A	constant equal to 1.4794
B	constant equal to .67753
C	function of jet Reynolds number
D	function of jet outlet conditions and jet Reynolds number
F	function of $\frac{\zeta}{U_m}$
M	function of jet outlet conditions and jet Reynolds number
S	shear similarity function of η
T	shear similarity function of η
U	mean velocity in x direction
V	mean velocity in y direction
W	shear similarity function of η
Z	shear similarity function of η
d	jet slot height
e	exponential function
f	similarity function of η
g	similarity function of η
h	similarity function of η
j	similarity function of η
u	non-dimensional x velocity component, U/V_j
v	non-dimensional y velocity component, V/V_j
x	longitudinal distance from jet exit
y	vertical distance above wall

α	constant, $\int_0^\infty f^2(\eta)d\eta$ (also constant in Glauert's analysis)
β	constant, $\int_0^\infty f(\eta)[2g(\eta) - 1]d\eta$
γ	constant, $\int_0^\infty g(\eta)[g(\eta) - 1]d\eta + 2\int_0^\infty f(\eta)h(\eta)d\eta$
δ	characteristic jet thickness
ζ	velocity ratio, U_∞/V_j
η	similarity variable, y/δ
λ	similarity parameter
μ	viscosity coefficient
ν	kinematic viscosity
ρ	mass density
σ	constant, $\int_0^\infty h(\eta)[2g(\eta) - 1]d\eta + 2\int_0^\infty f(\eta)j(\eta)d\eta$
τ	turbulent shearing stress
U_*	shearing velocity, $\sqrt{\frac{\tau}{\rho}}$
u_*	non-dimensional shearing velocity, U_*/V_j
V_j	jet outlet velocity
$\bar{x}$	non-dimensional longitudinal coordinate, x/d
$\bar{y}$	non-dimensional vertical coordinate, y/d
U_{max}	maximum velocity in jet profile
U_m	non-dimensional maximum velocity, U_{max}/V_j
$\bar{\delta}$	non-dimensional jet thickness, δ/d
τ_w	wall shearing stress
U_τ	skin friction velocity, $\sqrt{\frac{\tau_w}{\rho}}$
u_τ	non-dimensional skin friction velocity, U_τ/V_j

C_f	skin friction coefficient
η_*	value of η where $S(\eta)$ vanishes
η_m	value of η where $f'(\eta)$ vanishes
Re_o	jet outlet Reynolds number
K_i	constant $(i = 1, 2, \cdots)$
U_∞	free stream velocity
$\eta_{1/2}$	function of ζ/U_m

I INTRODUCTION

The behavior of a jet blowing tangentially to a solid surface is of great interest because of the application of such jets to boundary layer control of aircraft. In the absence of a pressure gradient, the flow field produced by such a jet, commonly called a wall jet, is a combination of a boundary layer and a free turbulent flow. This flow field may be further complicated by the presence of a secondary free stream as in the case of any normal boundary layer control application.

For the case of a plane wall jet, Glauert (1) has obtained a theoretical solution of the boundary layer equations for both laminar and turbulent flow. However, the analysis of the laminar wall jet in which a similarity solution was found is of little practical interest because of the extremely low critical Reynolds number of mixing layer flows. For the turbulent case, a near similarity solution was obtained by assuming that the variation of shear stress with mean velocity near the wall was the same as that in a turbulent pipe flow. Outside of the velocity maximum, an eddy viscosity which remained constant across the breadth of the jet was assumed, the value being chosen to give the best agreement with experiment. As a result of these assumptions, the shear stress at the maximum velocity location necessarily vanished, a result which has been questioned by several recent experimental investigators (2, 3, 4).

The more practical case of a wall jet beneath a uniform free stream is not as easily treated by the concept of similar profiles since the ratio of free stream velocity to maximum velocity in the jet profile varies continuously with the downstream coordinate. However, tentative theories in which a form of downstream similarity is assumed have been suggested by George (5) and Carriere, Eichelbrenner, and Poisson-Quinton (6).

As in the case of the plane turbulent wall jet, the correspondence of the point of zero shear stress with the maximum velocity location has also been questioned experimentally. This apparent lack of dependence of the Reynolds stress on the mean velocity gradient seems to disprove the validity of mixing length theory and, in particular, the concept of an eddy viscosity when applied to an asymmetric velocity distribution. Furthermore, Glauert's assumption that the flow may be divided, for purposes of calculation, into layers each having the properties of some known type of shear flow is also subject to question.

Based upon the experimental results of this investigation as well as those of George (7) and Myers, Schauer, and Eustis (8) for the plane turbulent wall jet, the present analysis assumes that similarity exists with respect to the velocity profiles over the entire useful range of downstream positions. The assumption that the shear stress distribution also remains similar leads to a relation between the jet thickness and maximum velocity in the jet profile. This relation, together with the consideration of the effect of introducing a "wall" into a two-dimensional turbulent jet, yields an approximate relation for the growth of the jet and decay of maximum velocity in the plane turbulent wall jet.

The present analysis of the turbulent wall jet beneath an external free stream expresses the velocity profiles and also the shear stress distribution in terms of a series of similarity functions. The results for the plane turbulent wall jet are appropriately modified in order to predict the growth of the jet and decay of maximum velocity in the presence of a free stream. Because of the difficulties encountered in obtaining precise analytic representations for the similarity functions, an approximate form for the velocity distribution which includes only four such functions has been adopted. This approximation remains valid as long as the maximum velocity in the profile is at least as great as the free stream velocity.

II THEORETICAL ANALYSIS

Part I: Plane Turbulent Wall Jet

A. Equations of Motion

The turbulent wall jet may be regarded as a combination of a boundary layer and a free turbulent flow. Since problems in free turbulent flow are of a "boundary layer" nature (i.e., the transverse gradients are large and the region in which a solution is sought does not extend far in the transverse direction as compared with the longitudinal direction of flow), it is expected that the conventional boundary layer equations are also applicable to the case of a wall jet. For a two-dimensional, incompressible flow in the absence of a pressure gradient, these equations are (9)

$$U \frac{\partial U}{\partial x} + V \frac{\partial U}{\partial y} = \frac{1}{\rho} \frac{\partial \tau}{\partial y} \tag{1.1a}$$

and

$$\frac{\partial U}{\partial x} + \frac{\partial V}{\partial y} = 0 \tag{1.1b}$$

where U and V refer to mean velocities and τ denotes the turbulent shearing stress.

Defining the shearing velocity as

$$U_* \equiv \sqrt{\frac{\tau}{\rho}} \tag{1.2}$$

and non-dimensionalizing

$$u = \frac{U}{V_j} \tag{1.3a}$$

$$v = \frac{V}{V_j} \tag{1.3b}$$

$$u_* = \frac{U_*}{V_j} \tag{1.3c}$$

$$\bar{x} = \frac{x}{d} \qquad (1.3d)$$

$$\bar{y} = \frac{y}{d} \qquad (1.3e)$$

where V_j is the jet outlet velocity and d the jet slot height, the boundary layer equations become

$$u \frac{\partial u}{\partial \bar{x}} + v \frac{\partial u}{\partial \bar{y}} = \frac{\partial u_*^2}{\partial \bar{y}} \qquad (1.4a)$$

and

$$\frac{\partial u}{\partial \bar{x}} + \frac{\partial v}{\partial \bar{y}} = 0 \qquad (1.4b)$$

B. Similar Velocity Profiles

For the plane turbulent wall jet, the general form of the mean velocity profile is as shown below, the maximum velocity in the profile being denoted by U_{max}. In general, the flow in the outer part of the profile is virtually the same as that in a two-dimensional free turbulent jet provided the jet momentum is very much greater than the wall friction. Except for the loss of momontum due to this surface friction, the flow is at constant momentum so that at least the overall characteristics of the flow will depend on this momentum.

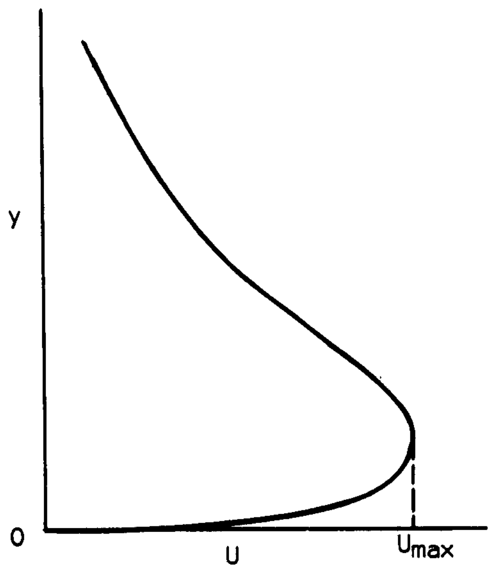

If these profiles are to be independent of the downstream coordinate (i.e., if there is to be a similarity solution), then the general form of the velocity distribution must be

$$\frac{U}{U_{max}} = f(\eta) \tag{1.5}$$

where

$$\eta = \frac{y}{\delta} \ , \tag{1.6}$$

δ being some characteristic thickness of the jet profile. Several properties of this similarity function $f(\eta)$ can be readily deduced, namely

$$f(0) = 0 \tag{1.7a}$$

$$f(\infty) = 0 \tag{1.7b}$$

and

$$f_{max} = 1 \tag{1.7c}$$

occurring at some $\eta = \eta_m$.

Assuming that

$$\bar{\delta} \equiv \frac{\delta}{d} \tag{1.8}$$

and

$$U_m \equiv \frac{U_{max}}{V_j} \tag{1.9}$$

are functions only of $\bar{x}$, then integration of the continuity equation results in

$$v = U_m \frac{d\bar{\delta}}{d\bar{x}} \eta \ f(\eta) - \frac{d}{d\bar{x}} (\bar{\delta} \ U_m) \int_0^{\eta} f(z)dz \tag{1.10}$$

With regard to the characteristic jet thickness δ, two possible choices are available, one being the value of y where the maximum velocity occurs and the other being that value of y in the outer portion of the jet where the velocity is half the maximum value. Since the latter choice is more easily measured experimentally, it is usually taken as the representative thickness of the wall jet. This then imposes another condition on the similarity function, namely,

$$f(1) = 1/2 \qquad (1.11)$$

C. Shear Similarity

Making use of equations (1.5) and (1.10), the momentum equation (1.1a) may be written

$$U_m \frac{dU_m}{d\bar{x}} f^2(\eta) - \frac{U_m}{\bar{\delta}} \frac{d}{d\bar{x}} (\bar{\delta} U_m)\, f'(\eta) \int_0^\eta f(z)\,dz = \frac{\partial U_*^2}{\partial \bar{y}} \qquad (1.12)$$

Integrating this equation with respect to y from zero to ∞ gives

$$\frac{1}{V_j^2} \frac{\tau_w}{\rho} = - U_m \left[2\bar{\delta} \frac{dU_m}{d\bar{x}} + U_m \frac{d\bar{\delta}}{dx} \right] \int_0^\infty f^2(\eta)\,d\eta \qquad (1.13)$$

where τ_w is the wall shearing stress. Defining the skin friction velocity as

$$U_\tau \equiv \sqrt{\frac{\tau_w}{\rho}} \qquad (1.14)$$

with

$$u_\tau \equiv \frac{U_\tau}{V_j} \qquad (1.15)$$

and letting

$$\alpha = \int_0^\infty f^2(\eta)\,d\eta \qquad (1.16)$$

equation (1.13) may be written

$$u_\tau^2 = - \alpha \frac{d}{d\bar{x}} (\bar{\delta}\, U_m^2) \qquad (1.17)$$

Defining a skin friction coefficient by

$$C_f \equiv \frac{\tau_w}{1/2\, \rho\, U_{max}^2} = 2 \frac{U_\tau^2}{U_m^2} \qquad (1.18)$$

then from equation (1.17)

$$C_f = - \frac{2\alpha}{U_m^2} \frac{d}{dx} (\bar{\delta} \, U_m^2) \qquad (1.19)$$

On the basis of Forthmann's (10) calculations, it may be assumed that similarity also exists with respect to the shear stress distribution in a turbulent wall jet flow. That is,

$$u_*^2 = u_T^2 \, S(\eta) \qquad (1.20)$$

where $S(\eta)$ is the shear similarity function. This is also consistent with the claim of Eskinazi and Kruka (4) that it is a characteristic shearing velocity and not a characteristic mean velocity which brings similarity to turbulent velocities (i.e., to turbulent shear stress).

Making use of equation (1.20), the momentum equation (1.12) may then be written

$$U_m \frac{dU_m}{d\bar{x}} f^2(\eta) - \frac{U_m}{\bar{\delta}} \frac{d}{d\bar{x}} (\bar{\delta} \, U_m) \, f'(\eta) \int_0^\eta f(z)dz = \frac{u_T^2}{\bar{\delta}} S'(\eta)$$

The conditions which must be satisfied by the similarity function $S(\eta)$ are

$$S(0) = 1 \qquad (1.21a)$$

$$S(\infty) = 0 \qquad (1.21b)$$

$$S'(0) = 0 \qquad (1.21c)$$

Making use of equation (1.17), the momentum equation may be written

$$U_m \frac{dU_m}{d\bar{x}} \left[f^2(\eta) - f'(\eta) \int_0^\eta f(z)dz + 2\alpha \, S'(\eta) \right] =$$

$$\frac{U_m^2}{\bar{\delta}} \frac{d\bar{\delta}}{d\bar{x}} \left[f'(\eta) \int_0^\eta f(z)dz - \alpha S'(\eta) \right] \qquad (1.22)$$

If there is to be a similarity solution (i.e., a solution which is independent of $\bar{x}$), then both sides of this equation must vary in the same manner with $\bar{x}$. This implies, for some constant λ,

$$\frac{U_m^2}{\bar{\delta}}\frac{d\bar{\delta}}{d\bar{x}} = -\lambda U_m \frac{dU_m}{d\bar{x}}$$

or

$$\frac{\lambda}{U_m}\frac{dU_m}{d\bar{x}} + \frac{1}{\bar{\delta}}\frac{d\bar{\delta}}{d\bar{x}} = 0 \tag{1.23}$$

Therefore, the momentum equation becomes

$$f^2(\eta) + (\lambda - 1)\, f'(\eta)\int_0^{\eta} f(z)dz + (2 - \lambda)\alpha S'(\eta) = 0 \tag{1.24}$$

which is the similarity equation governing the flow in a plane turbulent wall jet.

The general shape of the shear function is shown below

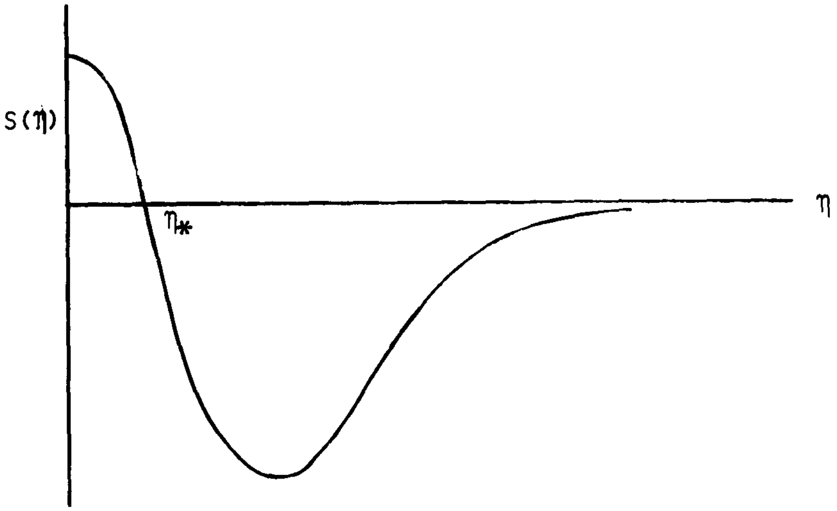

Denoting the value of η where $S(\eta)$ vanishes by η_*, then equation (1.24) may be integrated giving

$$(\lambda - 1)\ f(\eta_*) \int_0^{\eta_*} f(\eta)d\eta + (\lambda - 2) \int_{\eta_*}^{\infty} f^2(\eta)d\eta = 0 \qquad (1.25)$$

D. Similarity Function

A solution of equation (1.24) cannot be found unless some further assumptions are made concerning the velocity distribution $f(\eta)$ or the shear distribution $S(\eta)$. Glauert (1) has obtained a solution for the plane turbulent wall jet assuming that the inner part of the flow near the wall is governed by Blasius' formula and the outer part by Prandtl's hypothesis, the matching taking place at the maximum velocity point. Blasius' formula implies that $U \sim y^{1/7}$ near the wall while Prandtl's hypothesis states that the eddy viscosity is constant across the outer portion of the flow and is proportional to the product of the maximum mean velocity and the thickness of the jet.

As a result of the assumptions concerning the eddy viscosity, the solution involves one disposable constant, and exact similarity of the velocity profiles at all downstream positions does not exist since the eddy viscosity in the inner and outer parts of the jet vary in a slightly different manner with the Reynolds number based on jet thickness and maximum velocity. However, the velocity profiles are relatively invariant for given orders of the Reynolds number, the general nature of these profiles being characterized by a parameter α which is indicative of the proportional extent of the inner layer, between the wall and point of maximum velocity, to that of the outer layer, between the velocity maximum and the stationary fluid far from the wall.

The relative invariance of the velocity profiles in a plane turbulent wall jet has been adequately verified by previous experimental investigations as well as by the present one. Those investigators who have related their results to Glauert's solution have all adopted profiles corresponding to a narrow range of the parameter α (i.e., $1.2 \leq \alpha \leq 1.3$). This possibly indicates that complete similarity does exist to a greater extent than predicted by Glauert's assumptions concerning the eddy viscosity which are of doubtful validity.

On the basis of this information, it will therefore be assumed that the velocity profiles in a plane turbulent wall jet can be adequately represented by a universal similarity function $f(\eta)$. The shear stress distribution is then given by the similarity function $S(\eta)$ which is expressable in terms of $f(\eta)$ by means of equation (1.24).

From the standpoint of obtaining some sort of solution of equation (1.24), it is much more practical, although not as mathematically satisfying, to make some plausible assumptions concerning the velocity distribution, since the general shape of the mean velocity profile in a plane turbulent wall jet is reasonably well defined. One such assumption is that the inner portion of the flow, which closely approximates a turbulent boundary layer, is related to Blasius' formula which implies $f(\eta) \sim \eta^{1/7}$ near the wall.

For the case of a free jet boundary, H. Goertler has obtained a solution for the velocity distribution in terms of the Error function making use of Prandtl's hypothesis. Therefore, a reasonable form for the similarity function $f(\eta)$ suggested by Blasius' formula and Goertler's solution is

$$f(\eta) = A\eta^{1/7} [1 - \operatorname{erf} (B\eta)] \qquad (1.26)$$

where A and B are constants. This function automatically satisfies conditions (1.7a) and (1.7b) so that the remaining conditions (1.7c) and (1.11) serve to determine the constants A and 3. These constants were found to be 1.4794 and .67753 respectively so that

$$f(\eta) = 1.4794\, \eta^{1/7} \left[1 - \operatorname{erf}(.67753\, \eta) \right] \tag{1.27}$$

with $\eta_m = .16539$.

From equation (1.24)

$$S'(\eta) = \frac{f^2(\eta)}{\alpha(\lambda - 2)} + \frac{\lambda - 1}{\alpha(\lambda - 2)}\, f'(\eta) \int_0^\eta f(z)\,dz \tag{1.28}$$

which can be integrated by parts to give

$$S(\eta) = 1 + \frac{\lambda - 1}{\alpha(\lambda - 2)}\, f(\eta) \int_0^\eta f(z)\,dz - \frac{1}{\alpha} \int_0^\eta f^2(z)\,dz \tag{1.29}$$

since $S(0) = 1$. One obvious shortcoming of the assumed form of $f(\eta)$ is the fact that $f'(\eta)$ increases without limit as η approaches zero. However, since

$$\lim_{\eta \to 0} f'(\eta) \int_0^\eta f(z)\,dz = 0$$

$S'(\eta)$ as defined by equation (1.28) exhibits no such behavior.

The function $f(\eta)$ was programed for the computer and the values of $f'(\eta)$, $f(\eta)$, $\int_0^\eta f(z)\,dz$, and $\int_0^\eta f^2(z)\,dz$ are tabulated in Table 1. The procedure used in dealing with the singularity $f'(0)$ is described in the Appendix. The constant α defined by equation (1.16) was found to be

$$\alpha = \int_0^\infty f^2(\eta)\,d\eta = .75437 \tag{1.30}$$

From equation (1.25), the similarity parameter λ can be written as

$$\lambda = \frac{f(\eta_*) \int_0^{\eta_*} f(\eta)\,d\eta + 2 \int_{\eta_*}^\infty f^2(\eta)\,d\eta}{f(\eta_*) \int_0^{\eta_*} f(\eta)\,d\eta + \int_{\eta_*}^\infty f^2(\eta)\,d\eta} \tag{1.31}$$

which is clearly a function of the point of zero shear stress η_*. Glauert has assumed in his analysis that the shear stress is zero at the maximum velocity point. However, the validity of this assumption has been questioned by several recent investigators (2, 3, 4) who have found that the point of zero shear stress occurred, for the most part, on the wall side of the maximum velocity point where the velocity gradient was largest (i.e., $\eta_* < \eta_m$). If it is assumed that the point of zero shear stress coincides with the maximum velocity point, then equation (1.31), together with the assumed form for the velocity distribution, yields

$$\lambda = 1.7977 \tag{1.32}$$

The effect of a different location for the zero shear point on the similarity parameter is shown in Figure 1. It can be seen that the value of λ is not greatly affected and varies almost linearly with η_* provided the zero shear point η_* is reasonably close to η_m. The location of the zero shear point will, however, have a much stronger effect on $S'(\eta)$ and $S(\eta)$ as given by equations (1.28) and (1.29).

The values of $S(\eta)$ and $S'(\eta)$ corresponding to $\lambda = 1.7977$ (i.e., $\eta_* = \eta_m$) are tabulated in Table I along with the similarity function $f(\eta)$. The effect of a different location for the zero shear point on these functions can then be obtained from the Taylor series expansions

$$S(\eta; \lambda) = S(\eta; 1.7977) + \frac{dS}{d\lambda}(\eta; 1.7977)(\lambda - 1.7977) + \cdots \tag{1.33a}$$

and

$$S'(\eta; \lambda) = S'(\eta; 1.7977) + \frac{dS'}{d\lambda}(\eta; 1.7977)(\lambda - 1.7977) + \cdots \tag{1.33b}$$

where the derivatives $\frac{d^nS}{d\lambda^n}$ and $\frac{d^nS'}{d\lambda^n}$ can be obtained from equations (1.28) and (1.29).

E. Variation of Velocity and Length Scales

The characteristic jet thickness δ as well as the maximum velocity in the jet profile U_{max} are functions of the jet outlet velocity, the downstream coordinate, the density and viscosity of the fluid, and the height of the jet outlet. A dimensional analysis yields

$$\frac{\delta}{d} = F_1 \left(\frac{x}{d}, \frac{V_j d}{\nu} \right)$$

or

$$\bar{\delta} = F_1 \; (\bar{x}, Re_0) \qquad (1.34a)$$

and

$$\frac{U_{max}}{V_j} = U_m = F_2 \; (\bar{x}, Re_0) \qquad (1.34b)$$

where Re_0 is the jet outlet Reynolds number.

The variation of these velocity and length scales U_m and $\bar{\delta}$ with the downstream coordinate is partially governed by equation (1.23). This equation may be integrated directly with the result

$$U_m = (\text{constant}) \cdot \bar{\delta}^{\,-1/\lambda} \qquad (1.35)$$

where λ has been assumed constant. If the region of similarity in the flow extended as far upstream as the jet outlet, then the constant appearing in this equation could be evaluated from conditions at the jet outlet. That is, at $\bar{x} = 0$

$$U_m = \frac{U_{max}}{V_j} = 1$$

and

$$\bar{\delta} = \frac{\delta}{d} = 1$$

so that the constant would be unity. However, since conditions at the jet outlet are somewhat dependent on the local geometry of the outlet as well as the jet outlet Reynolds number, an additional factor M may be introduced which takes into account the effects of geometry and jet Reynolds number. Equation (1.35) may then be written

$$U_m = (1 + M)\,\bar{\delta}^{\,-1/\lambda} \tag{1.36}$$

From equation (1.17), the wall shear stress can then be written

$$u_T^2 = -\alpha(1 + M)^2 \frac{d}{d\bar{x}}\left(\bar{\delta}^{\,(\lambda-2)/\lambda}\right) \tag{1.37}$$

In the case of a two-dimensional free turbulent jet, it can be shown from momentum considerations that the maximum velocity in the jet profile varies as $x^{-1/2}$ while the jet thickness varies linearly with x, the shear stress being zero on the center line by reasons of symmetry. An examination of equation (1.31) shows that as the point of zero shear stress η_* approaches zero, λ approaches a value of two. Consequently, equations (1.36) and (1.37) both tend toward those governing a free turbulent jet flow.

Because the wall boundary layer represents only a small portion of the flow, the spreading and entrainment action of a wall jet is qualitatively similar to that of a free turbulent jet. The general forms of the velocity distribution in the turbulent wall jet and turbulent free jet are compared below.

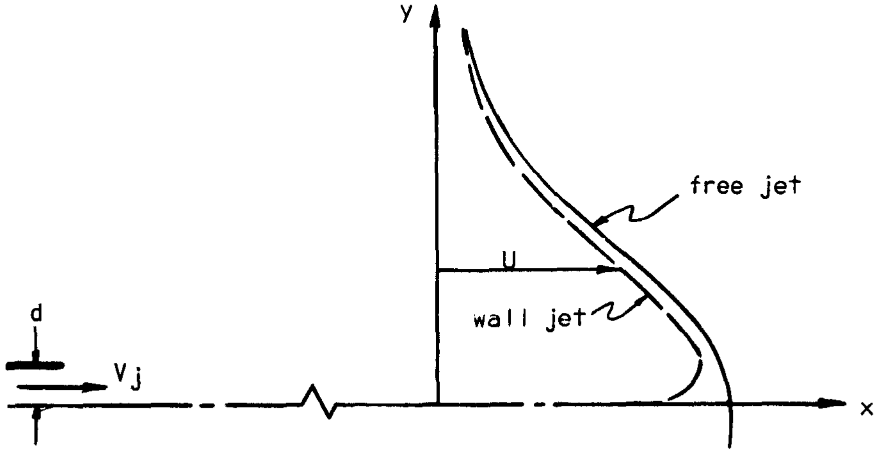

While there is no change in momentum in the free jet case, the wall jet does suffer a momentum loss due to the friction at the wall. The variation of this surface friction is given by equation (1.17).

In both cases, the total kinetic energy contained in the flow up to any point x is given by

$$KE(x) = \int^{x} \left[\int_{0}^{\infty} \left(\frac{\rho U}{2} \frac{\partial U^2}{\partial x} + \frac{\rho V}{2} \frac{\partial U^2}{\partial y} \right) dy \right] dx \qquad (1.38a)$$

Making use of the fact that similarity also exists for the free turbulent jet flow, this expression may be integrated with the result

$$KE(\bar{x}) = \frac{1}{2} \rho V_J^3 \, d \, \bar{\delta} \, U_m^3 \int_{0}^{\infty} f^3(\eta) d\eta \qquad (1.38b)$$

The amount of energy required to insert the "wall" into the free jet flow is given by $\int^{x} \tau_w [\, U_{max} \,]_{\substack{FREE \\ JET}} dx$ where $[\, U_{max} \,]_{\substack{FREE \\ JET}}$ is the maximum velocity which existed in the free jet velocity profile. It is therefore possible to write

$$[\, K_1 \, \bar{\delta} \, U_m^3 \,]_{\substack{FREE \\ JET}} - \int^{\bar{x}} u_\tau^2 \, [U_m]_{\substack{FREE \\ JET}} \, d\bar{x} = K_2 \, \bar{\delta} \, U_m^3 \qquad (1.39)$$

where the K_i ($i = 1, 2, \cdots$) are constants. Differentiating with respect to $\bar{x}$,

$$K_1 \frac{d}{d\bar{x}} [\, \bar{\delta} \, U_m^3 \,]_{\substack{FREE \\ JET}} - u_\tau^2 \, [U_m]_{\substack{FREE \\ JET}} = K_2 \frac{d}{d\bar{x}} (\bar{\delta} \, U_m^3) \qquad (1.40)$$

Making use of equations (1.36) and (1.37) and the known variations of $\bar{\delta}$ and U_m for a free turbulent jet, this becomes

$$K_3 \bar{x}^{-3/2} + \bar{x}^{-1/2} \frac{d}{d\bar{x}} \left(\bar{\delta}^{(\lambda-2)/\lambda} \right) + K_4 \frac{d}{d\bar{x}} \left(\bar{\delta}^{(\lambda-3)/\lambda} \right) = 0$$

or

$$\bar{\delta}^{-2/\lambda} \frac{d\bar{\delta}}{d\bar{x}} \left[\bar{x}^{-1/2} + K_5 \, \bar{\delta}^{-1/\lambda} \right] = K_6 \, \bar{x}^{-3/2} \qquad (1.41)$$

which may also be written

$$\frac{\bar{\delta}^{(\lambda-2)/\lambda}}{\bar{\delta}} \frac{d\bar{\delta}}{d\bar{x}} [\bar{x}^{-1/2} + K_5 \bar{\delta}^{-1/\lambda}] = K_6 \bar{x}^{-3/2} \qquad (1.42)$$

Previous experimental investigations have shown that $\bar{\delta}$ varies almost linearly with the downstream coordinate $\bar{x}$ in the case of a wall jet. In order to obtain an approximate solution to equation (1.42), the factors $\bar{\delta}^{(\lambda-2)/\lambda}$ and $\bar{\delta}^{-1/\lambda}$ may be assumed to vary as $\bar{x}^{(\lambda-2)/\lambda}$ and $\bar{x}^{-1/\lambda}$ respectively. Then

$$\frac{1}{\bar{\delta}} \frac{d\bar{\delta}}{d\bar{x}} = \frac{K_7 \bar{x}^{(4-5\lambda)/(2\lambda)}}{\bar{x}^{-1/2} + K_8 \bar{x}^{-1/\lambda}}$$

Substituting $z = \bar{x}^{(2-\lambda)/(2\lambda)}$ and integrating,

$$\begin{aligned} \ln \bar{\delta} &= K_9 \int^{z} \frac{z^2 dz}{z + K_8} + K_{10} \\ &= K_9 \left[\frac{z^2}{2} - K_8 z - \frac{3}{2} K_8^2 + K_8^2 \ln (z + K_8) \right] + K_{10} \end{aligned}$$

In terms of $\bar{x}$,

$$\ln \bar{\delta} = K_9 \left[\frac{1}{2} \bar{x}^{(2-\lambda)/\lambda} - K_8 \bar{x}^{(2-\lambda)/(2\lambda)} + K_8^2 \ln (\bar{x}^{(2-\lambda)/\lambda} + K_8) \right] + K_{11} \qquad (1.43)$$

As a further approximation, the second and third terms in the brackets may be dropped so that

$$\ln \bar{\delta} = C\bar{x}^{(2-\lambda)/\lambda} + K_{11}$$

or

$$\bar{\delta} = D \exp [C\bar{x}^{(2-\lambda)/\lambda}] \qquad (1.44)$$

The constants C and D appearing in this equation will depend on the jet outlet Reynolds number as well as the local conditions at the jet outlet. Referring back to equation (1.36) it can be seen that there are three factors (i.e., C, D, and M) describing the variation of the velocity and length scales which must be determined experimentally.

From equations (1.36) and (1.44), the maximum velocity decay is given by

$$U_m = (1 + M)\, D^{-1/\lambda} \exp\left[- \frac{C}{\lambda}\, \bar{x}^{(2-\lambda)/\lambda} \right] \qquad (1.45)$$

Likewise, from equations (1.37) and (1.44) the wall shear stress variation can be expressed as

$$u_\tau^2 = \frac{\tau_w}{\rho V_j^2} = \alpha C\, (1 + M)^2\, D^{(\lambda-2)/\lambda} \left(\frac{\lambda-2}{\lambda} \right)^2 \bar{x}^{(2-2\lambda)/\lambda} \exp \left[\frac{\lambda-2}{\lambda}\, C\, \bar{x}^{(2-\lambda)/\lambda} \right] \qquad (1.46)$$

Because of the approximations involved in obtaining a solution of equation (1.41), the above expressions for $\bar{\delta}$ and U_m do not tend toward the corresponding expressions for the free turbulent jet as λ approaches a value of two. It is also interesting to note that the preceding analysis does not involve the idea of a virtual origin or hypothetical point where the jet is assumed to originate. This is advantageous because in many cases it has been found that the virtual origin location for the maximum velocity decay did not coincide with that for the jet thickness variation.

F. Comparison With Glauert's Theory

As mentioned previously, Glauert has obtained a theoretical solution for the velocity distribution as well as the variation of the velocity and length scales in a plane turbulent wall jet. Glauert's solution for several values of the parameter α are shown in Figure 2 along with the profile defined by equation (1.27) for purposes of comparison.

Glauert's profiles have been constructed from the figures given in Reference 1 and no great accuracy is claimed. Near the wall, equation (1.27) coincides almost exactly with the profile corresponding to α = 1.2, while far from the wall it lies somewhat above Glauert's solutions for those values of α which are shown.

The rate of growth of the jet and rate of decay of maximum velocity are predicted by Glauert's analysis as functions of the Reynolds number based on jet thickness and maximum velocity in the jet profile. If U_{max} and δ are assumed to vary as x^a and x^b respectively, then the exponents a and b are related to the parameter α, which depends on the Reynolds number, in two possible ways. That is,

$$a = \frac{-4\alpha}{5 + 4\alpha}$$

$$b = \frac{4 + 4\alpha}{5 + 4\alpha}$$

or

$$a = \frac{-\alpha}{1 + \alpha}$$

$$b = 1$$

This last set of relations appears to be more acceptable experimentally. If the shear stress at the point of maximum velocity were zero as Glauert has assumed, then these two relations along with equations (1.32) and (1.35) imply that $\alpha \approx 1.25$. Glauert's profile for $\alpha = 1.25$ is shown in Figure 3 along with equation (1.27), and it can be seen that the differences between the two are not appreciable.

Part 2: Turbulent Wall Jet Beneath a Uniform Free Stream

A. Similar Solution

For the more practical case of a turbulent wall jet beneath a secondary uniform stream, the boundary layer equations (1.1a) and (1.1b) of the preceding part are still applicable. The general form of the mean velocity distribution for this case is as shown below, the secondary free stream velocity being denoted by U_∞.

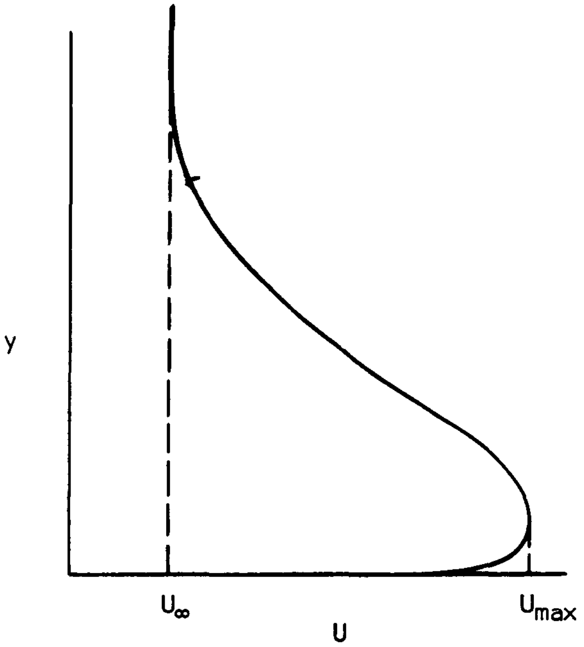

Because the ratio of U_∞ to U_{max} varies continuously in the downstream direction from a large value near the jet outlet to unity when the jet disappears, a similar solution of the form (1.5) cannot be found. However, a different type of similarity can be found which utilizes the two similarity functions found in the analysis of the plane turbulent wall jet. That is, a solution of the form

$$u = U_m\, f(\eta) + \zeta\, g(\eta) + \frac{\zeta^2}{U_m}\, h(\eta) + \frac{\zeta^3}{U_m^2}\, j(\eta) + \cdots \tag{2.1}$$

may be sought where

$$\zeta \equiv \frac{U_\infty}{V_j} \tag{2.2}$$

and

$$\eta = y/\delta, \tag{2.3}$$

δ again being some characteristic thickness of the jet profile.

Several properties of the similarity functions $g(\eta)$, $h(\eta)$, $j(\eta)$,$\cdots$ can be immediately stated, namely

$$g(0) = h(0) = j(0) = \cdots = 0 \tag{2.4a}$$

$$g(\infty) = 1 \tag{2.4b}$$

and

$$h(\infty) = j(\infty) = \dots = 0 \tag{2.4c}$$

At the point of maximum velocity η_m,

$$g(\eta_m) = h(\eta_m) = j(\eta_m) = \cdots = 0 \tag{2.5a}$$

and

$$g'(\eta_m) = h'(\eta_m) = j'(\eta_m = \cdots = 0 \tag{2.5b}$$

Integration of the continuity equation, making use of equation (2.1), results in

$$\begin{aligned} v = {} & U_m \frac{d\bar{\delta}}{d\bar{x}} \eta f(\eta) - \frac{d}{d\bar{x}} (\bar{\delta} U_m) \int_0^\eta f(z)dz + \zeta \frac{d\bar{\delta}}{d\bar{x}} [\ \eta g(\eta) \\ & - \int_0^\eta g(z)dz\ ] + \zeta^2 [\ \frac{1}{U_m} \frac{d\bar{\delta}}{d\bar{x}} \eta h(\eta) - \frac{d}{d\bar{x}} (\bar{\delta}/U_m) \int_0^\eta h(z)dz\ ] \\ & + \zeta^3 [\frac{1}{U_m^2} \frac{d\bar{\delta}}{d\bar{x}} \eta j(\eta) - \frac{d}{d\bar{x}} (\bar{\delta}/U_m^2) \int_0^\eta j(z)dz] + \cdots \end{aligned} \tag{2.6}$$

B. Shear Similarity

With the aid of equations (2.1) and (2.6), the momentum equation may be written

$$
\begin{aligned}
&U_m \frac{dU_m}{d\bar{x}} f^2(\eta) - \frac{U_m}{\bar{\delta}} \frac{d}{d\bar{x}} (\bar{\delta} U_m) f'(\eta) \int_0^\eta f(z)dz + \zeta \Big[\frac{dU_m}{d\bar{x}} f(\eta)\, g(\eta) \\
&\quad - \frac{U_m}{\bar{\delta}} \frac{d\bar{\delta}}{d\bar{x}} f'(\eta) \int_0^\eta g(z)dz - \frac{1}{\bar{\delta}} \frac{d}{d\bar{x}} (\bar{\delta} U_m) g'(\eta) \int_0^\eta f(z)dz \Big] \\
&\quad - \zeta^2 \Big[\frac{1}{\bar{\delta}} \frac{d\bar{\delta}}{d\bar{x}} g'(\eta) \int_0^\eta g(z)dz + \frac{1}{U_m \bar{\delta}} \frac{d}{d\bar{x}} (\bar{\delta} U_m)\, h'(\eta) \int_0^\eta f(z)dz \\
&\quad + \frac{U_m}{\bar{\delta}} \frac{d}{d\bar{x}} (\bar{\delta}/U_m)\, f'(\eta) \int_0^\eta h(z)dz \Big] - \zeta^3 \Big\{ \frac{1}{U_m^2} \frac{dU_m}{d\bar{x}} \big[f(\eta) j(\eta) \\
&\quad + g(\eta) h(\eta) \big] + \frac{1}{\bar{\delta} U_m^2} \frac{d}{d\bar{x}} (\bar{\delta} U_m)\, j'(\eta) \int_0^\eta f(z)dz + \frac{1}{\bar{\delta} U_m} \frac{d\bar{\delta}}{dx} h'(\eta) \\
&\quad \cdot \int_0^\eta g(z)dz + \frac{1}{\bar{\delta}} \frac{d}{d\bar{x}} (\bar{\delta}/U_m)\, g'(\eta) \int_0^\eta h(z)dz + \frac{U_m}{\bar{\delta}} \frac{d}{d\bar{x}} (\bar{\delta}/U_m^2) \\
&\quad \cdot f'(\eta) \int_0^\eta j(z)dz \Big\} \quad + \cdots = \frac{\partial u_*^2}{\partial \bar{y}} \qquad (2.7)
\end{aligned}
$$

Assuming that the shear stress in the free stream is zero, this equation may be integrated with respect to y from zero to ∞ in order to determine the shear stress at the wall. That is,

$$
\begin{aligned}
u_\tau^2 &= - \alpha \frac{d}{d\bar{x}} (\bar{\delta} U_m^2) - \zeta \frac{d}{d\bar{x}} (\bar{\delta} U_m) \Big[2 \int_0^\infty f(\eta)\, g(\eta) d\eta - \int_0^\infty f(\eta)\, d\eta \Big] \\
&\quad - \zeta^2 \frac{d\bar{\delta}}{d\bar{x}} \Big[\int_0^\infty g^2(\eta) d\eta - \int_0^\infty g(\eta) d\eta + 2 \int_0^\infty f(\eta)\, h(\eta) d\eta \Big] \\
&\quad - \zeta^3 \frac{d}{d\bar{x}} (\bar{\delta}/U_m) \Big[2 \int_0^\infty f(\eta)\, j(\eta) d\eta + 2 \int_0^\infty g(\eta)\, h(\eta)\, d\eta \\
&\quad - \int_0^\infty h(\eta)\, d\eta \Big] - \cdots \qquad (2.8)
\end{aligned}
$$

Defining

$$\beta = \int_0^\infty f(\eta) \left[2\, g(\eta) - 1 \right] d\eta \qquad (2.9)$$

$$\gamma = \int_0^\infty g(\eta) \left[g(\eta) - 1 \right] d\eta + 2 \int_0^\infty f(\eta)\, h(\eta) d\eta \qquad (2.10)$$

$$\sigma = \int_0^\infty h(\eta) \left[2g(\eta) - 1 \right] d\eta + 2 \int_0^\infty f(\eta)\, j(\eta) d\eta \qquad (2.11)$$

then equation (2.8) may be written

$$u_\tau^2 = -\alpha \frac{d}{d\bar{x}}(\bar{\delta}U_m^2) - \zeta\beta\frac{d}{d\bar{x}}(\bar{\delta}U_m) - \zeta^2\gamma\frac{d\bar{\delta}}{d\bar{x}}$$

$$-\zeta^3\sigma\frac{d}{d\bar{x}}(\delta/U_m) - \cdots \qquad (2.12)$$

Likewise, the skin friction coefficient defined by equation (1.18) may be written

$$C_f = -\frac{2\alpha}{U_m^2}\frac{d}{d\bar{x}}(\bar{\delta}U_m^2) - \frac{2\zeta\beta}{U_m^2}\frac{d}{d\bar{x}}(\bar{\delta}U_m) - \frac{2\zeta^2\gamma}{U_m^2}\frac{d\bar{\delta}}{d\bar{x}}$$

$$-\frac{2\zeta^3\sigma}{U_m^2}\frac{d}{d\bar{x}}(\bar{\delta}/U_m) - \cdots \qquad (2.13)$$

Assuming that similarity exists for the shear stress in a wall jet beneath an external free stream, then analogous to equation (2.1)

$$u_*^2 = u_\tau^2\left[S(\eta) + \frac{\zeta}{U_m}T(\eta) + \frac{\zeta^2}{U_m^2}W(\eta) + \frac{\zeta^3}{U_m^3}Z(\eta) + \cdots\right. \qquad (2.14)$$

This equation may then be combined with the momentum equation (2.7). In order that the resulting equation be valid for all values of ζ, the coefficient of each ζ^n must vanish. For $n = 0$

$$U_m\frac{dU_m}{d\bar{x}}\left[f^2(\eta) - f'(\eta)\int_0^\eta f(z)\,dz + 2\alpha S'(\eta)\right] =$$

$$\frac{U_m^2}{\bar{\delta}}\frac{d\bar{\delta}}{d\bar{x}}\left[f'(\eta)\int_0^\eta f(z)\,dz - \alpha S'(\eta)\right] \qquad (2.15)$$

which is the same as equation (1.22).

For $n = 1$,

$$\bar{\delta}\frac{dU_m}{d\bar{x}}f(\eta)\,g(\eta) - U_m\frac{d\bar{\delta}}{d\bar{x}}f'(\eta)\int_0^\eta g(z)\,dz - \frac{d}{d\bar{x}}(\bar{\delta}U_m)g'(\eta)$$

$$\cdot\int_0^\eta f(z)\,dz = -\beta\frac{d}{d\bar{x}}(\bar{\delta}U_m)S'(\eta) - \frac{\alpha}{U_m}\frac{d}{d\bar{x}}(\bar{\delta}U_m^2)T'(\eta) \qquad (2.16)$$

For n = 2,

$$\frac{d\bar{\delta}}{d\bar{x}}\, g'(\eta) \int_0^\eta g(z)dz + \frac{1}{U_m}\frac{d}{d\bar{x}}(\bar{\delta}U_m)\, h'(\eta)\int_0^\eta f(z)dz + U_m \frac{d}{d\bar{x}}(\bar{\delta}/U_m)$$

$$\cdot\, f'(\eta)\int_0^\eta h(z)dz \;=\; \gamma \frac{d\bar{\delta}}{d\bar{x}}\, S'(\eta) + \frac{\beta}{U_m}\frac{d}{d\bar{x}}(\bar{\delta}U_m)\, T'(\eta)$$

$$+ \frac{\alpha}{U_m^2}\frac{d}{d\bar{x}}(\bar{\delta}U_m^2)\, W'(\eta) \qquad (2.17)$$

For n = 3,

$$\frac{\bar{\delta}}{U_m^2}\frac{dU_m}{d\bar{x}}\left[f(\eta)j(\eta) + g(\eta)h(\eta)\right] + \frac{1}{U_m^2}\frac{d}{d\bar{x}}(\bar{\delta}U_m)\, j'(\eta)\int_0^\eta f(z)dz$$

$$+ \frac{1}{U_m}\frac{d\bar{\delta}}{d\bar{x}}\, h'(\eta)\int_0^\eta g(z)dz + \frac{d}{d\bar{x}}(\bar{\delta}/U_m)\, g'(\eta)\int_0^\eta h(z)dz + U_m \frac{d}{d\bar{x}}$$

$$\cdot\, (\bar{\delta}/U_m^2)\, f'(\eta)\int_0^\eta j(z)dz \;=\; \sigma \frac{d}{d\bar{x}}(\bar{\delta}/U_m)\, S'(\eta) + \frac{\gamma}{U_m}\frac{d\bar{\delta}}{d\bar{x}}\, T'(\eta)$$

$$+ \frac{\beta}{U_m^2}\frac{d}{d\bar{x}}(\bar{\delta}U_m)\, W'(\eta) + \frac{\alpha}{U_m^3}\frac{d}{d\bar{x}}(\bar{\delta}U_m^2)\, Z'(\eta) \qquad (2.18)$$

The boundary conditions governing the shear similarity functions $T(\eta)$, $W(\eta)$, $Z(\eta)$, $\cdots$ may be written

$$T(0) = W(0) = Z(0) = \cdots = 0 \qquad (2.19a)$$

$$T(\infty) = W(\infty) = Z(\infty) = \cdots = 0 \qquad (2.19b)$$

$$T'(0) = W'(0) = Z'(0) = \cdots = 0 \qquad (2.19c)$$

In order that there be a similarity solution independent of the downstream coordinate, each of the equations (2.15) through (2.18) must be independent of $\bar{x}$. As before, equation (2.15) implies the condition

$$\frac{\lambda}{U_m}\frac{dU_m}{d\bar{x}} + \frac{1}{\bar{\delta}}\frac{d\bar{\delta}}{d\bar{x}} \;=\; 0 \qquad (2.20)$$

with solution given by equation (1.35). Equations (2.15) through (2.18) may then be written

$$f^2(\eta) + (\lambda-1)\, f'(\eta)\int_0^\eta f(z)dz + (2-\lambda)\,\alpha\, S'(\eta) = 0 \qquad (2.21)$$

$$f(\eta)\ g(\eta)\ +\lambda\ f'(\eta)\int_0^\eta g(z)dz + (\lambda-1)\ g'(\eta)\int_0^\eta f(z)dz$$

$$+ (1-\lambda)\beta\ S'(\eta) + (2-\lambda)\alpha\ T'(\eta) = 0 \qquad (2.22)$$

$$\lambda g'(\eta)\int_0^\eta g(z)dz + (\lambda-1)\ h'(\eta)\int_0^\eta f(z)dz + (\lambda+1)\ f'(\eta)$$

$$\cdot \int_0^\eta h(z)dz - \lambda\gamma\ S'(\eta) + (1-\lambda)\beta\ T'(\eta)$$

$$+ (2-\lambda)\alpha\ W'(\eta) = 0 \qquad (2.23)$$

$$f(\eta)j(\eta) + g(\eta)h(\eta) + (1-\lambda)j'(\eta)\int_0^\eta f(z)dz - \lambda h'(\eta)\int_0^\eta g(z)dz$$

$$- (\lambda+1)\ g'(\eta)\int_0^\eta h(z)dz - (2+\lambda)\ f'(\eta)\int_0^\eta j(z)dz + (\lambda+1)\sigma$$

$$\cdot\ S'(\eta) - \lambda\gamma\ T'(\eta) + (1-\lambda)\beta\ W'(\eta) + (2-\lambda)\alpha Z'(\eta) = 0 \qquad (2.24)$$

These are the similarity equations which govern the flow in a wall jet beneath a uniform free stream.

If the point of zero shear stress is again denoted by η_*, then in addition to equations (2.19)

$$T(\eta_*) = W(\eta_*) = Z(\eta_*) = \cdots = 0 \qquad (2.25)$$

It might also be pointed out that equation (1.25) relating the similarity parameter λ to η_* is still valid in the case of a wall jet beneath a secondary free stream.

C. Similarity Functions

Elimination of $S'(\eta)$ from equations (2.21) and (2.22) gives

$$f(\eta)\ g(\eta)\ +\lambda\ f'(\eta)\int_0^\eta g(z)dz + (\lambda-1)\ g'(\eta)\int_0^\eta f(z)dz + \frac{(1-\lambda)\beta}{(\lambda-2)\alpha}$$

$$\cdot \left[f^2(\eta) + (\lambda-1)\ f'(\eta)\int_0^\eta f(z)dz\right] + (2-\lambda)\alpha T'(\eta) = 0 \qquad (2.26)$$

As before, in order to obtain a solution of this equation, some further assumptions must be made concerning the velocity distribution $g(\eta)$ or the shear distribution $T(\eta)$. One possible form for the function $g(\eta)$ which satisfies the boundary conditions (2.4) and (2.5) and which is suggested by the function $f(\eta)$ found in the preceding part is

$$g(\eta) = \left\{ \mathrm{erf}(B\eta) \left[1 - e^{-1/2\,\eta^2} \right]^4 \left[1 - f(\eta) \right] \right\}^2 \qquad (2.27)$$

where B has the value .67753 as determined in the preceding part.

From equation (2.26)

$$T'(\eta) = \frac{(1-\lambda)\beta}{[(\lambda-2)\alpha]^2} \left[f^2(\eta) + (\lambda-1)\, f'(\eta) \int_0^\eta f(z)dz \right] + \frac{1}{(\lambda-2)\alpha}$$

$$\cdot \left[f(\eta)g(\eta) + \lambda f'(\eta) \int_0^\eta g(z)dz + (\lambda-1)g'(\eta) \int_0^\eta f(z)dz \right] \qquad (2.28)$$

which may be integrated giving

$$T(\eta) = \frac{(1-\lambda)\beta}{[(\lambda-2)\alpha]^2} \left[(2-\lambda) \int_0^\eta f^2(z(dz + (\lambda-1)f(\eta) \int_0^\eta f(z)dz \right.$$

$$+ \frac{1}{(\lambda-2)\alpha} \left[2(1-\lambda) \int_0^\eta f(z)g(z)dz + \lambda f(\eta) \int_0^\eta g(z)dz \right.$$

$$\left. + (\lambda-1)\; g(\eta) \int_0^\eta f(z)dz \right] \qquad (2.29)$$

If $S'(\eta)$ and $T'(\eta)$ are eliminated from equation (2.23), there results

$$\lambda g'(\eta) \int_0^\eta g(z)dz + (\lambda-1)h'(\eta) \int_0^\eta f(z)dz + (\lambda+1)f'(\eta) \int_0^\eta h(z)dz$$

$$+ \left\{ \left[\frac{(\lambda-1)\beta}{(\lambda-2)\alpha} \right]^2 - \frac{\lambda\gamma}{(\lambda-2)\alpha} \right\} \left[f^2(\eta) + (\lambda-1)f'(\eta) \int_0^\eta f(z)dz \right]$$

$$+ \frac{(1-\lambda)\beta}{(\lambda-2)\alpha} \left[f(\eta)g(\eta) + \lambda f'(\eta) \int_0^\eta g(z)dz + (\lambda-1)g'(\eta) \int_0^\eta f(z)dz \right]$$

$$+ (2-\lambda)\alpha\, W'(\eta) = 0 \qquad (2.30)$$

A reasonable form for the function $h(\eta)$ satisfying the required boundary conditions (2.4) and (2.5) is

$$h(\eta) = 50\, f(\eta)\, g(\eta) \tag{2.31}$$

From equation (2.30)

$$\begin{aligned} W'(\eta) = {} & \frac{1}{(\lambda-2)\alpha} \Big[\lambda g'(\eta) \int_0^\eta g(z)dz + (\lambda-1)\, h'(\eta) \int_0^\eta f(z)dz + (\lambda+1) f'(\eta) \\ & \cdot \int_0^\eta h(z)dz\Big] + \frac{(1-\lambda)\beta}{[(\lambda-2)\alpha]^2} \Big[f(\eta)g(\eta) + \lambda f'(\eta) \int_0^\eta g(z)dz + (\lambda-1) \\ & \cdot g'(\eta) \int_0^\eta f(z)dz\Big] + \frac{1}{[(\lambda-2)\alpha]^2} \left\{ \frac{[(\lambda-1)\beta]^2}{(\lambda-2)\alpha} - \lambda\, \gamma \right\} \Big[f^2(\eta) \\ & + (\lambda-1)\, f'(\eta) \int_0^\eta f(z)dz\Big] \end{aligned} \tag{2.32}$$

which may be integrated with the result

$$\begin{aligned} W(\eta) = {} & \frac{1}{(\lambda-2)\alpha} \Big[\lambda g(\eta) \int_0^\eta g(z)dz - \lambda \int_0^\eta g^2(z)dz + (\lambda-1)h(\eta) \int_0^\eta f(z)dz \\ & + (\lambda+1)\, f(\eta) \int_0^\eta h(z)dz - 2\lambda \int_0^\eta f(z)h(z)dz\Big] + \frac{(1-\lambda)\beta}{[(\lambda-2)\alpha]^2} \\ & \cdot \Big[2(1-\lambda) \int_0^\eta f(z)g(z)dz + \lambda f(\eta) \int_0^\eta g(z)dz + (\lambda-1)g(\eta) \int_0^\eta f(z)dz\Big] \\ & + \frac{1}{[(\lambda-2)\alpha]^2} \left\{ \frac{[(\lambda-1)\beta]^2}{(\lambda-2)\alpha} - \lambda\, \gamma \right\} \Big[(2-\lambda) \int_0^\eta f^2(z)dz \\ & + (\lambda-1)\, f(\eta) \int_0^\eta f(z)dz\Big] \end{aligned} \tag{2.33}$$

Following a procedure similar to the above, $S'(\eta)$, $T'(\eta)$, and $W'(\eta)$ may be eliminated from equation (2.24) by means of equations (1.28), (2.28), and (2.32). The resulting equation, however, still contains the two unknowns $j(\eta)$ and $Z'(\eta)$ and because of its length will not be stated here. One possible form for the function $j(\eta)$ which satisfies the prescribed boundary conditions is

$$j(\eta) = 160\, e^{-B\eta^2}\, f(\eta)\, h(\eta) \qquad (2.34)$$

With this assumption, the function $Z(\eta)$ may then be obtained by a straightforward integration.

An examination of equation (2.1) shows that a series representation of this form is valid only up to the point where the jet disappears (i.e., only when $(\zeta/U_m) = (U_\infty/U_{max}) < 1$). As long as ζ/U_m remains less than one, this series will converge provided each of the similarity functions is bounded. Beyond the point where the jet disappears, the flow becomes equivalent to a normal turbulent boundary layer in a zero pressure gradient.

Since the normal region of interest for the wall jet flow beneath an external free stream extends only up to a point where the ratio ζ/U_m is still somewhat less than unity, the velocity distribution can be adequately represented by the first four terms of equation (2.1). That is,

$$\frac{U}{U_m} = f(\eta) + \frac{\zeta}{U_m} g(\eta) + \frac{\zeta^2}{U_m^2} h(\eta) + \frac{\zeta^3}{U_m^3} j(\eta) \qquad (2.35)$$

Likewise, the shear stress distribution can be adequately represented by

$$u_*^2 = u_\tau^2 [S(\eta) + \frac{\zeta}{U_m} T(\eta) + \frac{\zeta^2}{U_m^2} W(\eta) + \frac{\zeta^3}{U_m^3} Z(\eta)] \qquad (2.36)$$

The next term in each of these expressions becomes important only in the case where ζ is relatively large, or very far downstream of the jet outlet where U_m becomes small.

The similarity functions $g(\eta)$, $h(\eta)$, and $j(\eta)$ were programmed for the computer along with the function $f(\eta)$ of the preceding part. Values of these functions are listed in Tables II, III, and IV. The constants β, γ, and σ defined by equations (2.9), (2.10), and (2.11) were found to be

$$\beta = \int_0^\infty f(\eta)\,[2g(\eta) - 1]\,d\eta = -1.0472 \tag{2.37}$$

$$\gamma = \int_0^\infty g(\eta)\,[g(\eta) - 1]\,d\eta + 2\int_0^\infty f(\eta)h(\eta)\,d\eta = -.09981 \tag{2.38}$$

and

$$\sigma = \int_0^\infty h(\eta)\,[2g(\eta) - 1]\,d\eta + 2\int_0^\infty f(\eta)j(\eta)\,d\eta = +.63250 \tag{2.39}$$

The shear similarity functions $T(\eta)$, $W(\eta)$, and $Z(\eta)$ together with their derivatives are also listed in the above tables. These values were computed under the assumption that the point of zero shear stress coincides with the maximum velocity location. The effect of a different location for the zero shear point on these functions (i.e., $\lambda \neq 1.7977$) can be obtained by simple Taylor series expansions as outlined in the preceding part.

D. Variation of Velocity and Length Scales

The presence of an external free stream above the wall jet alters the functional dependence of $\bar{\delta}$ and U_m as given by equations (1.34a) and (1.34b). To account for the secondary stream, these equations may be rewritten in the form

$$\bar{\delta} = F_1(\bar{x},\ \zeta,\ Re_0) \tag{2.40a}$$

and

$$U_m = F_2(\bar{x},\ \zeta,\ Re_0) \tag{2.40b}$$

As was pointed out earlier, equation (1.35) still relates the velocity and length scales even with the addition of the secondary free stream.

Due to the greater momentum in the jet profile, mass is entrained into the jet from the free stream but not to as great an extent as when the free stream is not present. Thus a wall jet necessarily mixes more slowly with a moving stream than with still air and only for very small values of ζ will the rate of growth of the jet approach that of the plane turbulent wall jet. Analogous to the still air case, the most obvious choice for the characteristic jet thickness, δ, is that value of y in the outer portion of the jet where the velocity lies halfway between the maximum and free stream velocities. This point is also measured very easily experimentally.

An examination of Tables I through IV reveals that the similarity functions as tabulated do not take into account the fact that the jet thickness is also dependent on the velocity ratio ζ. That, $y = \delta$ does not necessarily correspond to $\eta = 1$ except for the case $\zeta = 0$ which is that of the plane turbulent wall jet. This fact, however, can be used to determine the effect of the external free stream on the velocity and length scales. Denoting the value of η in equations (1.26), (2.27), (2.31), and (2.34) where the velocity lies halfway between the maximum and free stream velocities by $\eta_{1/2}$, then from equation (2.35)

$$\frac{1}{2}\left(1 + \frac{\zeta}{U_m}\right) = f(\eta_{1/2}) + \frac{\zeta}{U_m}\, g(\eta_{1/2}) + \frac{\zeta^2}{U_m^2}\, h(\eta_{1/2}) + \frac{\zeta^3}{U_m^3}\, j(\eta_{1/2}) \qquad (2.41)$$

This relation between $\eta_{1/2}$ and ζ/U_m is shown in Figure 4 and can be written symbolically in the form

$$\eta_{1/2} = F(\zeta/U_m) \qquad (2.42)$$

In constructing a given velocity profile by means of the Tables, each value of η must, therefore, be scaled by the factor $[F(\zeta/U_m)]^{-1}$ appropriate to the given profile. An example velocity profile construction is given in the Appendix.

The introduction of the scale factor, F, necessarily modifies equation (2.20) which must now be written

$$\frac{\lambda}{U_m}\frac{dU_m}{d\bar{x}} + \frac{1}{\bar{\delta}F}\frac{d}{d\bar{x}}(\bar{\delta}F) = 0$$

with solution

$$U_m = \text{const.}\ (\bar{\delta}F)^{-1/\lambda} \tag{2.43}$$

Analogous to equation (1.36) for the plane turbulent wall jet, this may be rewritten in the form

$$U_m = (1+M)\ (\bar{\delta}F)^{-1/\lambda} \tag{2.44}$$

where the factor M again takes into account local conditions at the jet outlet. Likewise, the wall shear stress must be expressed as

$$u_\tau^2 = -\alpha\frac{d}{d\bar{x}}(\bar{\delta}FU_m^2) - \zeta\beta\frac{d}{d\bar{x}}(\bar{\delta}FU_m) - \zeta^2\gamma\frac{d}{d\bar{x}}(\bar{\delta}F)$$

$$- \zeta^3\sigma\frac{d}{d\bar{x}}\left(\frac{\bar{\delta}F}{U_m}\right) - \cdots \tag{2.45}$$

It may be pointed out that these results are consistent with the results for the plane turbulent wall jet, since the scale factor F is unity for $\zeta = 0$.

The fact that the values of η in the Tables are correct only for $\zeta = 0$ and must be scaled by the factor F^{-1} for $\zeta \neq 0$ implies that the effect of the external free stream on the growth of the jet is given by the function $F(\zeta/U_m)$. From equation (1.44), the jet thickness variation is therefore given by

$$\bar{\delta} = D\ F(\zeta/U_m)\ \exp\left[C\bar{x}^{(2-\lambda)/\lambda}\right] \tag{2.46}$$

while the maximum velocity decay is given by

$$U_m = (1 + M)\ [D\ F^2(\zeta/U_m)]^{-1/\lambda}\ \exp[\ -\ \frac{C}{\lambda}\ \bar{x}^{(2-\lambda)/\lambda}\ ] \tag{2.47}$$

Again, the constants C and D appearing in these equations will depend on conditions in the neighborhood of the jet outlet.

If the above equations (2.46) and (2.47) are rewritten in the form

$$\frac{\bar{\delta}}{F} = D\ \exp[C\ \bar{x}^{(2-\lambda)/\lambda}\ ] \tag{2.48}$$

and

$$U_m\ F^{2/\lambda} = (1 + M)\ D^{-1/\lambda}\ \exp[\ -\ \frac{C}{\lambda}\ \bar{x}^{(2-\lambda)/\lambda}\ ] \tag{2.49}$$

then the quantities on the left are dependent on the velocity ratio ζ only to the extent that the factors C, D, and M are dependent on ζ. Except for the case $\zeta = 0$, a solution of these equations for given values of C, D, and M must be obtained by trial and error in conjunction with Figure 4 which describes the variation of F with ζ/U_m.

III EXPERIMENTAL INVESTIGATION

The experimental phase of this investigation was carried out in the Princeton University 2" x 36" two-dimensional smoke tunnel which has a maximum velocity capability of approximately 90 feet per second. A portion of the test section floor of this tunnel was removed in order to accommodate the jet and rear plate. The entire model was machined from aluminum and a sectional view of its installation is shown in Figure 5. The rear plate, or wall as it is commonly called, consists of two pieces and has an overall length of 34.5 inches. The height of the jet outlet could be varied between .03 inches and .15 inches by merely raising or lowering the rear plate. Sealing between the entire model and tunnel walls was accomplished by means of "O" ring segments and rubber fillers.

Located upstream of the jet outlet is a suction slot which provides some control over the boundary layer which exists above the jet outlet when the external free stream is used. The present investigation, however, does not include any measurements to determine the effect of this initial boundary layer on the flow field downstream of the jet outlet. In each case in which the external stream was used, a normal flat plate boundary layer was allowed to form on the jet lip.

The air issuing from the jet was supplied by two centrifugal compressors connected in series. To avoid any angularity in the flow with respect to the plane of symmetry of the tunnel, a small honeycomb element was installed in the plenum chamber just upstream of the jet outlet. With this arrangement, the velocity distribution at the jet outlet was found to be two-dimensional to within ± .5%, and the maximum Reynolds number based on jet velocity and jet slot height which could be attained was in the neighborhood of 21,000. Both the plenum chamber and suction chamber were effectively sealed by means of "0" ring segments. The height of the jet outlet could be held to within ± .001 inches of any desired value by means of a set of cylindrical plug guages.

The initial phase of the experimental program consisted mainly of a verification of the fact that the flow remained sufficiently two-dimensional for a reasonable distance downstream of the jet outlet. Transverse velocity distributions in the jet were measured at various downstream locations both with and without the external free stream. This was accomplished with the aid of a rake consisting of ten evenly spaced total head tubes .032 inches in diameter, the pressures being measured by means of a bank of alcohol manometers. In all cases, it was found that the flow remained two-dimensional to within ± 5% in a central lane approximately one inch wide extending as far as 20 inches downstream. Consequently, all subsequent measurements were carried out in this narrow region.

In order to determine the static pressure variation in the longitudinal direction, the rear plate of the model was equipped with a series of static pressure taps. The location at which the longitudinal pressure gradient essentially became zero could then easily be determined, and all measurements were performed well downstream of this point.

The velocity profiles normal to the rear plate were measured by means of a total head tube having an internal diameter of .020 inches and an external diameter of .032 inches. This probe was mounted on a carriage as shown in Figure 6 as was the total head rake used in the two-dimensionality study. The carriage was guided during its fore and aft movement by a small track which is an integral part of the rear plate.

The long threaded rod extending downstream from the rear of the carriage was used to control the longitudinal position of the carriage and total head tube. The vertical movement of the probe was powered by a small direct current electric motor mounted on the carriage, the details of the drive mechanism also being shown in Figure 6. The vertical position error of this system was found to be less than .002 inches over the entire range of movement of the probe. When the external free stream was employed, the pitot static tube located at the top of the carriage was used to measure its velocity.

Initially, the pressures sensed by the total head probe were fed to an inclined manometer whose angle of inclination could be varied between 7 and 45 degrees. Data for several velocity profiles were recorded using this manometer, but it was found that because the length of time involved in making such measurements was so long, any appreciable change in ambient conditions could substantially alter the results. Consequently, the data for the remaining profiles were recorded with the aid of a differential pressure transducer having a range of ± .6 psi. Because of the nearly instantaneous response of such a device, the measurement time was drastically reduced without any appreciable loss in accuracy.

IV DISCUSSION

A. Comparison of Experimental Results With Theory

1. Plane Turbulent Wall Jet

Velocity profiles in the plane turbulent wall jet (i.e., $\zeta = 0$) were measured for two different values of the jet outlet Reynolds number. These profiles are shown in Figures 7 and 8 along with the similarity function $f(\eta)$ defined by equation (1.27) for comparison purposes. These results apparently verify the assumption that similarity with respect to the velocity profiles exists at least as far as 417 slot widths downstream of the outlet.

The data presented in Figure 7 were recorded with the aid of the inclined manometer discussed previously while those in Figure 8 were recorded by means of the pressure transducer. Extreme care was taken in making the measurements in the outer portion of the jet where the velocity tends to zero. There is an appreciable source of error in this region due to the fact that the turbulence level is very high and, because of the mass entrainment, the transverse inflow velocity is relatively large resulting in a yawed flow relative to the total head tube. Both of these effects combine to cause the total head tube to read low in the outer portion of the jet. There is also a source of measurement error in the region within a few total head tube diameters from the wall. Here, errors may arise from viscous effects, the fact that there is a velocity gradient across the face of the tube, and the displacement effect due to the presence of the wall. Since these latter two effects tend to cancel each other, the overall error in this region is not appreciable and no corrections to the data were employed.

As a further verification of its usefulness in predicting the turbulent wall jet velocity profiles, the data of several other investigations have been compared with the similarity function defined by equation (1.27). The data of George (7) and Myers, Schauer, and Eustis (8) are presented in Figures 9 and 10 respectively and, because of the wide range of downstream positions over which the data were taken, they offer further support for the similar velocity profiles assumption. The data of Patel (11), Sigalla (12), Schwarz and Cosart (2), and Förthmann (10) covering a somewhat more limited range of downstream positions are presented in Figures 11, 12, 13, and 14 respectively. Except for the data of George, all data were taken from the references cited and are thereby limited in accuracy. It is easily seen that the over-all agreement of the assumed form for the velocity distribution with the experimental results of this investigation as well as with those of other previous investigations is remarkably good. Only in the extreme outer portion of the profile is there any appreciable discrepancy, the data points lying consistently below the curve as expected.

As a check on equation (1.44), the approximate solution found for the variation of jet thickness with downstream coordinate, the data have been plotted in the form $\ln \bar{\delta}$ versus $\bar{x}^{(2-\lambda)/\lambda}$. These data are shown in Figure 15 where $\lambda = 1.7977$ has been assumed. Likewise, the data of George, Myers, Schauer, and Eustis, Patel, and Förthmann for $\bar{x}$ greater than 20 are presented in Figures 16, 17, and 18 in the same manner. The data of Schwarz and Cosart were not available while the data of Sigalla were not easily adaptable to the above manner of presentation. The constants C and D appearing in equation (1.44) were then determined to give a reasonable fit to the data in each case. The value of $(1+M) = U_m\bar{\delta}^{1/\lambda}$, as defined by equation (1.36), was determined by simply averaging the values of $U_m\bar{\delta}^{1/\lambda}$ in each case.

The variation of $\bar{\delta}$ and U_m with the downstream coordinate $\bar{x}$ for each of the investigations mentioned above is presented in Figures 19 through 26. It is easily seen from these figures that $\bar{\delta}$ varies almost linearly with $\bar{x}$, which means that the influence of the wall is fairly small since the jet thickness varies linearly with $\bar{x}$ for the free turbulent jet. It is also evident that the assumption $\lambda = 1.7977$ (i.e., that the point of zero shear stress coincides with the maximum velocity location) is reasonable as far as the prediction of the growth of the jet and decay of maximum velocity is concerned.

In Figure 27, the transverse shear stress calculations of Förthmann are compared with the shear similarity function $S(\eta)$ defined by equation (1.29) for $\lambda = 1.7977$. Only the data corresponding to values of $\bar{x}$ greater than 20 are shown since the similarity assumption is not valid for smaller values of $\bar{x}$. The agreement between the two is reasonable and adequately verifies the assumption of shear stress similarity.

2. Turbulent Wall Jet Beneath a Uniform Free Stream

Velocity profiles in the turbulent wall jet beneath a secondary uniform stream were measured for two different values of the jet outlet Reynolds number which also corresponds to two different values of the velocity ratio ζ. These profiles are shown in Figures 28 through 32, along with the similarity expansion defined by equation (2.35) for comparison purposes. All of these data were recorded with the aid of the pressure transducer discussed previously. These results verify that an expansion in terms of similarity functions as defined by equation (2.35) is certainly valid for at least 400 slot widths downstream of the outlet provided the ratio ζ/U_m remains approximately less than .4.

The addition of a secondary stream considerably reduces the experimental errors arising in the outer portion of the jet as a result of pitot tube incidence. Consequently, the outer portion of the velocity profile for a turbulent wall jet beneath a secondary stream exhibits a longer 'tail' than a profile for a wall jet issuing into a region of stationary fluid. However, the sources of measurement error in the region near the wall still remain, but again the over-all error in this region is not appreciable and can be neglected.

Again, as a further verification of its usefulness in predicting the velocity profiles in the turbulent wall jet beneath a secondary uniform stream, the data of several previous investigations have been compared with the velocity profiles constructed on the basis of equation (2.35). The measurements of Eskinazi (13) at three different values of jet outlet Reynolds number and velocity ratio ζ are shown in Figures 33 through 42. These measurements were made in a range extending as far as 465 slot widths downstream of the jet outlet. The data of George (5), extending as far as 400 slot widths downstream of the jet outlet, are shown in Figures 43, 44, and 45. The data of Patel (11), covering a more limited range of downstream positions, are presented in Figures 46 to 49 inclusive. These measurements were made at two different values of the jet outlet Reynolds number and velocity ratio ζ.

An examination of these velocity profiles shows that once the ratio ζ/U_m exceeds approximately .4, the tail of the profile constructed on the basis of equation (2.35) begins to show a certain amount of waviness, the amplitude of these oscillations or waves increasing as ζ/U_m

The addition of a secondary stream considerably reduces the experimental errors arising in the outer portion of the jet as a result of pitot tube incidence. Consequently, the outer portion of the velocity profile for a turbulent wall jet beneath a secondary stream exhibits a longer 'tail' than a profile for a wall jet issuing into a region of stationary fluid. However, the sources of measurement error in the region near the wall still remain, but again the over-all error in this region is not appreciable and can be neglected.

Again, as a further verification of its usefulness in predicting the velocity profiles in the turbulent wall jet beneath a secondary uniform stream, the data of several previous investigations have been compared with the velocity profiles constructed on the basis of equation (2.35). The measurements of Eskinazi (13) at three different values of jet outlet Reynolds number and velocity ratio ζ are shown in Figures 33 through 42. These measurements were made in a range extending as far as 465 slot widths downstream of the jet outlet. The data of George (5), extending as far as 400 slot widths downstream of the jet outlet, are shown in Figures 43, 44, and 45. The data of Patel (11), covering a more limited range of downstream positions, are presented in Figures 46 to 49 inclusive. These measurements were made at two different values of the jet outlet Reynolds number and velocity ratio ζ.

An examination of these velocity profiles shows that once the ratio ζ/U_m exceeds approximately .4, the tail of the profile constructed on the basis of equation (2.35) begins to show a certain amount of waviness, the amplitude of these oscillations or waves increasing as ζ/U_m

increases. This of course is primarily due to the fact that only the first four terms of the asymptotic expansion (2.1) were used to represent the profile. The value of ζ/U_m at which this oscillatory behavior begins to appear could easily be increased by simply including more terms in the profile representation. It is also interesting to notice that the inner portion of the profile (i.e., $\eta \leq 1$) remains relatively well behaved for all values of ζ/U_m shown and gives a very good representation of the experimental data in this range. This is due to the fact that the similarity functions $g(\eta)$, $h(\eta)$, and $j(\eta)$ as defined by equations (2.27), (2.31), and (2.34) are extremely small in the region $0 \leq \eta \leq 1$. This also bears out the conclusion reached by Seban and Back (14) that the outer free stream has very little influence on the inner portion of the flow.

The variation of $\bar{\delta}$ and U_m with the downstream coordinate $\bar{x}$ for each of the investigations mentioned above is presented in Figures 50 through 57. The predicted variations, as given by equations (2.48) and (2.49), are also shown. As before, the constants C and D were determined to give a reasonable fit to the experimental data in each case and the value of $(1+M)$, as defined by equation (2.44), was determined by simply averaging the values of $U_m(\bar{\delta}F)^{1/\lambda}$. Again the assumption that the point of zero shear stress coincides with the maximum velocity location (i.e., $\lambda = 1.7977$) was employed. It is evident that this assumption is also reasonable in this more general case as far as the prediction of the growth of the jet and decay of maximum velocity is concerned. From these figures it is easily seen that the variation of $\bar{\delta}/F$ with the downstream coordinate is approximately linear. This is consistent with the previous results for the special case $\zeta = 0$, since in this case the scale factor F is unity.

B. Jet Outlet Conditions

For a short distance downstream of the outlet, the conditions in the jet will be strongly dependent on the nature of the flow immediately at the nozzle. For the plane turbulent wall jet, the two most important factors which influence the flow in this region, usually referred to as the jet core and transition region, are the jet outlet Reynolds number and the local geometry of the outlet itself. Initial turbulence in the jet has little influence on the flow except in a region on the order of one slot width from the jet outlet.

Because of the large amount of momentum in the jet, the rate mass entrainment near the nozzle is very great and the transverse velocity gradient is at a maximum. This mixing process induces a slight pressure rise in this region and only beyond 30 to 40 slot widths downstream of the outlet does the pressure gradient become essentially zero. At this point the flow has already reached a fully developed or self-preserving state and only beyond this point is the assumption of similar velocity profiles valid. Normally, the maximum velocity in the jet remains roughly constant for about ten slot widths downstream of the outlet before decreasing while the jet thickness begins to increase immediately. This possibly accounts for the fact that in many cases it has been found that the so-called virtual origin locations for the maximum velocity decay and jet thickness variation do not coincide.

In an attempt at a more accurate determination of the effect of local conditions at the jet exit on the downstream flow, the constants C, D, and 1+M employed in Figures 19 through 26 are presented in Figure 58 as functions of the jet outlet Reynolds number. There appears to be some evidence that each of these factors is a rather slowly varying function of the Reynolds number and that the effect of local geometry differences is not overly great.

In addition to the jet outlet Reynolds number and local geometrical configuration, the conditions near the jet outlet in the more general case of a turbulent wall jet beneath a secondary stream are also affected by the presence of the secondary stream itself and the boundary layer on the lip of the jet arising as a result of this secondary stream. Much of the practical interest in wall jets is in flows with an external stream and particularly in the mixing of a wall jet with such a boundary layer. However, it has been found that except for relatively large values of the velocity ratio ζ, the initial boundary layer has very little effect on the fully developed velocity profiles which appear at approximately 30 slot widths downstream of the jet outlet. That is, the momentum deficit of the initial boundary layer is absorbed so quickly that the influence of the initial boundary layer is confined to the region immediately downstream of the outlet. Specifically, Bradshaw and Gee (3) have stated that the fully developed jet is not greatly affected by the initial boundary layer provided the jet momentum excess is approximately five times as large as the boundary layer momentum deficit. Therefore, for all practical applications the initial boundary layer is important only in so far as it affects conditions immediately downstream of the jet outlet.

Qualitatively, the presence of the secondary free stream and resulting boundary layer above the turbulent wall jet affects the conditions in the vicinity of the jet outlet very little. There is still the slight induced pressure rise just down-stream of the jet outlet with an essentially zero pressure gradient beyond about 30 to 40 slot widths downstream of the outlet. The potential core or region of undiminished total pressure in which the maximum velocity remains roughly constant still exists followed by the transition region in which the velocity profiles reach the fully developed state. Only beyond this point where the velocity profiles become fully developed is the expansion in terms of similarity functions valid.

For this more general case, the constants C, D, and I+M employed in Figures 50 through 57 are presented in Figure 59 as functions of the jet outlet Reynolds number. It appears that any dependence on the Reynolds number which may exist has been completely overshadowed by the effects of the secondary stream and, in particular, the effects of the initial boundary layer. It is interesting to note that the numerical range of each of these constants has not been greatly affected by the addition of the secondary stream.

V CONCLUSIONS

It has been found that the velocity profiles in the plane turbulent wall jet and turbulent wall jet beneath a secondary uniform stream can be adequately predicted by an asymptotic expansion of the form

$$\frac{U}{U_m} = f(\eta) + \frac{\zeta}{U_m} g(\eta) + \frac{\zeta^2}{U_m^2} h(\eta) + \frac{\zeta^3}{U_m^3} j(\eta)$$

(provided $0 \leq (\zeta/U_m) \leq .4$,) where

$$\eta = y/\delta, \qquad \zeta = U_\infty/V_j$$

This upper bound on the expansion parameter ζ/U_m could be increased somewhat by simply adding more terms to the above series expansion.

Based on the assumption that the shear stress distribution in the jet can also be represented by an expansion in terms of similarity functions, the relation

$$U_m(\bar{\delta}F)^{1/\lambda} = \text{constant} = 1 + M$$

between the jet thickness $\bar{\delta}$ and maximum velocity in the profile U_m is obtained. The scale factor F is related to the expansion parameter ζ/U_m by the expression

$$\frac{1}{2}\left(1 + \frac{\zeta}{U_m}\right) = f(F) + \frac{\zeta}{U_m} g(F) + \frac{\zeta^2}{U_m^2} h(F) + \frac{\zeta^3}{U_m^3} j(F)$$

By considering the effect of introducing a wall into a two-dimensional, free turbulent jet, an approximate relation for the growth of the jet is obtained, namely

$$\bar{\delta} = D\, F \exp[C\, \bar{x}^{(2-\lambda)/\lambda}]$$

where C and D are constants. The similarity parameter λ was found to be dependent on the location of the point of zero shear stress, which lies somewhere in the vicinity of the point of maximum velocity in the profile.

It was found that the assumption that the point of zero shear stress coincided with the maximum velocity location was quite reasonable as far as the prediction of the jet thickness and maximum velocity decay is concerned.

Because of the complex nature of the turbulent wall jet flow, exact solutions for the similarity functions $f(\eta)$, $g(\eta)$, $h(\eta)$, and $j(\eta)$ could not be obtained. Instead, empirical analytic expressions satisfying the required boundary conditions were adopted and these proved to be quite adequate. Because the functions $g(\eta)$, $h(\eta)$, and $j(\eta)$, as well as any additional similarity functions which may be employed, are extremely small in the region $0 \leq \eta \leq 1$, the scale factor F can be determined quite accurately by using only very few terms of the above series expansion. For this reason, the above relations for the growth of the jet and decay of maximum velocity are reasonably accurate over a much larger range of the expansion parameter ζ/U_m than that for the velocity profiles themselves.

VI REFERENCES

1. Glauert, M. B., "The Wall Jet," Journal of Fluid Mechanics, Volume 1, Part 6, December, 1956, pp. 625-643.

2. Schwarz, W. H., and Cosart, W. P., "The Two-Dimensional Turbulent Wall Jet," Journal of Fluid Mechanics, Volume 10, Part 4, June 1961.

3. Bradshaw, P., and Gee, M. T., "Turbulent Wall Jets With and Without an External Stream," Aeronautical Research Council R. & M. No. 3252, June 1960.

4. Eskinazi, S., and Kruka, V., "Turbulence Measurements in a Two-Dimensional Rectangular Wall Jet With a Longitudinal Free Stream," Syracuse University Report No. ME 937-6205 P, May 1962.

5. George, A. R., "An Investigation of a Wall Jet in a Free Stream," Princeton University Report No. 479, September 1959.

6. Carriere, E., Eichelbrenner, E., and Poisson-Quinton, Ph., "Étude du Contrôl de la Couche Limite," Advances in Aeronautical Sciences, Volume 2, Pergaman Press, 1959, p. 620.

7. George, A. R., Unpublished Data, Princeton University, Department of Aeronautical Engineering, 1959.

8. Myers, G. E., Schauer, J. J., and Eustis, R. H., "The Plane Turbulent Wall Jet: Part I - Jet Development and Friction Factor," Stanford University Mechanical Engineering Department, Technical Report No. 1, June 1961.

9. Schlichting, H., Boundary Layer Theory, McGraw-Hill Book Company, Inc., New York, New York, 1960.

10. Förthmann, E., "Turbulent Jet Expansion," NACA TM-789, March 1936.

11. Patel, R. P., "Self Preserving, Two-Dimensional Turbulent Jets and Wall Jets in a Moving Stream," McGill University Thesis, April 1962.

12. Sigalla, A., "Measurements of Skin Friction in a Plane Turbulent Wall Jet," Journal of the Royal Aeronautical Society, Volume 62, Number 576, December 1958, pp. 873-877.

13. Eskinazi, S., and Helmbold, H. B., "The Turbulent Mixing of a Two-Dimensional Wall Jet with a Secondary Stream," Syracuse University Report No. ME 6700-670-6051, April 1960.

14. Seban, R. A., and Back, L. H., "Velocity and Temperature Profiles in a Wall Jet," International Journal of Heat and Mass Transfer, Volume 3, Number 4, December 1961, pp. 255-265.

15. Liepmann, H. W., and Laufer, J., "Investigations of Free Turbulent Mixing," NACA TN-1257, August 1947.

16. Patel, R. P., and Newman, B. G., "Self Preserving, Two-Dimensional Turbulent Jets and Wall Jets in a Moving Stream," McGill University Report No. Ae 5, September 1961.

17. Sigalla, A., "Experimental Data on Turbulent Wall Jets," Aircraft Engineering, Volume 30, Number 351, May 1958, pp. 131-134.

18. Eskinazi, S., and Kruka, V., "Mixing of a Turbulent Wall Jet into a Free Stream," Journal of Engineering Mechanics Division, Proceedings of the ASCE, Volume 88, Number EM2, Part I, April 1962, pp. 125-143.

19. Bakke, P., "An Experimental Investigation of a Wall Jet," Journal of Fluid Mechanics, Volume 2, July 1957, pp. 467-472.

20. Iwagaki, Y, and Tsuchiya, Y., "Boundary Layer Growth in Wall Jets Issuing from a Submerged Outlet," Proceedings of Japan National Congress for Applied Mechanics, 1959, pp. 259-264.

VII APPENDIX

1. Singularity in $f'(\eta)$:

If the conditions

$$f(1) = 1$$

and

$$f'(1) = 0$$

are used to determine the constants A and B, then

$$A = [1 - \mathrm{erf}(B)]^{-1} = 1.14406$$

$$B = .112060$$

and

$$f(\eta_m^{-1}) = .5$$

Integrating by parts, using the new values of A and B

$$\int_0^1 f(\eta)d\eta = A \int_0^1 \eta^{1/7} [1 - \mathrm{erf}(B\eta)]d\eta$$
$$= \frac{7}{8} + \frac{7\ AB}{4\sqrt{\pi}} \int_0^1 \eta^{8/7} e^{-B^2\eta^2} d\eta$$

Expanding in series and integrating term by term

$$\int_0^1 f(\eta)d\eta = \frac{7}{8} + \frac{49\ AB}{4\sqrt{\pi}} \left[\frac{1}{15} - \frac{B^2}{29} + \frac{B^4}{86} - \cdots \right]$$

$$= .933688$$

Therefore, for the function satisfying conditions (1.7c) and (1.11),

$$\int_0^{\eta_m} f(\eta)d\eta = .933688 \cdot \eta_m = .154427$$

The numerical evaluation of $\int_0^{\eta} f(z)dz$ and $\int_0^{\eta} f^2(z)dz$ was then carried out using a stepwise integration technique in which a finite value of $f'(0)$ was chosen such that

$$\int_0^{\eta_m} f(\eta)d\eta = .154427$$

The value of $\int_0^\infty f(\eta)d\eta$ was found to be 1.09790 which can also be determined analytically as a further check on the accuracy of the integration technique. Integrating by parts

$$\int_0^\infty A\eta^{1/7}\,[1 - \mathrm{erf}(B\eta)]d\eta = \frac{7\,AB}{4\sqrt{\pi}}\int_0^\infty \eta^{8/7}\,e^{-B^2\eta^2}d\eta$$

$$= \frac{7\,AB^{-8/7}}{8\sqrt{\pi}}\int_0^\infty z^{1/14}\,e^{-z}\,dz$$

where the substitution $z = B^2\eta^2$ has been made. This is expressable in terms of a Gamma function so that

$$\int_0^\infty f(\eta)d\eta = \frac{7\,AB^{-8/7}}{4\sqrt{\pi}}\,\Gamma\,(15/14) = 1.09797$$

which agrees almost exactly with the value obtained from the stepwise integration.

2. Example Velocity Profile Construction

Given ζ, $\bar{x}$, and the constants C, D, and 1+M, the values of $\bar{\delta}/F$ and $U_mF^{2/\lambda}$ can be obtained from equations (2.48) and (2.49). If a value of U_m is chosen, the value of the scale factor F as a function of ζ/U_m can be determined from Figure 4. A new estimate of U_m can then be obtained since $U_mF^{2/\lambda}$ is known. This procedure is then repeated until U_m and F have been determined. The jet thickness $\bar{\delta}$ can now be determined since $\bar{\delta}/F$ is known.

Knowing ζ/U_m, values of u/U_m can be calculated using equation (2.35) and Tables I, II, III, and IV. The non-dimensional vertical coordinate y/δ is then obtained by scaling the values of η in the tables by the factor F^{-1} found above. A plot of u/U_m versus y/δ then completes the velocity profile construction.

TABLE I

η	$f(\eta)$	$f'(\eta)$	$\int_0^\eta f\,d\eta$	$\int_0^\eta f^2\,d\eta$	$S(\eta)$	$S'(\eta)$
.000	.00000	-	.0000	.00000	1.00000	.0000
.010	.76040	10.2770	.0067	.00460	.96738	-4.1466
.020	.83308	5.3039	.0147	.01101	.92147	-4.9538
.030	.87591	3.4859	.0232	.01834	.86929	-5.4497
.040	.90552	2.5204	.0322	.02629	.81297	-5.7955
.050	.92748	1.9136	.0413	.03470	.75368	-6.0489
.060	.94440	1.4931	.0507	.04347	.69220	-6.2387
.070	.95771	1.1827	.0602	.05252	.62906	-6.3811
.080	.96829	.9430	.0698	.06180	.56470	-6.4866
.090	.97673	.7515	.0796	.07126	.49943	-6.5624
.100	.98343	.5946	.0894	.08086	.43353	-6.6138
.120	.99277	.3519	.1091	.10041	.30070	-6.6577
.140	.99792	.1719	.1290	.12023	.16763	-6.6401
.160	.99991	.0324	.1490	.14020	.03541	-6.5755
.180	.99941	-.0790	.1690	.16019	-.09514	-6.4738
.200	.99688	-.1703	.1890	.18013	-.22334	-6.3424
.300	.96383	-.4548	.2873	.27670	-.81368	-5.4033
.400	.91050	-.5968	.3811	.36478	-1.29683	-4.2425
.500	.84667	-.6714	.4690	.44211	-1.66124	-3.0507
.600	.77753	-.7061	.5503	.50815	-1.90940	-1.9301
.700	.70633	-.7142	.6245	.56324	-2.05157	-.9379
.800	.63532	-.7032	.6915	.60827	-2.10224	-.1031
.900	.56615	-.6783	.7516	.64438	-2.07779	.5642
1.000	.50000	-.6432	.8049	.67280	-1.99487	1.0677
1.100	.43774	-.6010	.8517	.69478	-1.86931	1.4198
1.200	.37995	-.5541	.8926	.71149	-1.71535	1.6389
1.300	.32700	-.5046	.9279	.72398	-1.54525	1.7462
1.400	.27906	-.4541	.9581	.73316	-1.36910	1.7636
1.500	.23615	-.4041	.9838	.73979	-1.19480	1.7125
1.600	.19817	-.3558	1.0055	.74450	-1.02823	1.6122
1.700	.16491	-.3099	1.0236	.74779	-.87344	1.4796
1.800	.13609	-.2672	1.0387	.75005	-.73292	1.3288
1.900	.11136	-.2280	1.0510	.75158	-.60791	1.1710
2.000	.09036	-.1926	1.0610	.75259	-.49867	1.0146
2.100	.07270	-.1611	1.0692	.75326	-.40474	.8657
2.200	.05801	-.1335	1.0757	.75368	-.32516	.7282
2.300	.04589	-.1095	1.0809	.75395	-.25864	.6046
2.400	.03599	-.0889	1.0849	.75412	-.20374	.4958
2.500	.02799	-.0716	1.0881	.75422	-.15898	.4018
2.600	.02159	-.0570	1.0906	.75428	-.12291	.3220
2.700	.01650	-.0450	1.0925	.75432	-.09415	.2552
2.800	.01251	-.0352	1.0939	.75434	-.07147	.2002
2.900	.00940	-.0273	1.0950	.75435	-.05376	.1554
3.000	.00700	-.0209	1.0958	.75435	-.04009	.1195

TABLE II

η	$g(\eta)$	$g'(\eta)$	$\int_0^\eta g\,d\eta$	$T(\eta)$	$T'(\eta)$
.000	.00000	.0000	.0000	.0000	.000
.010	.00000	.0000	.0000	.1785	22.691
.020	.00000	.0000	.0000	.4297	27.108
.030	.00000	.0000	.0000	.7153	29.821
.040	.00000	.0000	.0000	1.0235	31.714
.050	.00000	.0000	.0000	1.3479	33.101
.060	.00000	.0000	.0000	1.6844	34.139
.070	.00000	.0000	.0000	2.0298	34.918
.080	.00000	.0000	.0000	2.3821	35.496
.090	.00000	.0000	.0000	2.7392	35.911
.100	.00000	.0000	.0000	3.0998	36.192
.120	.00000	.0000	.0000	3.8267	36.432
.140	.00000	.0000	.0000	4.5549	36.336
.160	.00000	.0000	.0000	5.2784	35.982
.180	.00000	.0000	.0000	5.9928	35.426
.200	.00000	.0000	.0000	6.6944	34.707
.300	.00000	.0000	.0000	9.9248	29.568
.400	.00000	.0000	.0000	12.5687	23.216
.500	.00000	.0000	.0000	14.5628	16.694
.600	.00000	.0000	.0000	15.9208	10.562
.700	.00000	.0000	.0000	16.6988	5.132
.800	.00000	.0000	.0000	16.9760	.564
.900	.00001	.0002	.0000	16.8422	-3.088
1.000	.00006	.0010	.0000	16.3883	-5.847
1.100	.00029	.0040	.0000	15.7001	-7.788
1.200	.00104	.0124	.0001	14.8540	-9.029
1.300	.00315	.0322	.0003	13.9128	-9.717
1.400	.00811	.0709	.0008	12.9236	-10.017
1.500	.01821	.1360	.0021	11.9171	-10.089
1.600	.03631	.2308	.0047	10.9091	-10.063
1.700	.06526	.3517	.0097	9.9053	-10.013
1.800	.10716	.4874	.0182	8.9066	-9.955
1.900	.16268	.6212	.0316	7.9156	-9.853
2.000	.23072	.7350	.0512	6.9394	-9.648
2.100	.30854	.8147	.0780	5.9912	-9.288
2.200	.39225	.8523	.1131	5.0879	-8.748
2.300	.47758	.8475	.1565	4.2474	-8.037
2.400	.56052	.8057	.2085	3.4849	-7.195
2.500	.63781	.7364	.2685	2.8109	-6.277
2.600	.70724	.6501	.3358	2.2301	-5.342
2.700	.76760	.5567	.4096	1.7414	-4.441
2.800	.81861	.4640	.4890	1.3395	-3.613
2.900	.86062	.3777	.5730	1.0157	-2.881
3.000	.89446	.3009	.6608	.7598	-2.255

TABLE III

η	$h(\eta)$	$h'(\eta)$	$\int_0^\eta h d\eta$	$W(\eta)$	$W'(\eta)$
.000	.00000	.0000	.0000	.000	.00
.010	.00000	.0000	.0000	-.939	-119.29
.020	.00000	.0000	.0000	-2.259	-142.52
.030	.00000	.0000	.0000	-3.761	-156.79
.040	.00000	.0000	.0000	-5.381	-166.73
.050	.00000	.0000	.0000	-7.086	-174.02
.060	.00000	.0000	.0000	-8.855	-179.48
.070	.00000	.0000	.0000	-10.672	-183.58
.080	.00000	.0000	.0000	-12.523	-186.62
.090	.00000	.0000	.0000	-14.401	-188.80
.100	.00000	.0000	.0000	-16.297	-190.28
.120	.00000	.0000	.0000	-20.118	-191.54
.140	.00000	.0000	.0000	-23.947	-191.03
.160	.00000	.0000	.0000	-27.751	-189.17
.180	.00000	.0000	.0000	-31.506	-186.25
.200	.00000	.0000	.0000	-35.195	-182.47
.300	.00000	.0000	.0000	-52.178	-155.45
.400	.00000	.0000	.0000	-66.078	-122.06
.500	.00000	.0000	.0000	-76.562	-87.77
.600	.00000	.0000	.0000	-83.701	-55.53
.700	.00000	.0001	.0000	-87.792	-26.98
.800	.00004	.0009	.0000	-89.250	-2.97
.900	.00030	.0054	.0000	-88.547	16.22
1.000	.00157	.0237	.0001	-86.165	30.64
1.100	.00625	.0787	.0004	-82.568	40.60
1.200	.01977	.2073	.0016	-78.180	46.53
1.300	.05144	.4466	.0050	-73.377	49.00
1.400	.11315	.8055	.0129	-68.469	48.81
1.500	.21507	1.2380	.0290	-63.668	47.04
1.600	.35980	1.6411	.0574	-59.072	44.91
1.700	.53808	1.8890	.1021	-54.662	43.49
1.800	.72912	1.8852	.1654	-50.329	43.39
1.900	.90579	1.6041	.2474	-45.942	44.54
2.000	1.04241	1.0988	.3452	-41.402	46.29
2.100	1.12161	.4759	.4540	-36.694	47.74
2.200	1.13765	-.1457	.5674	-31.891	48.08
2.300	1.09577	-.6700	.6796	-27.130	46.86
2.400	1.00877	-1.0427	.7851	-22.575	44.00
2.500	.89274	-1.2515	.8803	-18.374	39.82
2.600	.76333	-1.3150	.9632	-14.639	34.78
2.700	.63340	-1.2684	1.0330	-11.429	29.41
2.800	.51201	-1.1505	1.0902	-8.754	24.14
2.900	.40452	-.9956	1.1359	-6.587	19.30
3.000	.31323	-.8301	1.1716	-4.874	15.06

TABLE IV

η	$j(\eta)$	$j'(\eta)$	$\int_0^\eta j\,d\eta$	$Z(\eta)$	$Z'(\eta)$
.000	.00000	.0000	.0000	.000	.00
.010	.00000	.0000	.0000	5.304	674.20
.020	.00000	.0000	.0000	12.768	805.45
.030	.00000	.0000	.0000	21.253	886.08
.040	.00000	.0000	.0000	30.410	942.29
.050	.00000	.0000	.0000	40.049	983.51
.060	.00000	.0000	.0000	50.046	1014.36
.070	.00000	.0000	.0000	60.311	1037.51
.080	.00000	.0000	.0000	70.776	1054.67
.090	.00000	.0000	.0000	81.388	1067.00
.100	.00000	.0000	.0000	92.103	1075.35
.120	.00000	.0000	.0000	113.701	1082.48
.140	.00000	.0000	.0000	135.336	1079.63
.160	.00000	.0000	.0000	156.834	1069.12
.180	.00000	.0000	.0000	178.060	1052.58
.200	.00000	.0000	.0000	198.906	1031.22
.300	.00000	.0000	.0000	294.889	878.53
.400	.00000	.0000	.0000	373.446	689.80
.500	.00000	.0000	.0000	432.696	496.02
.600	.00002	.0006	.0000	473.044	313.82
.700	.00030	.0075	.0000	496.161	152.52
.800	.00273	.0534	.0001	504.408	16.97
.900	.01577	.2469	.0009	500.483	-90.75
1.000	.06394	.7951	.0044	487.205	-170.12
1.100	.19295	1.8767	.0164	467.381	-221.94
1.200	.45306	3.3534	.0474	443.642	-249.15
1.300	.85641	4.6053	.1118	418.171	-257.86
1.400	1.33883	4.8131	.2214	392.399	-256.62
1.500	1.76940	3.5605	.3779	366.894	-253.57
1.600	2.01346	1.2038	.5690	341.539	-253.68
1.700	2.00375	-1.3470	.7720	315.900	-258.05
1.800	1.76754	-3.2113	.9621	289.547	-265.17
1.900	1.39840	-3.9870	1.1211	262.232	-272.53
2.000	1.00262	-3.7977	1.2410	233.958	-277.57
2.100	.65749	-3.0492	1.3233	204.990	-278.07
2.200	.39759	-2.1510	1.3753	175.844	-272.35
2.300	.22334	-1.3655	1.4057	147.234	-259.68
2.400	.11729	-.7925	1.4223	119.951	-240.42
2.500	.05792	-.4255	1.4307	94.737	-215.96
2.600	.02703	-.2132	1.4348	72.160	-188.31
2.700	.01198	-.1005	1.4367	52.544	-159.62
2.800	.00505	-.0448	1.4375	36.012	-131.79
2.900	.00204	-.0190	1.4378	22.420	-106.23
3.000	.00079	.0077	1.4379	11.517	-83.77

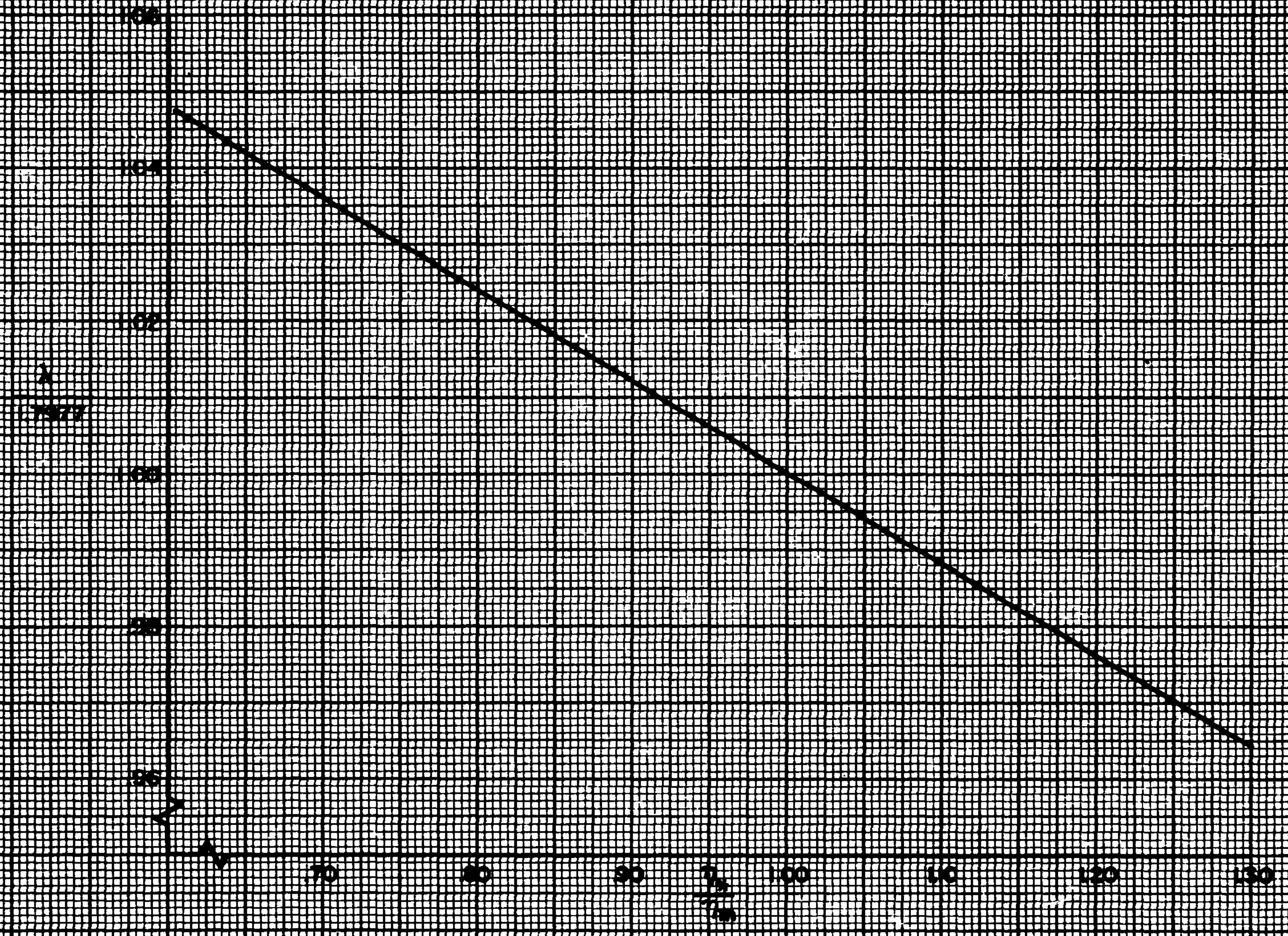

FIGURE 1. EFFECT OF ZERO SHEAR POINT ON SIMILARITY PARAMETER

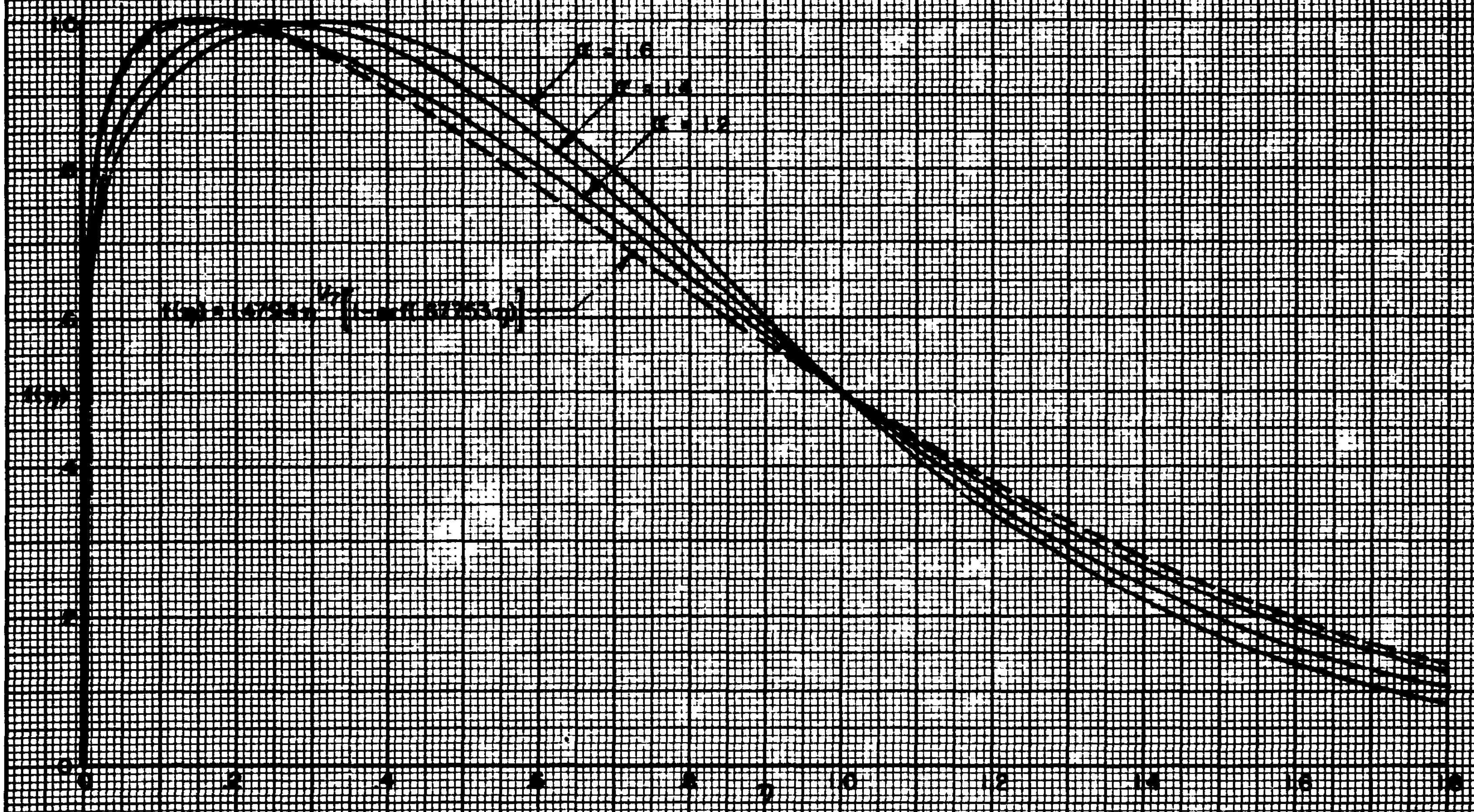

FIGURE 2. COMPARISON WITH GLAUERT'S PROFILES

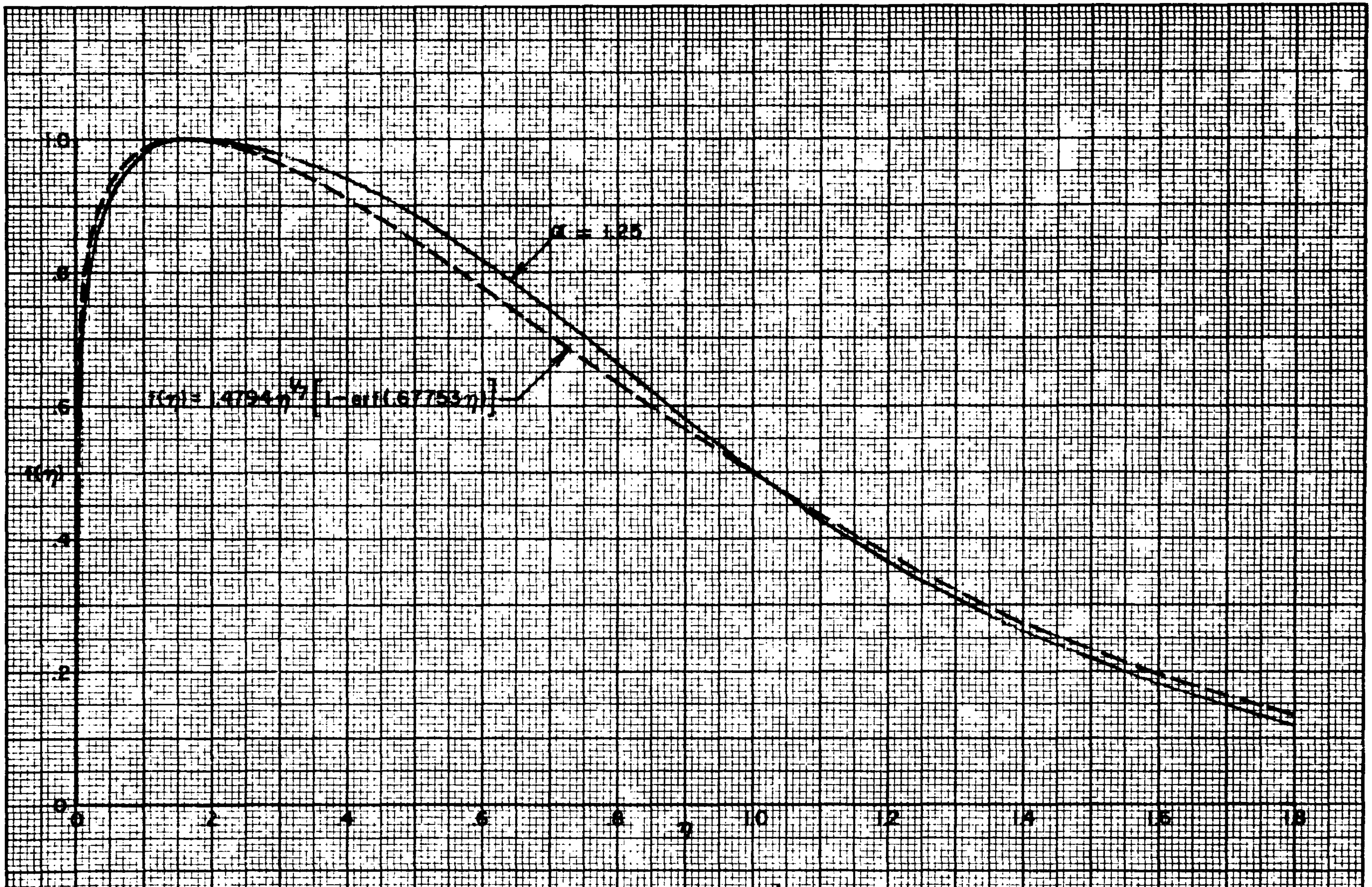

FIGURE 3. COMPARISON WITH GLAUERT'S PROFILE FOR $\alpha = 1.25$

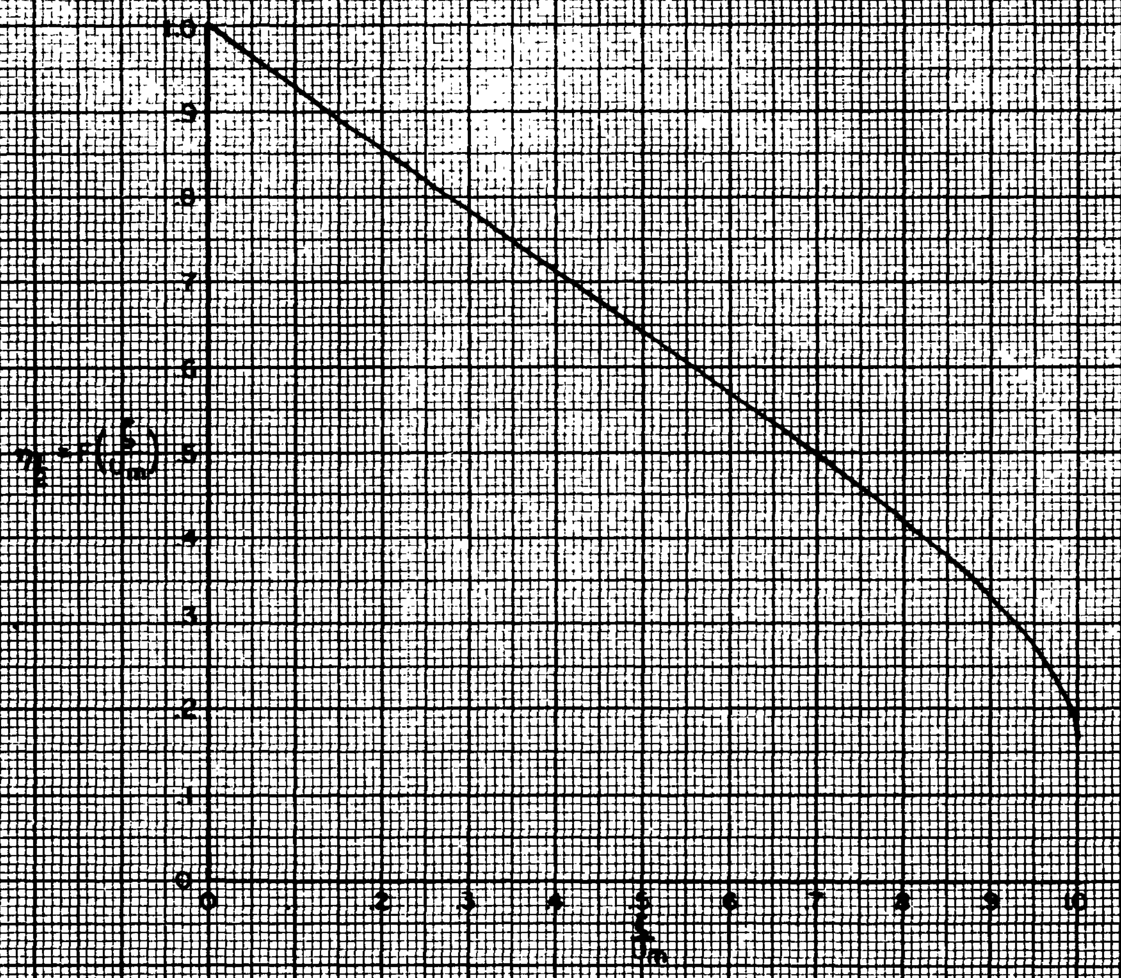

FIGURE 4. SCALE FACTOR

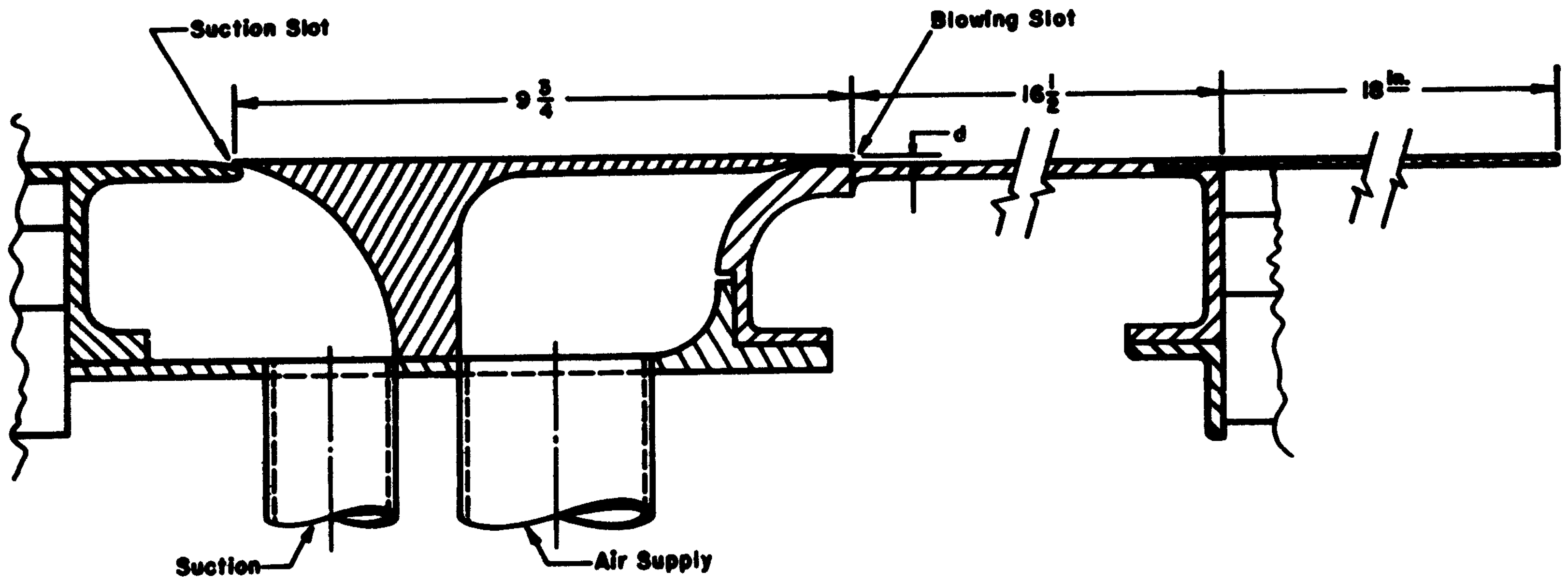
Suction Slot
Blowing Slot
9 3/4
16 1/2
18 in.
d
Suction
Air Supply

FIGURE 5. SECTIONAL VIEW OF WALL JET

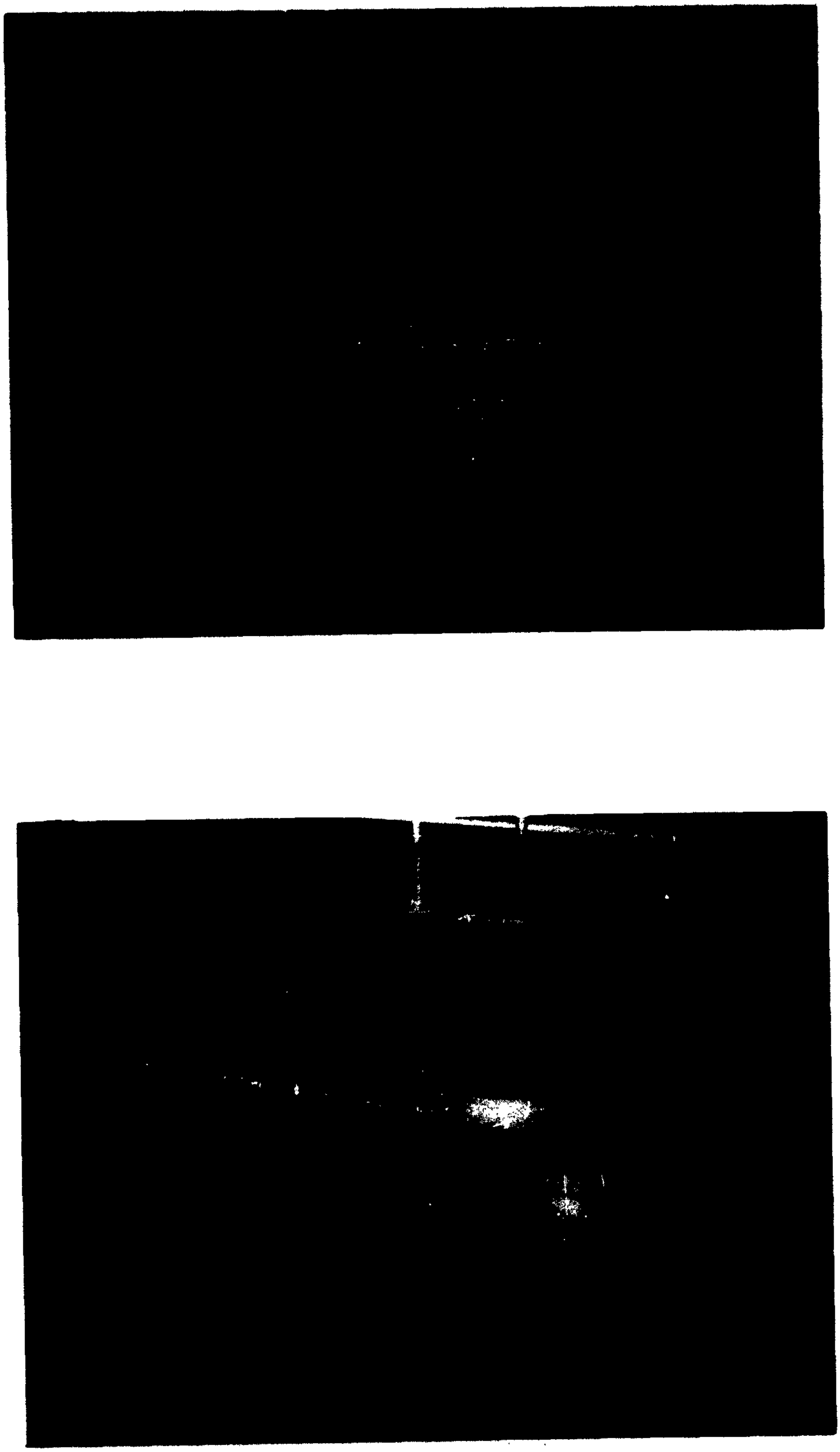

FIGURE 6. TOTAL HEAD PROBE AND CARRIAGE

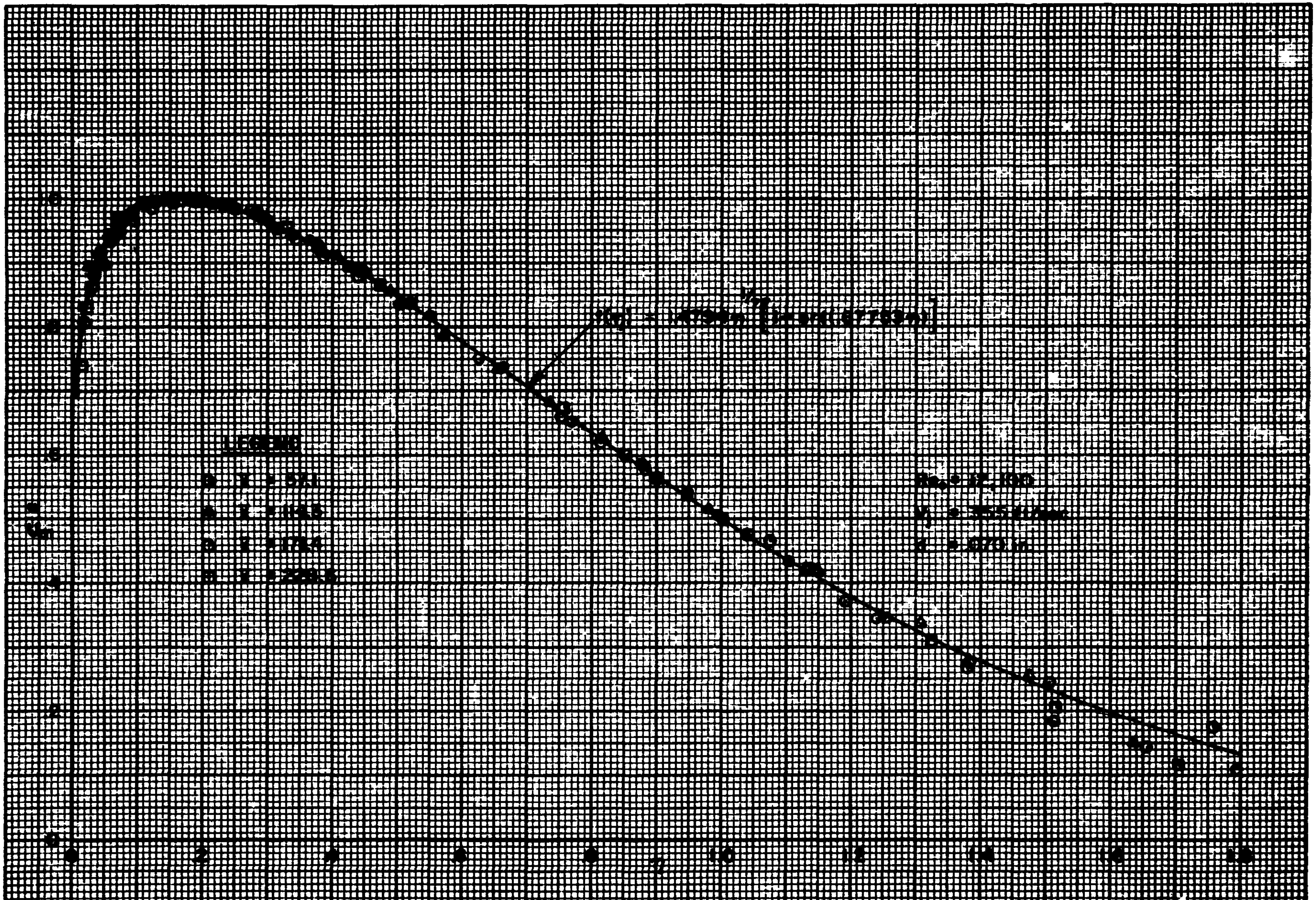

FIGURE 7 COMPARISON WITH EXPERIMENTAL DATA

$\xi = 0$

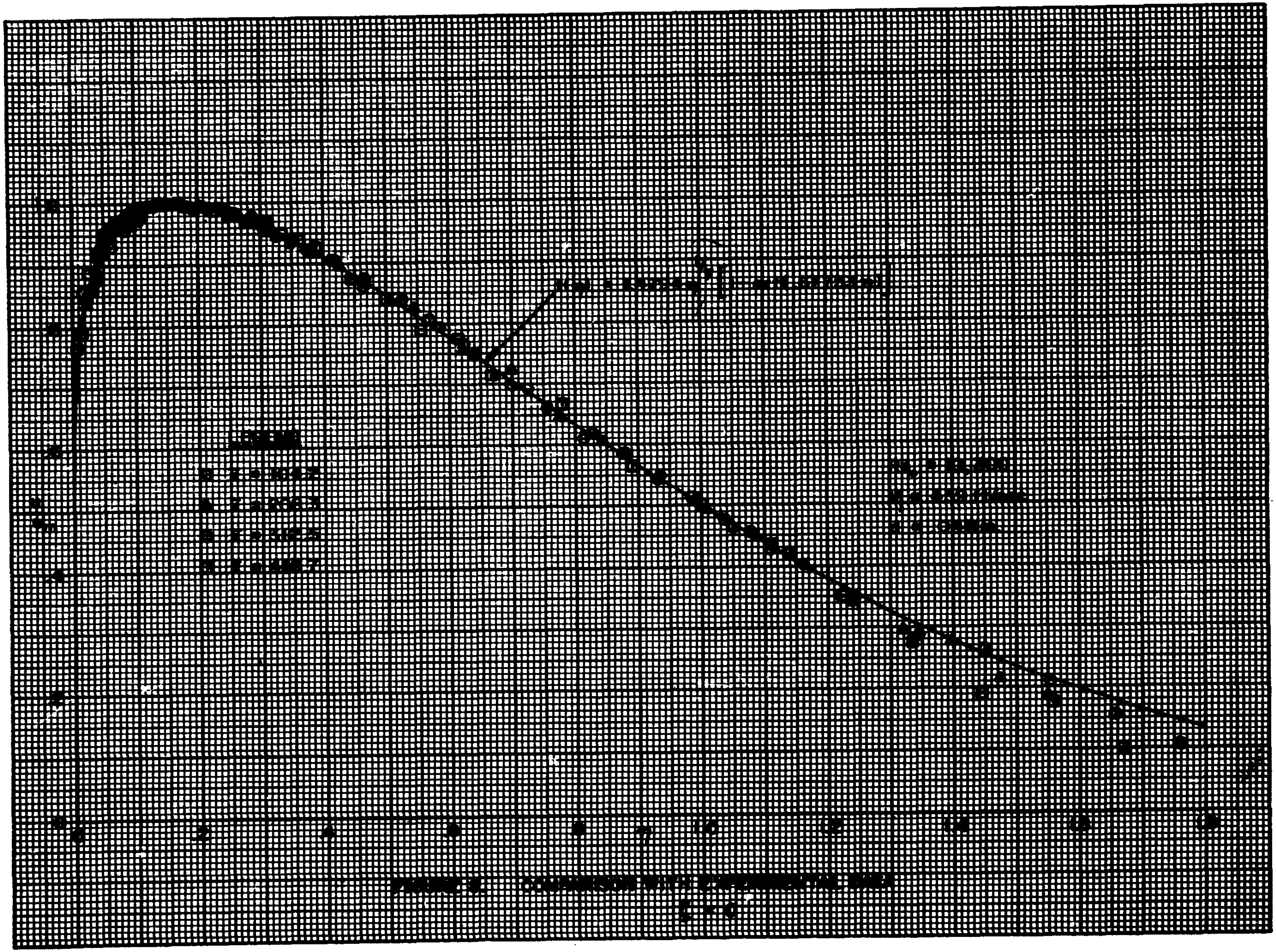

FIGURE 8. COMPARISON WITH EXPERIMENTAL DATA

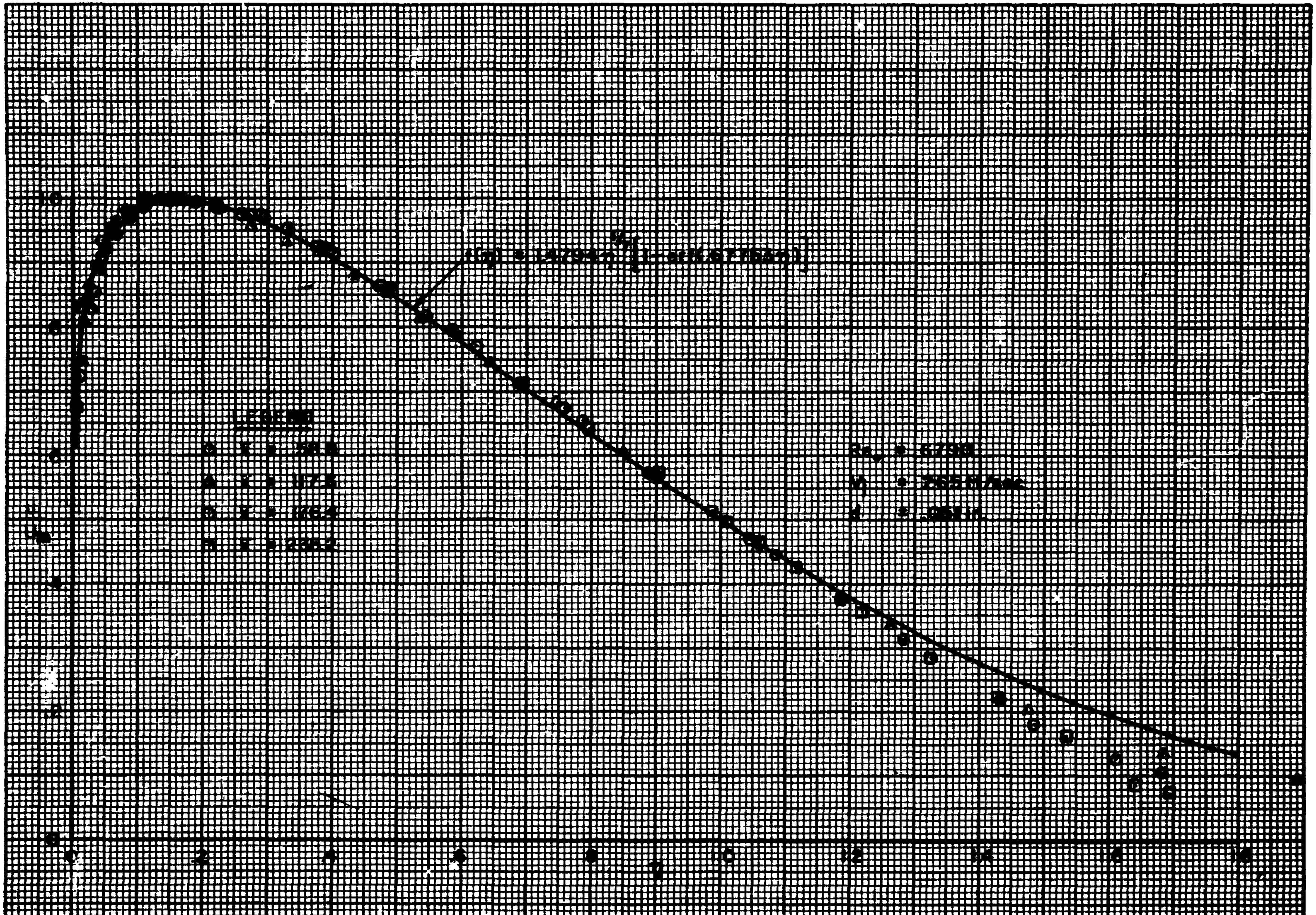

FIGURE 8. COMPARISON WITH GEORGE'S DATA

$\zeta = 0$

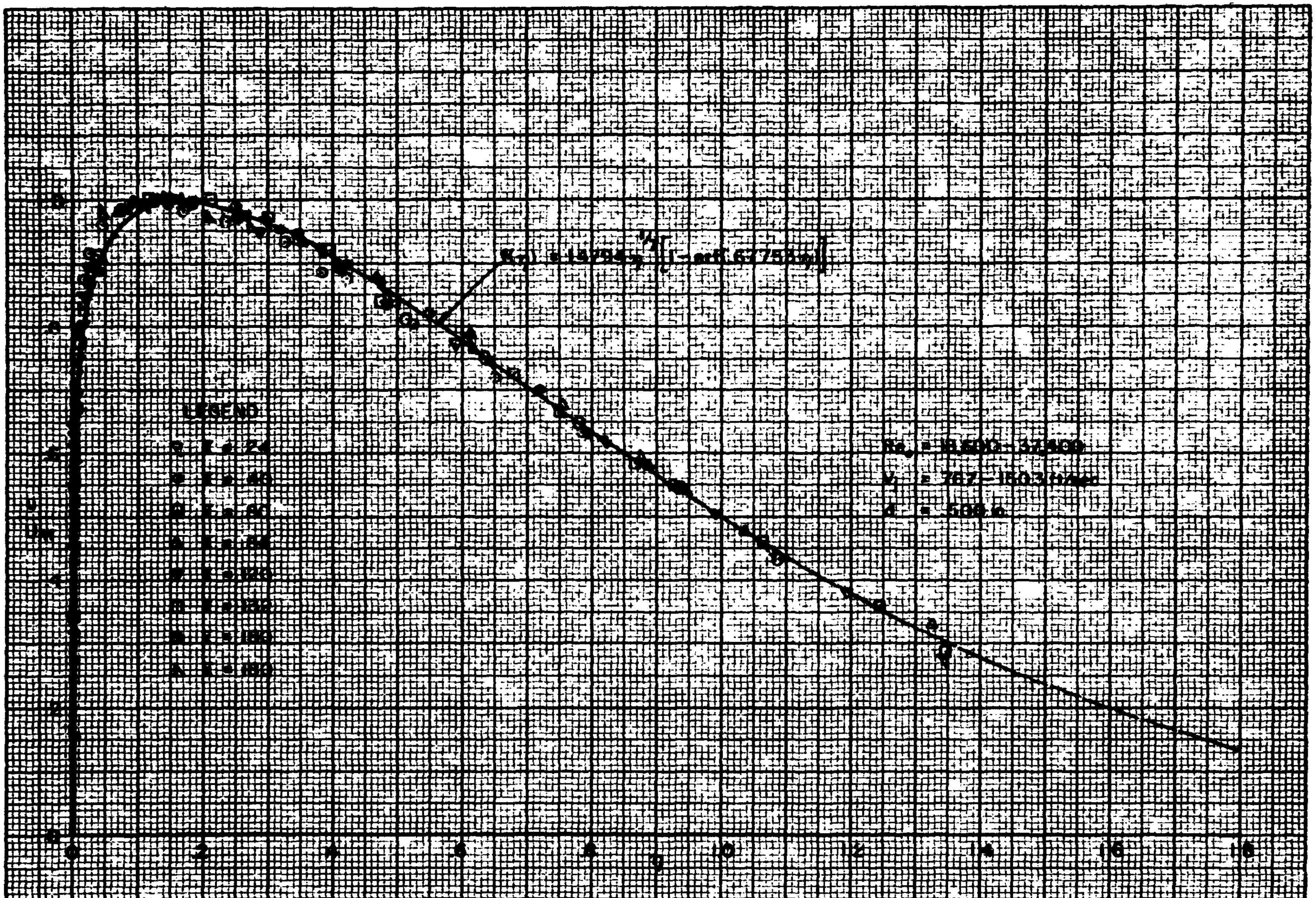

FIGURE 10. COMPARISON WITH DATA OF MYERS, SCHAUER, AND EUSTIS

$\zeta = 0$

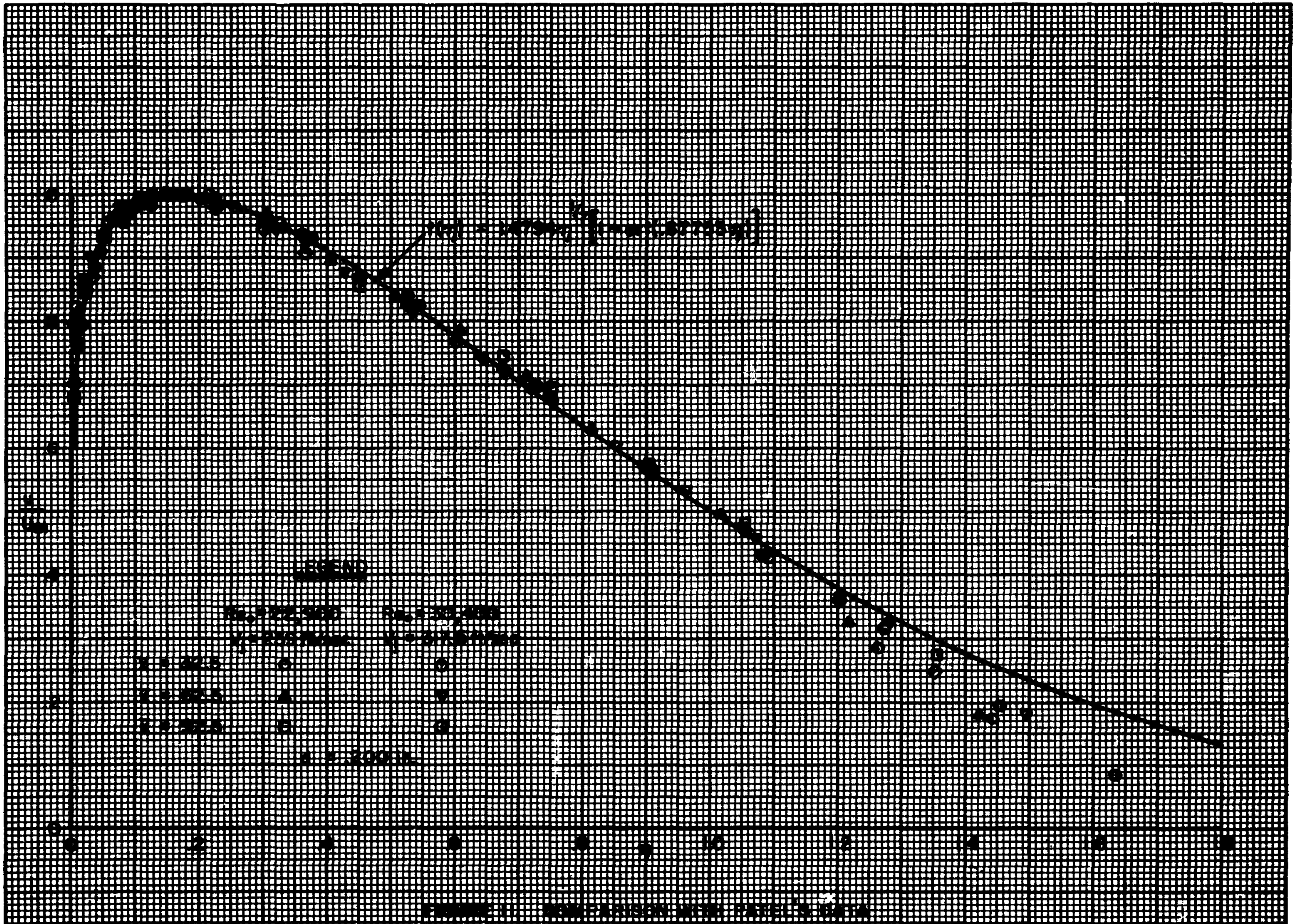

FIGURE 11. COMPARISON WITH PATEL'S DATA

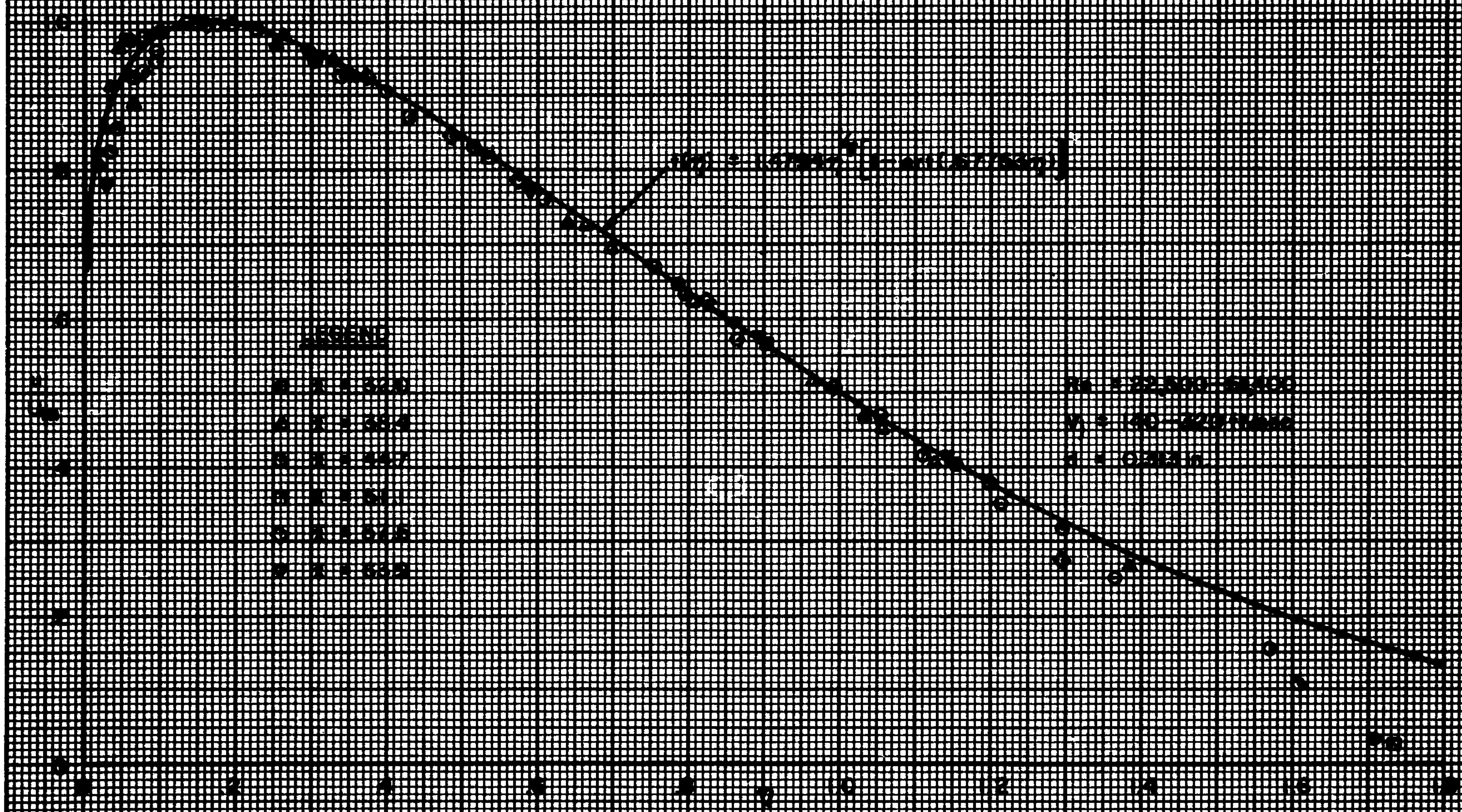

FIGURE 12. COMPARISON WITH SIGALLA'S DATA
ξ > 0

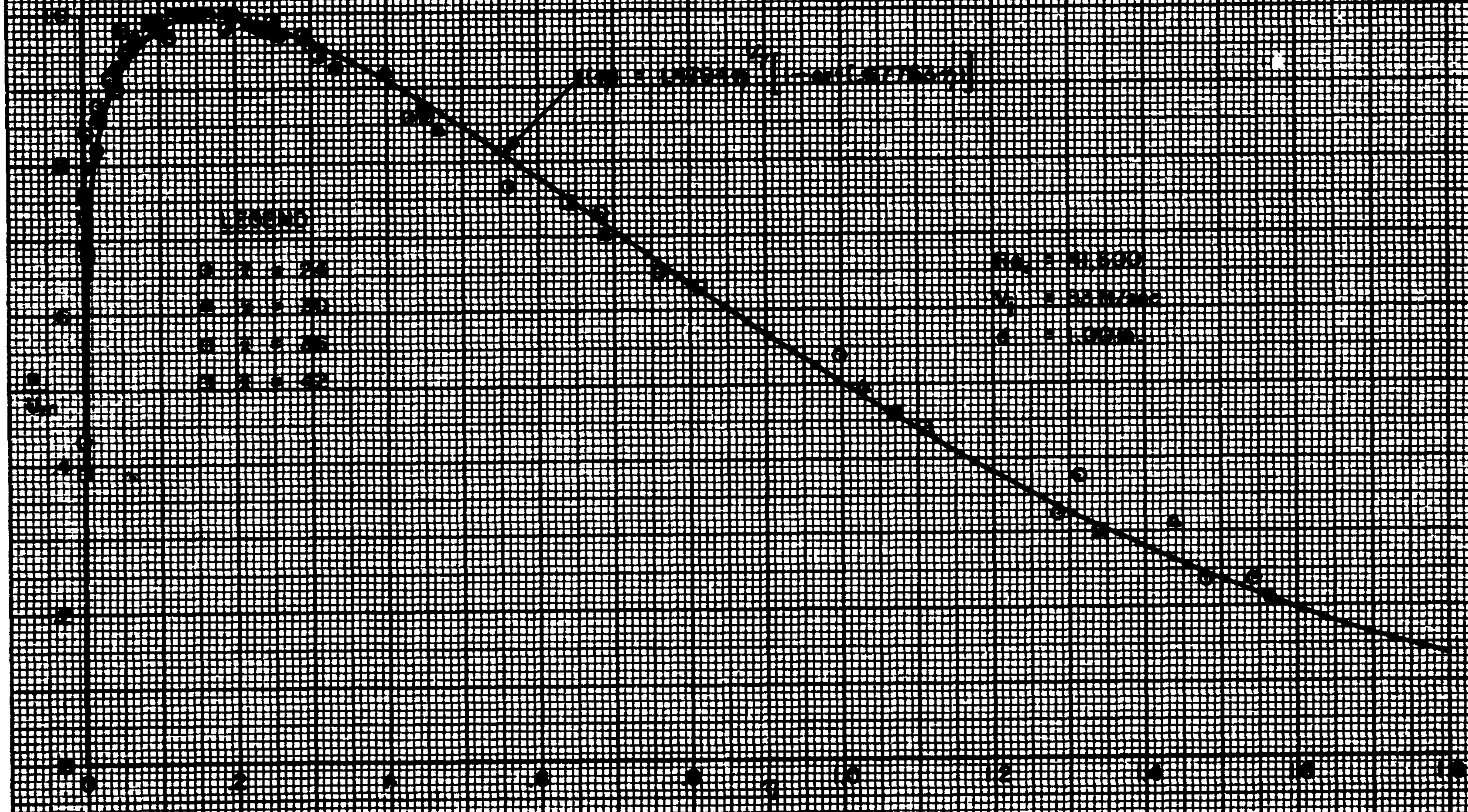

FIGURE 8. COMPARISON WITH SCHWARZ AND COSART'S DATA

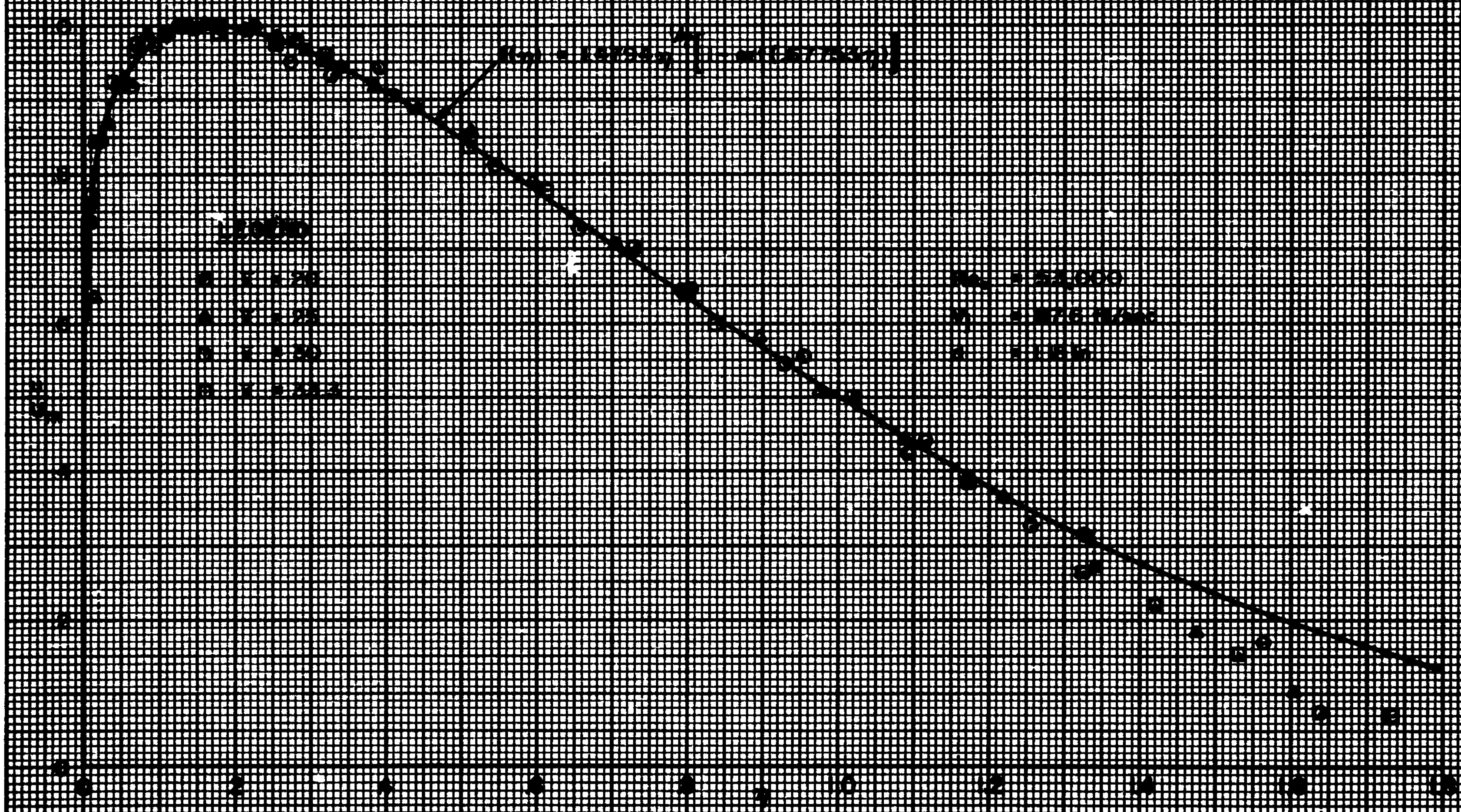

FIGURE 14. COMPARISON WITH FÖRTHMANN'S DATA
$\zeta = 0$

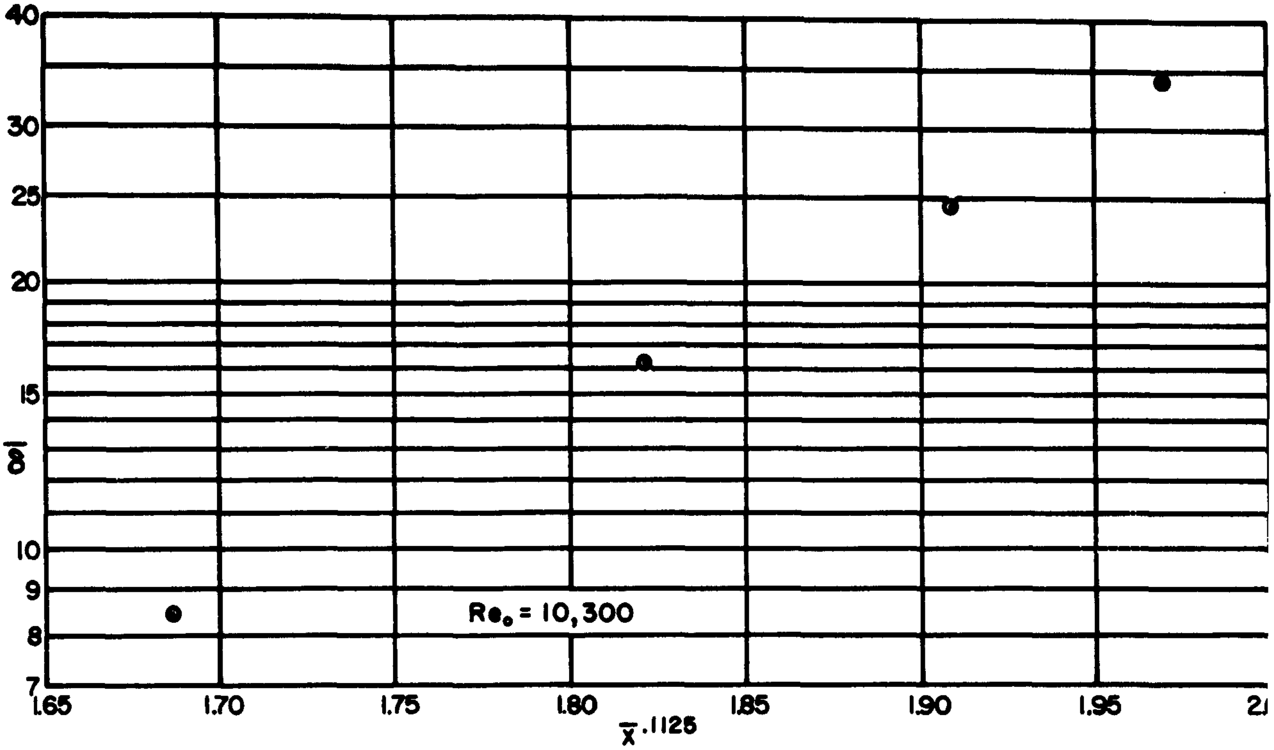

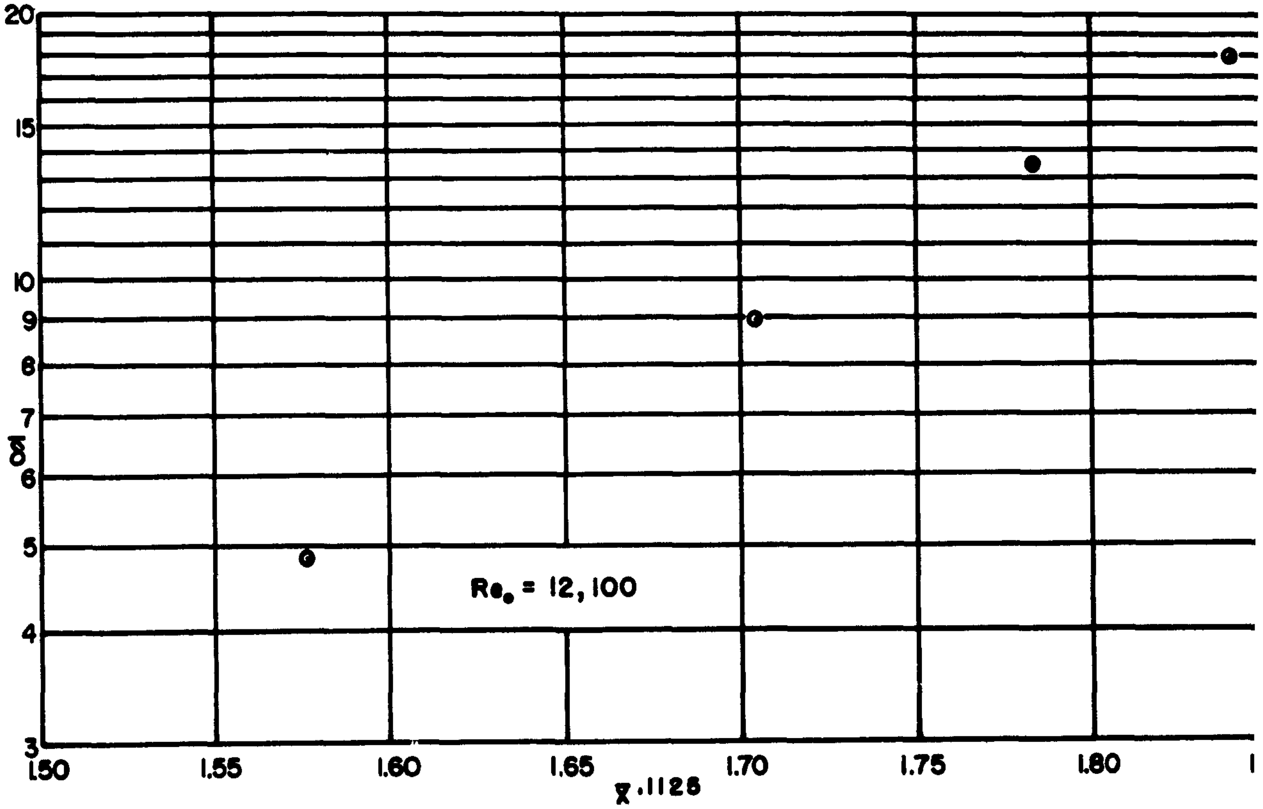

FIGURE 15. EXPERIMENTAL JET THICKNESS DATA
$\zeta = 0$

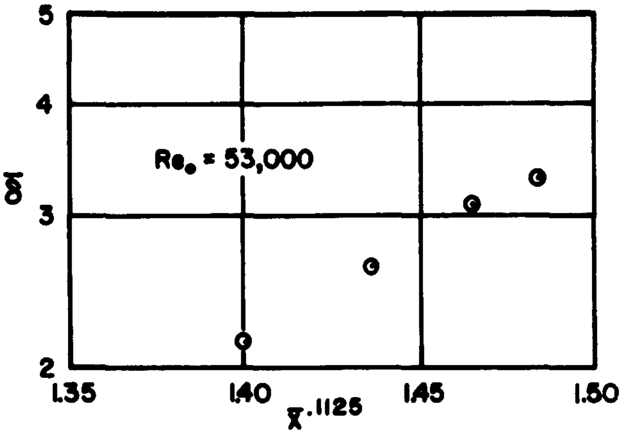

DATA OF FÖRTHMANN
$\zeta = 0$

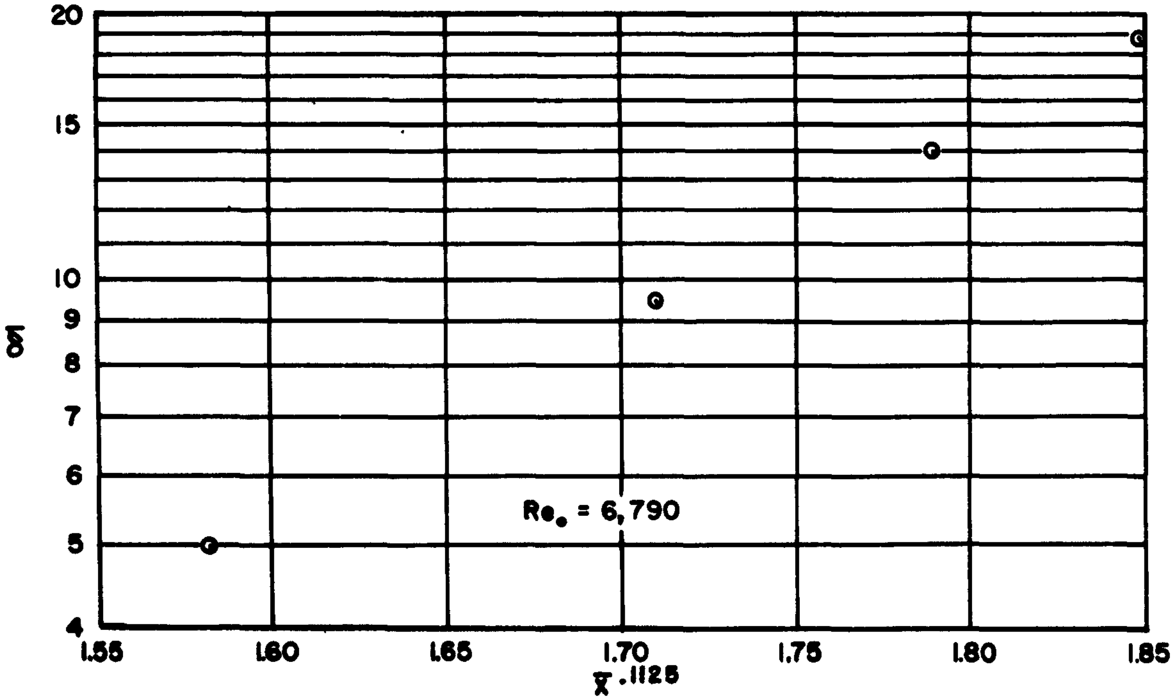

DATA OF GEORGE $\zeta = 0$

FIGURE 16

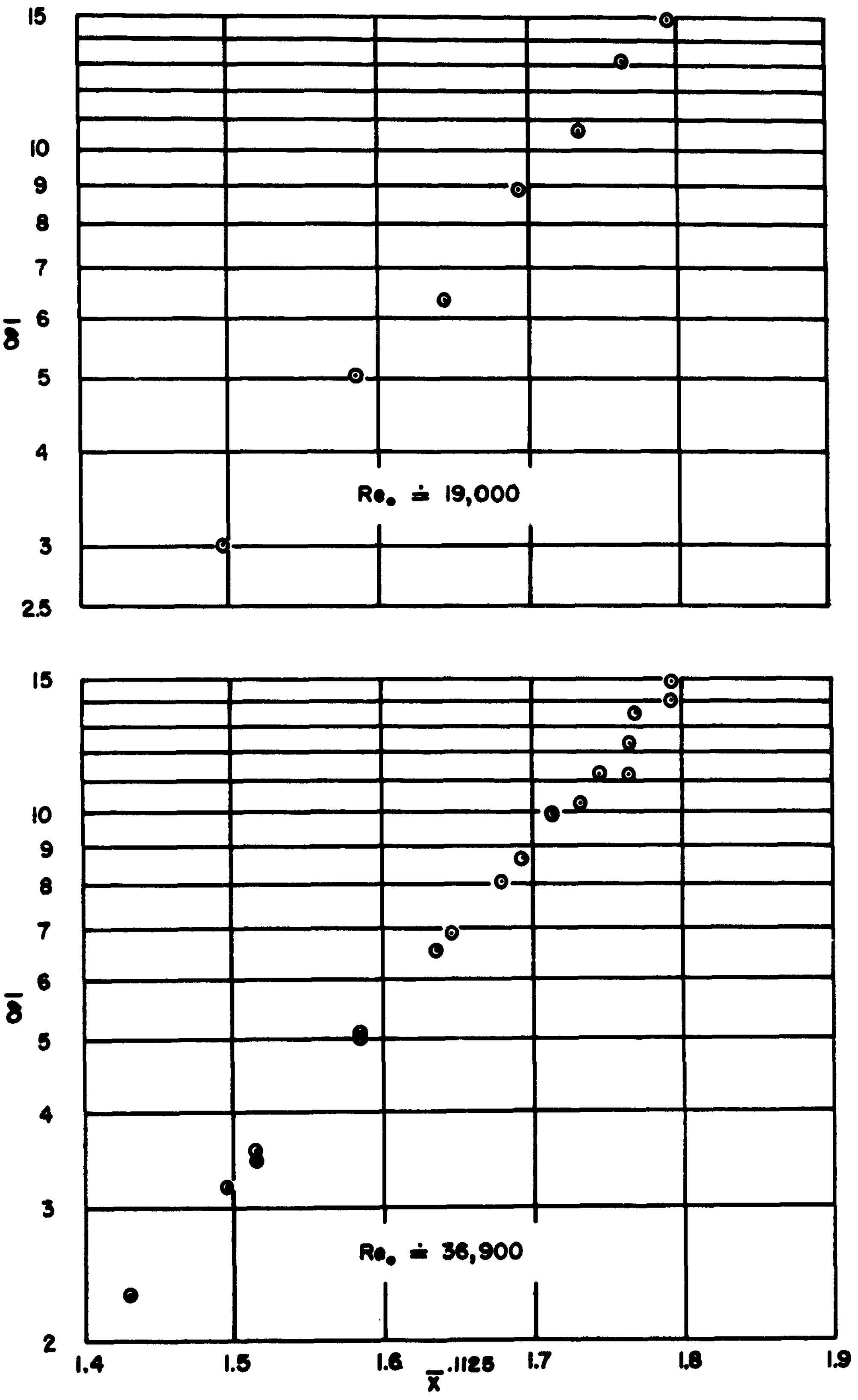

FIGURE 17. DATA OF MYERS, SCHAUER, AND EUSTIS

$\zeta = 0$

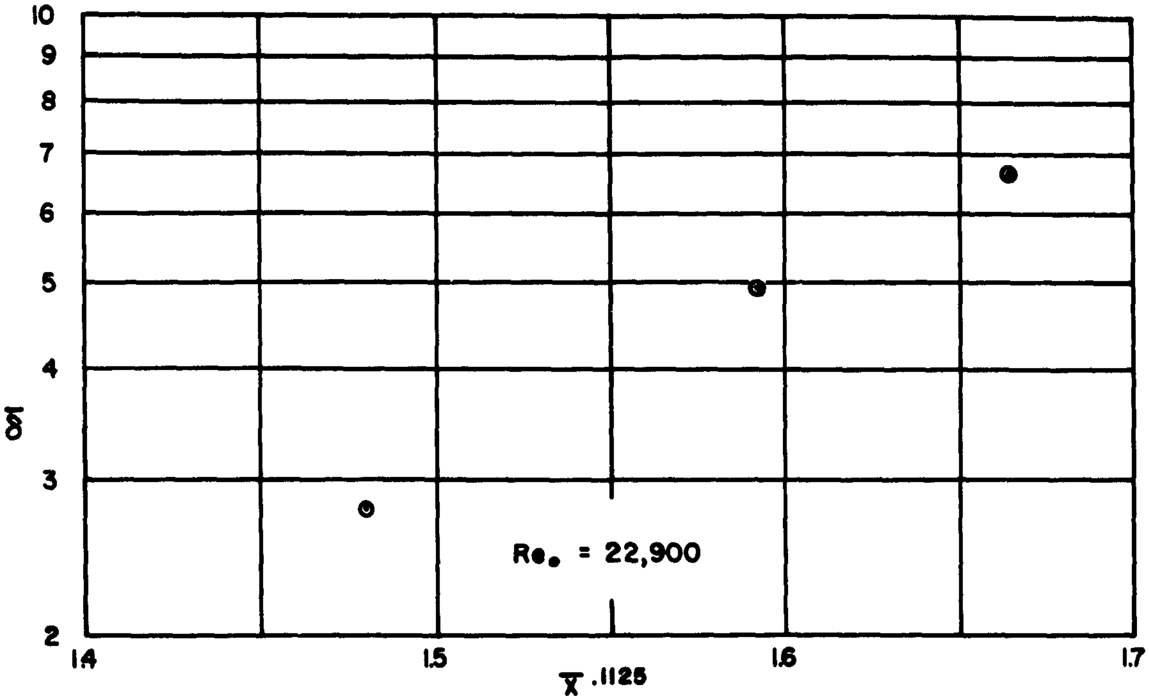

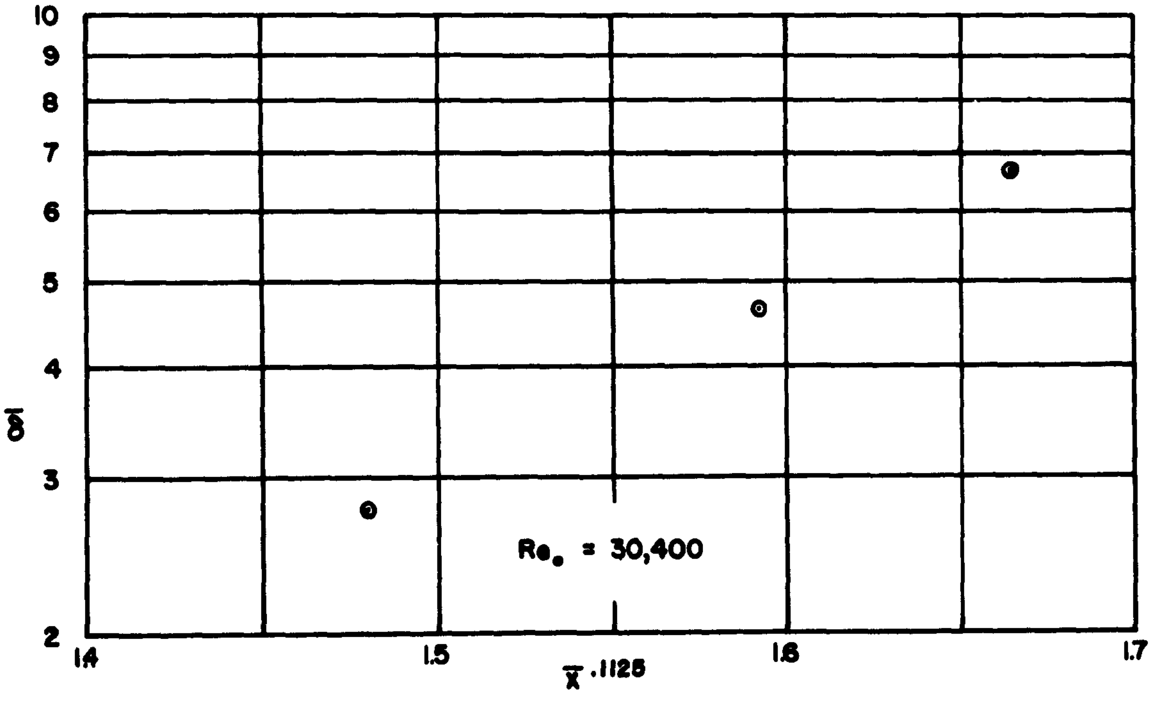

FIGURE 18. DATA OF PATEL

$\zeta = 0$

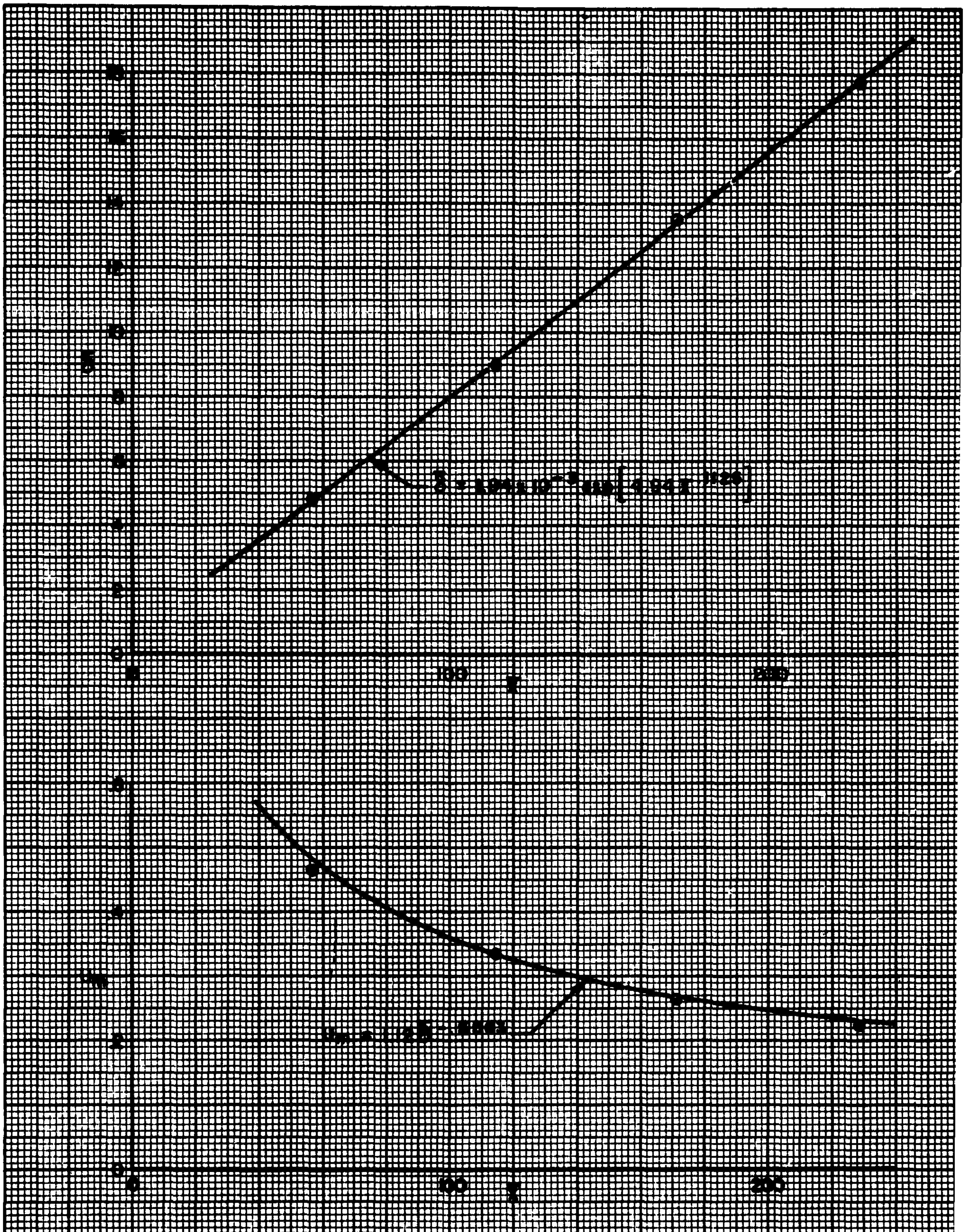

FIGURE 19. VARIATION OF VELOCITY AND LENGTH SCALES
Re_o = 12,100 ξ = 0

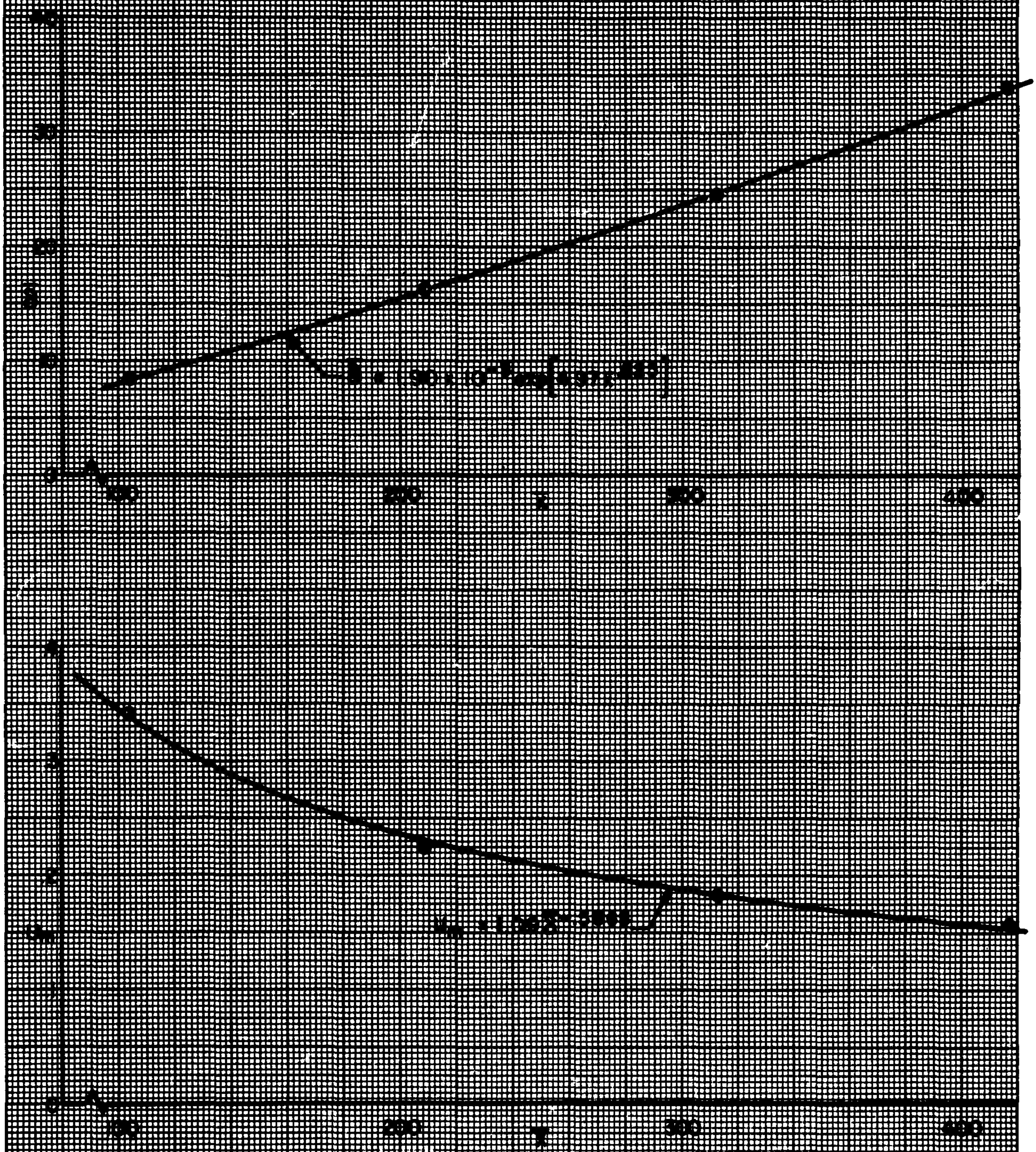

FIGURE 20.   VARIATION OF VELOCITY AND LENGTH SCALES

$Re_o = 10,300$ $\zeta = 0$

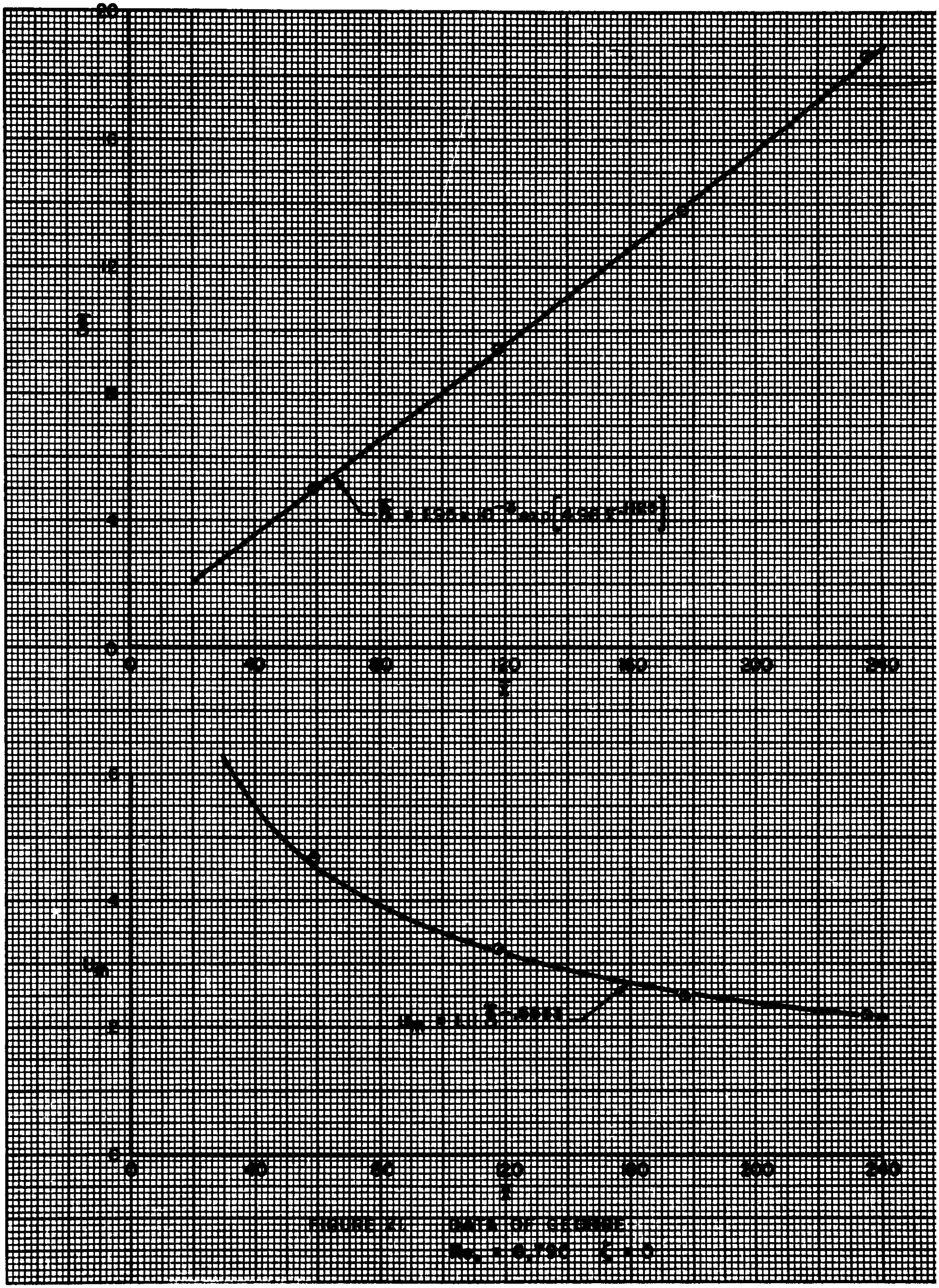

FIGURE 27. DATA OF GEORGE

$Re_1 = 6,750 \quad \zeta = 0$

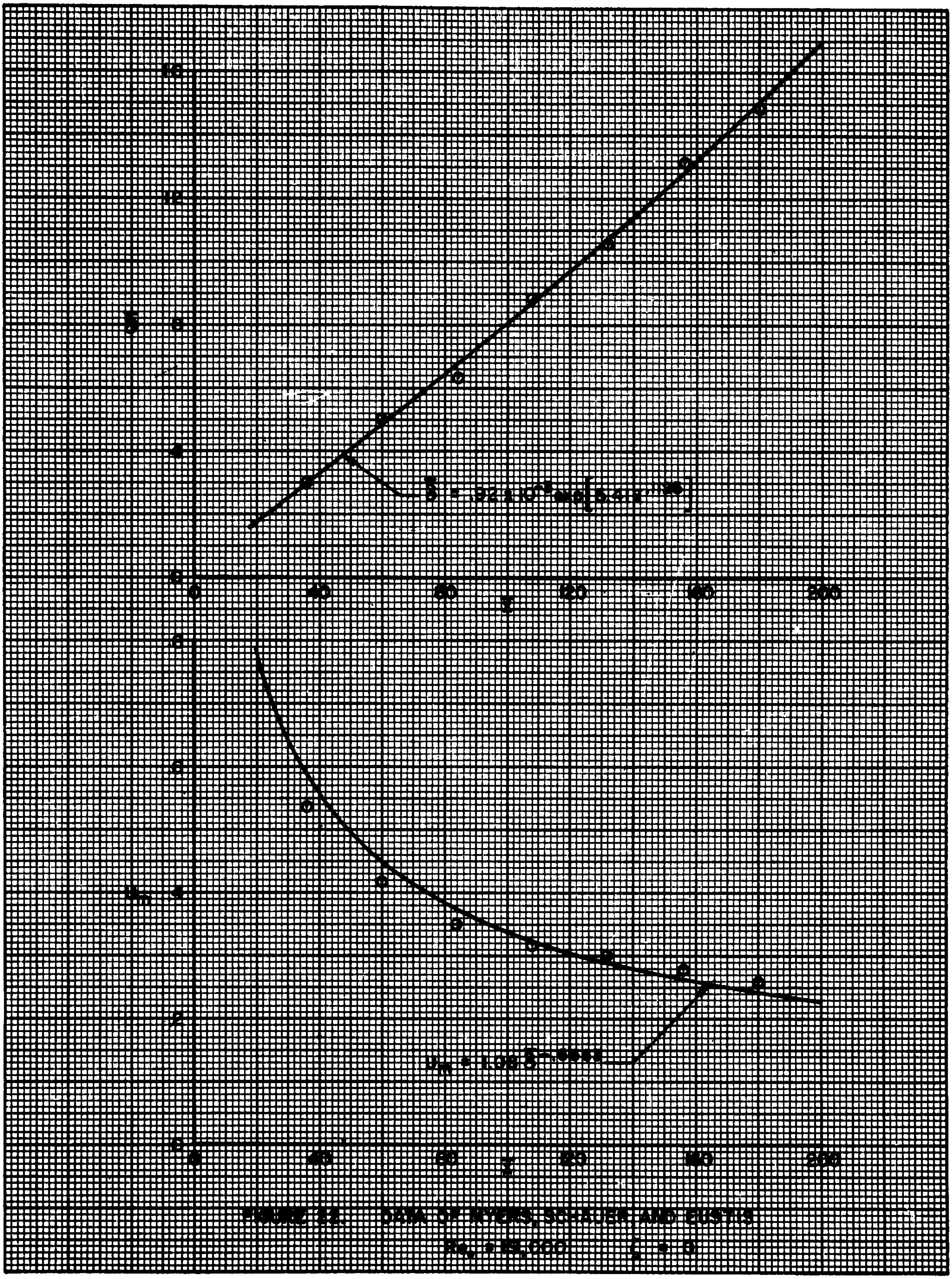

FIGURE 22. DATA OF MYERS, SCHAUER, AND EUSTIS

$Re_0 = 15,000 \qquad \zeta = 0$

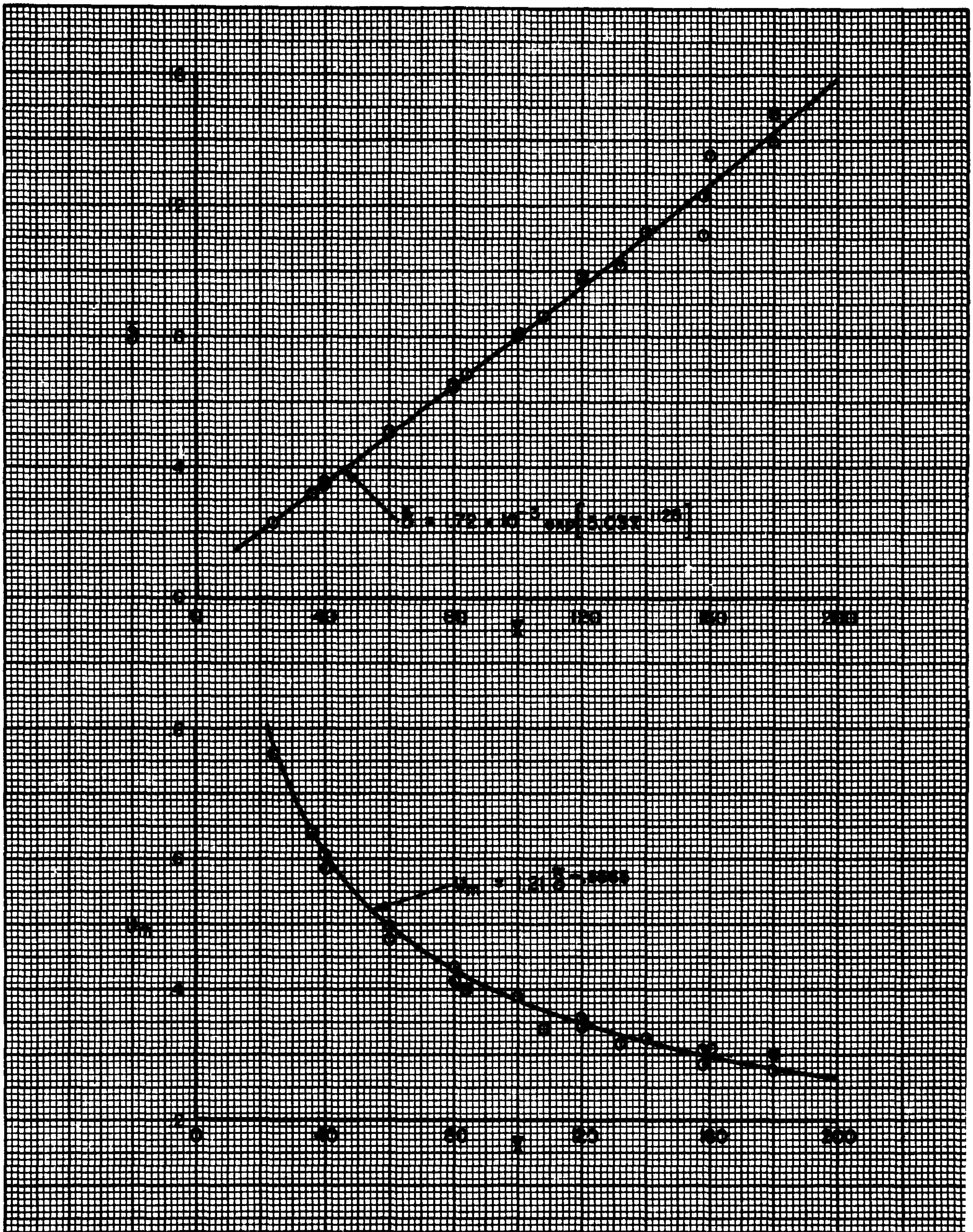

FIGURE E3. DATA OF MYERS, SCHAUER, AND EUSTIS

Re_o = 56,900 ξ = 6

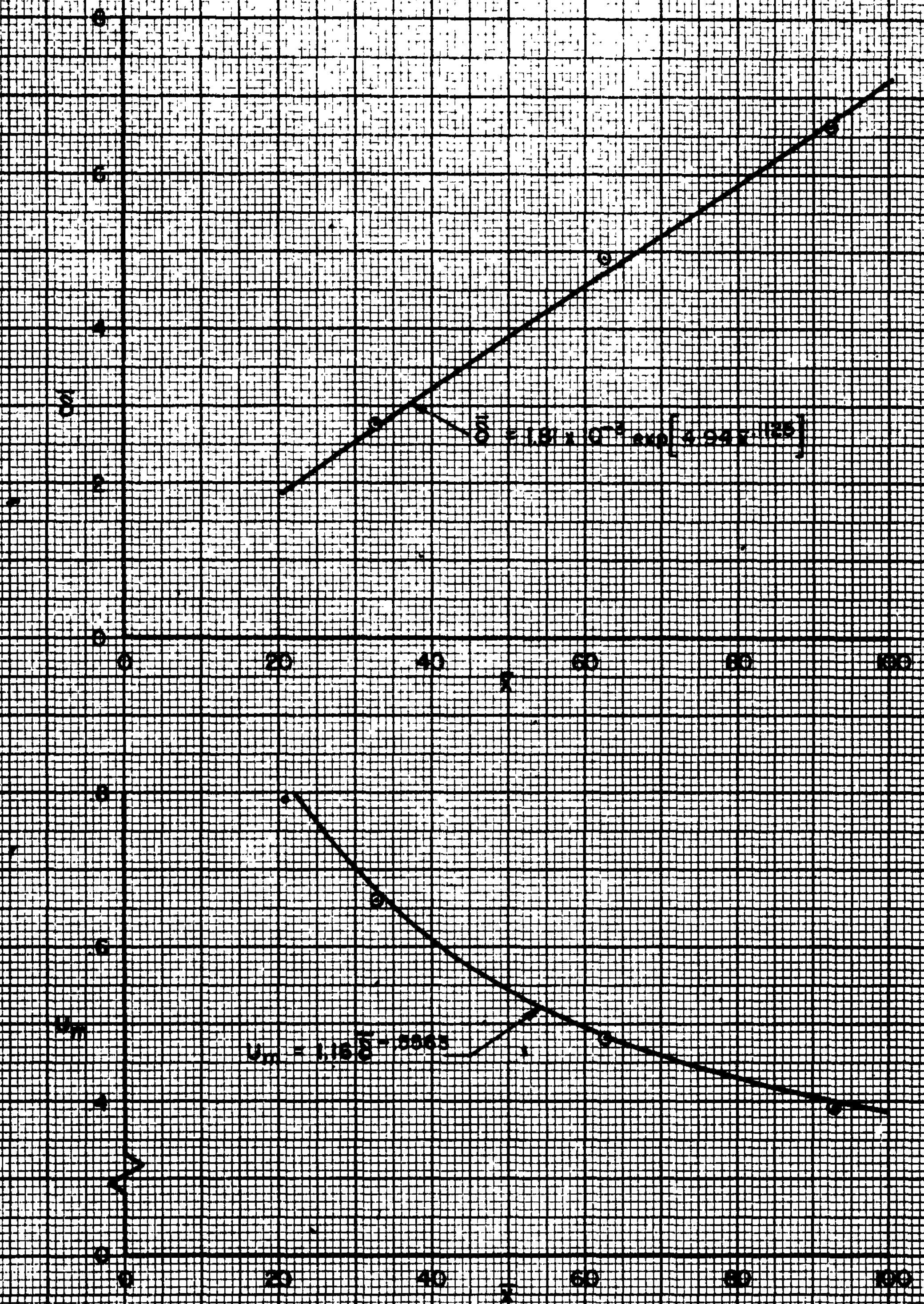

FIGURE 24 DATA OF PATEL

$Re_\theta = 22{,}900 \quad \xi = 0$

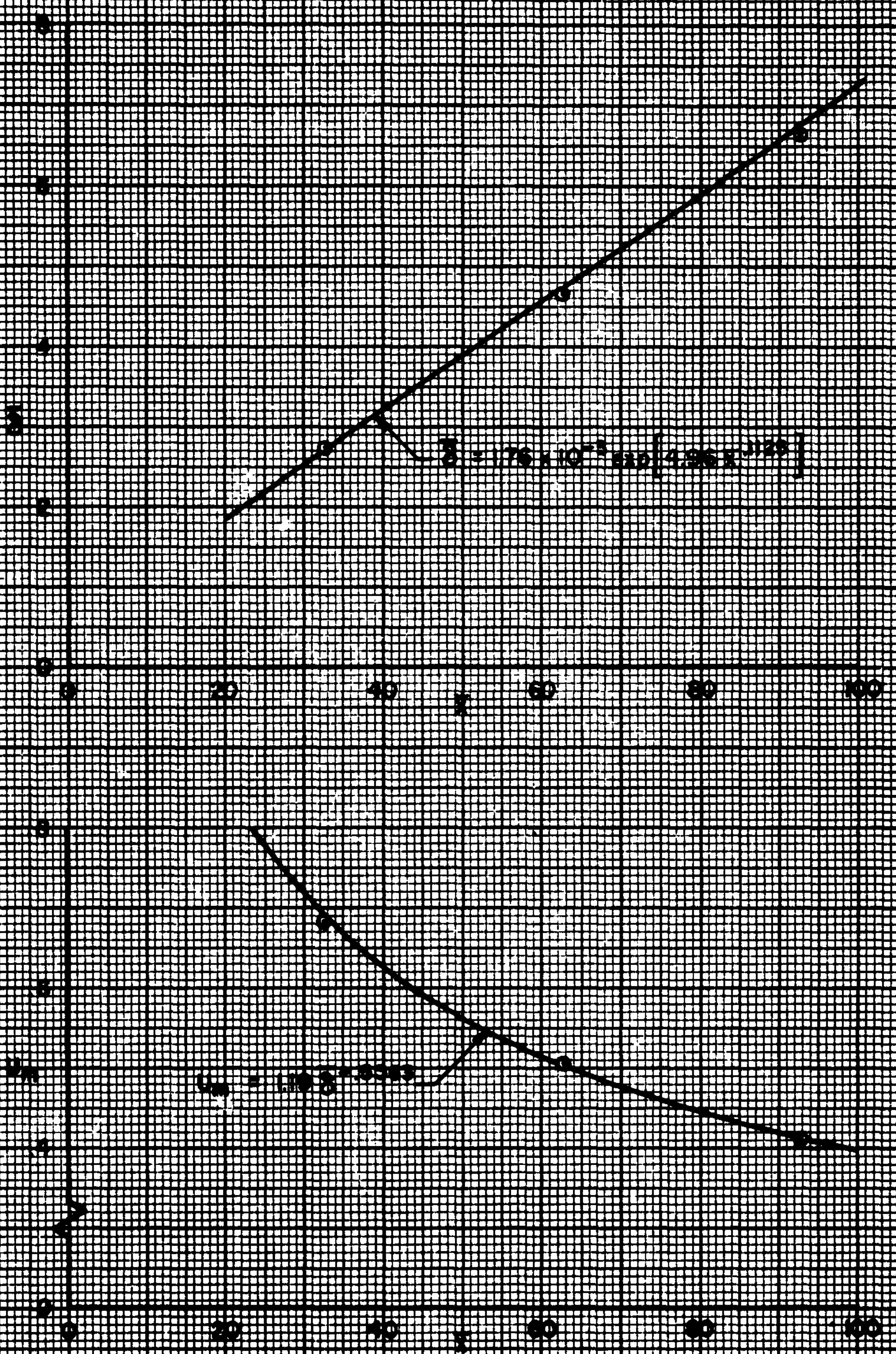

FIGURE 25. DATA OF PATEL

$Re_x = 30{,}400 \quad \frac{\xi}{\delta} = 0$

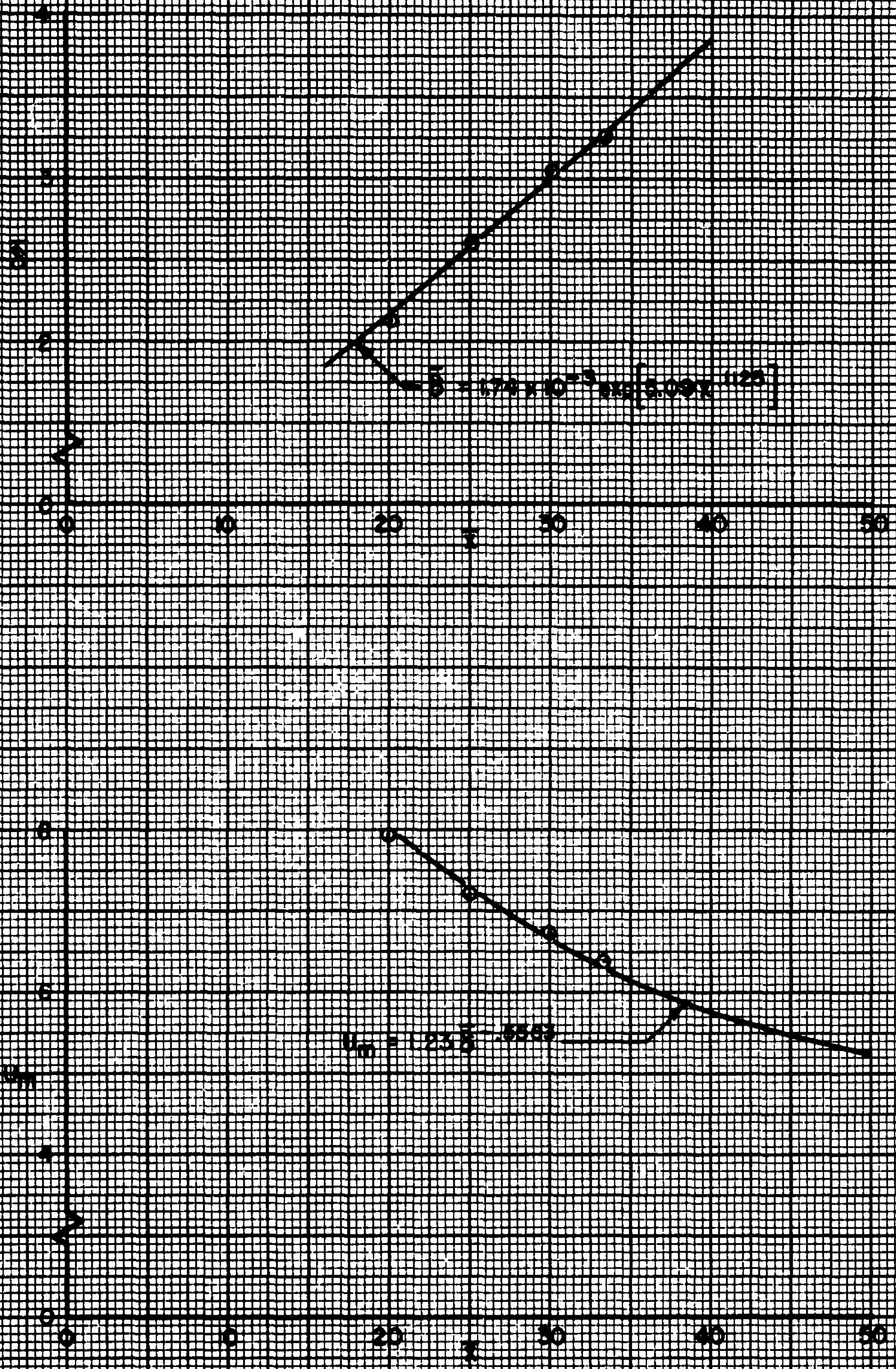

FIGURE 26. DATA OF FÖRTHMANN

$Re_o = 53{,}000$ $\zeta = 0$

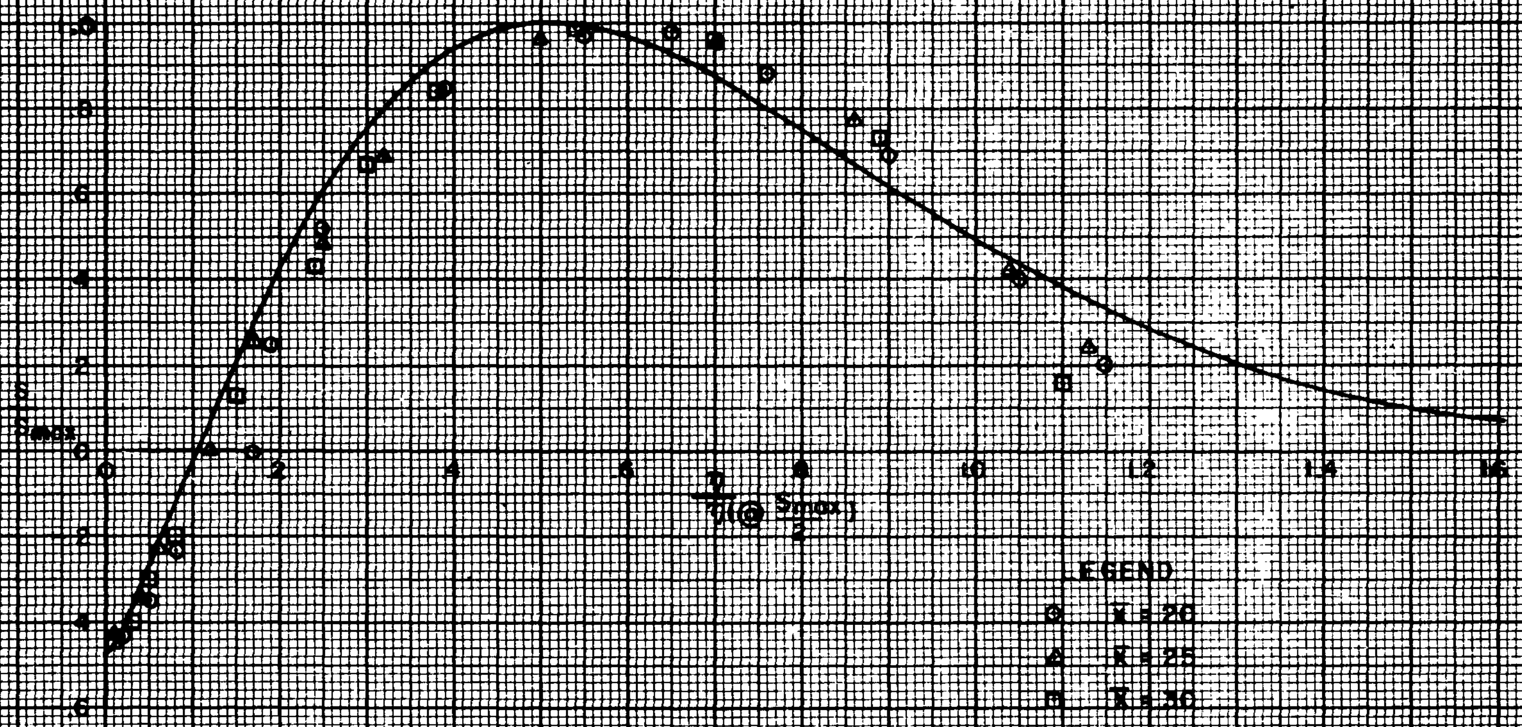

FIGURE 27. COMPARISON WITH FÖRTHMANN'S SHEAR STRESS CALCULATIONS

$\zeta = 0$

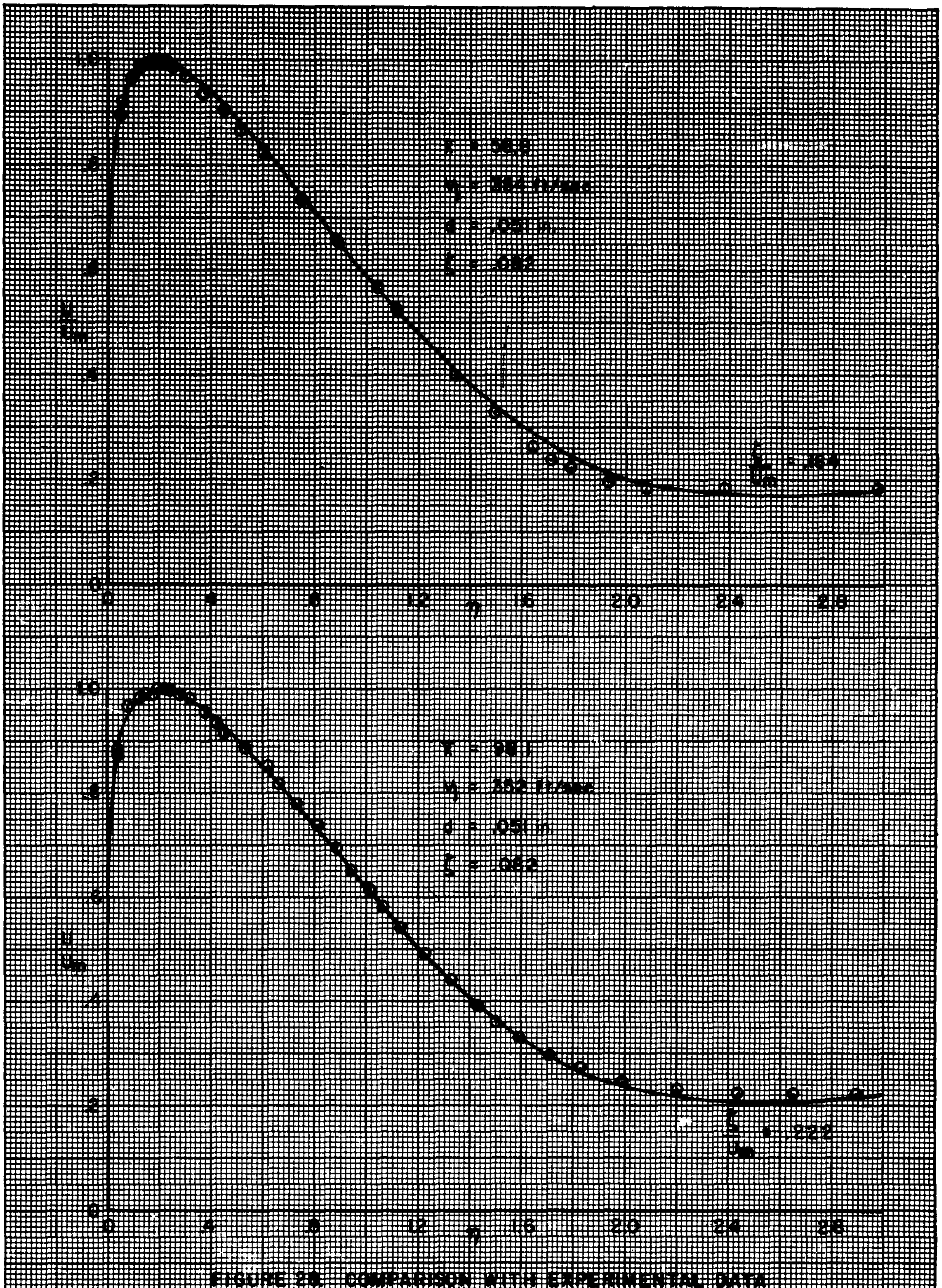

FIGURE 28. COMPARISON WITH EXPERIMENTAL DATA
Re_d = 8900

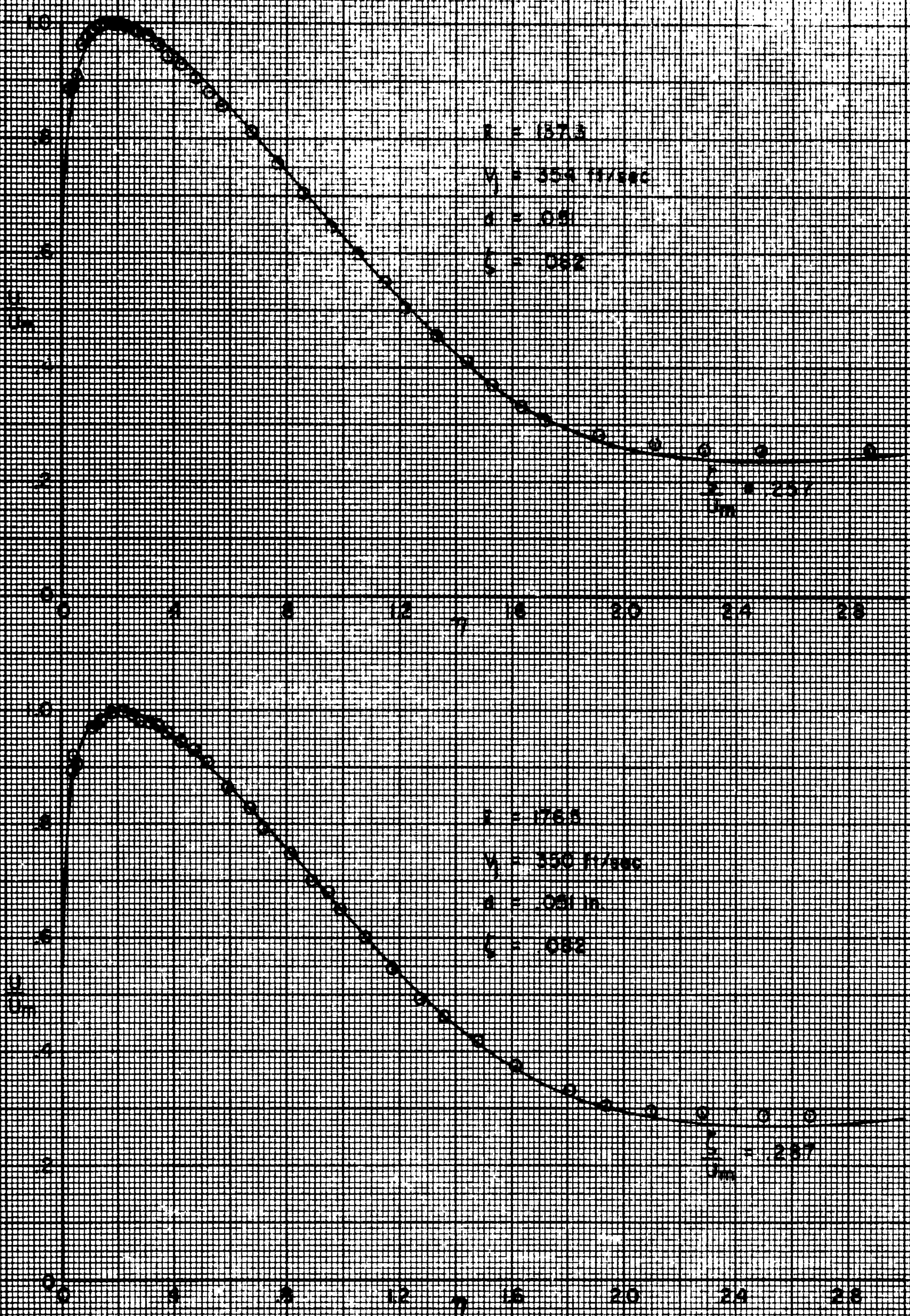

FIGURE 29. COMPARISON WITH EXPERIMENTAL DATA

$Re_o = 8900$

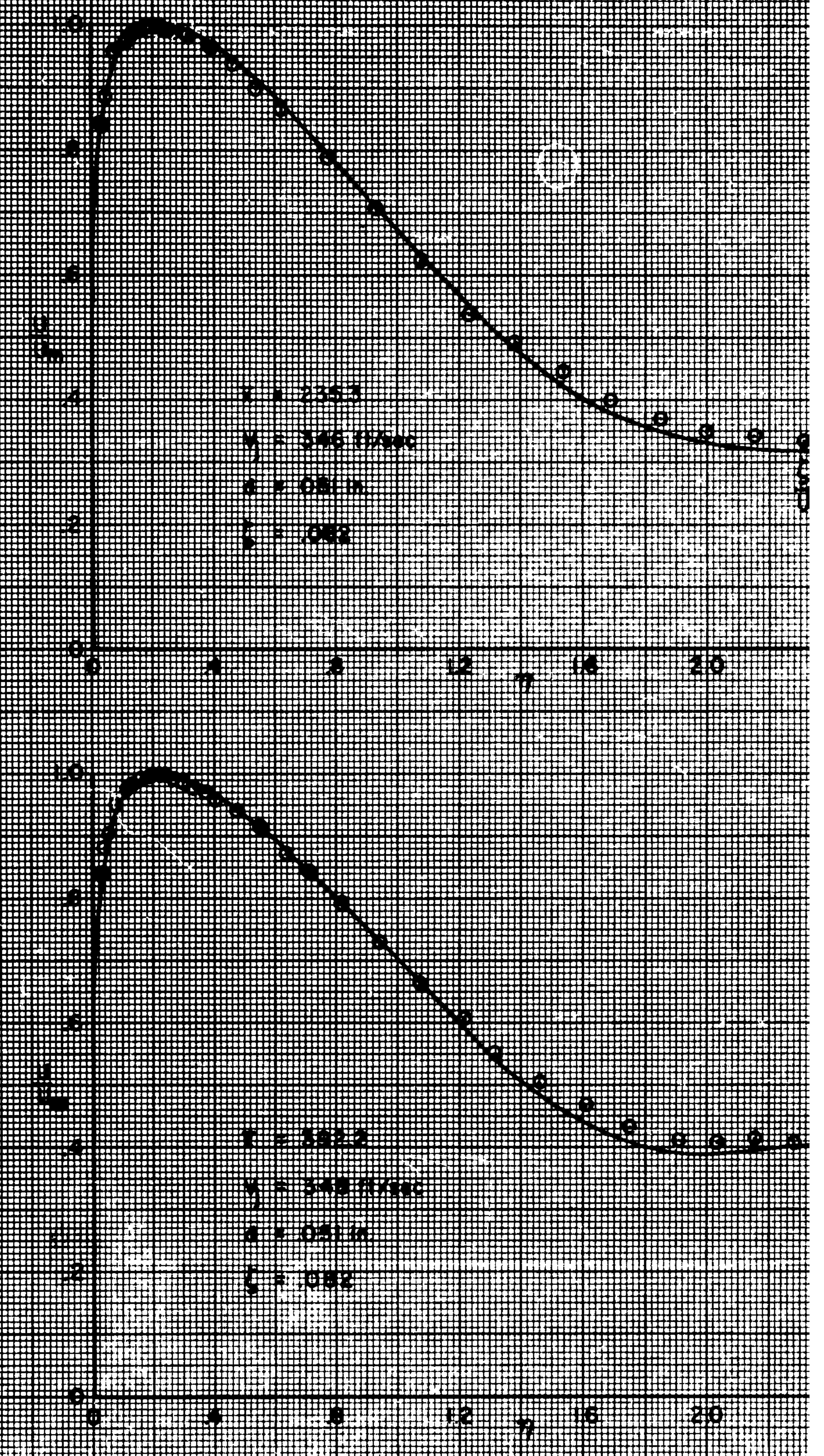

FIGURE 50. COMPARISON WITH EXPERIMENTAL D

Re_o = 8900

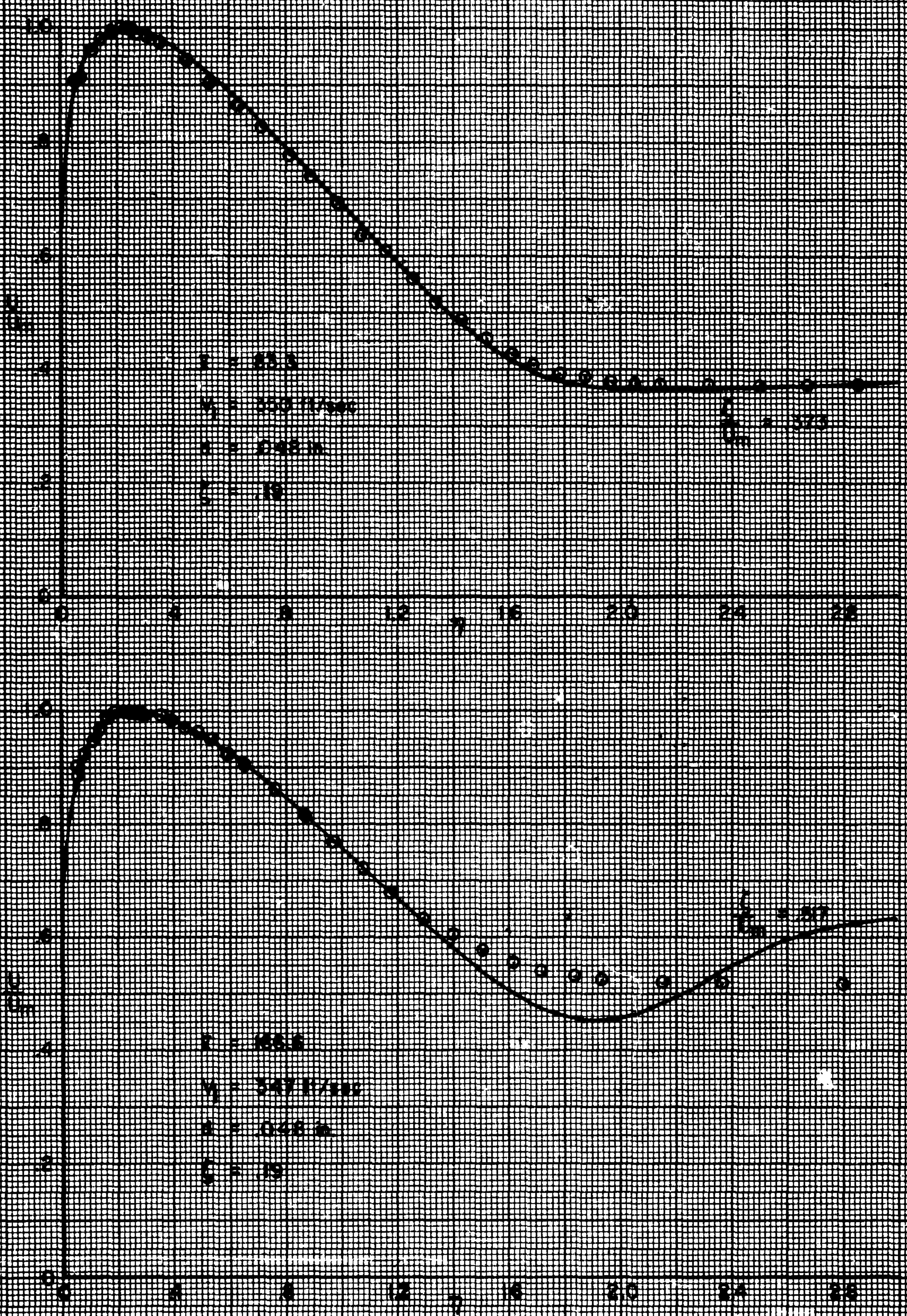

FIGURE 31. COMPARISON WITH EXPERIMENTAL DATA

$Re_s = 8400$

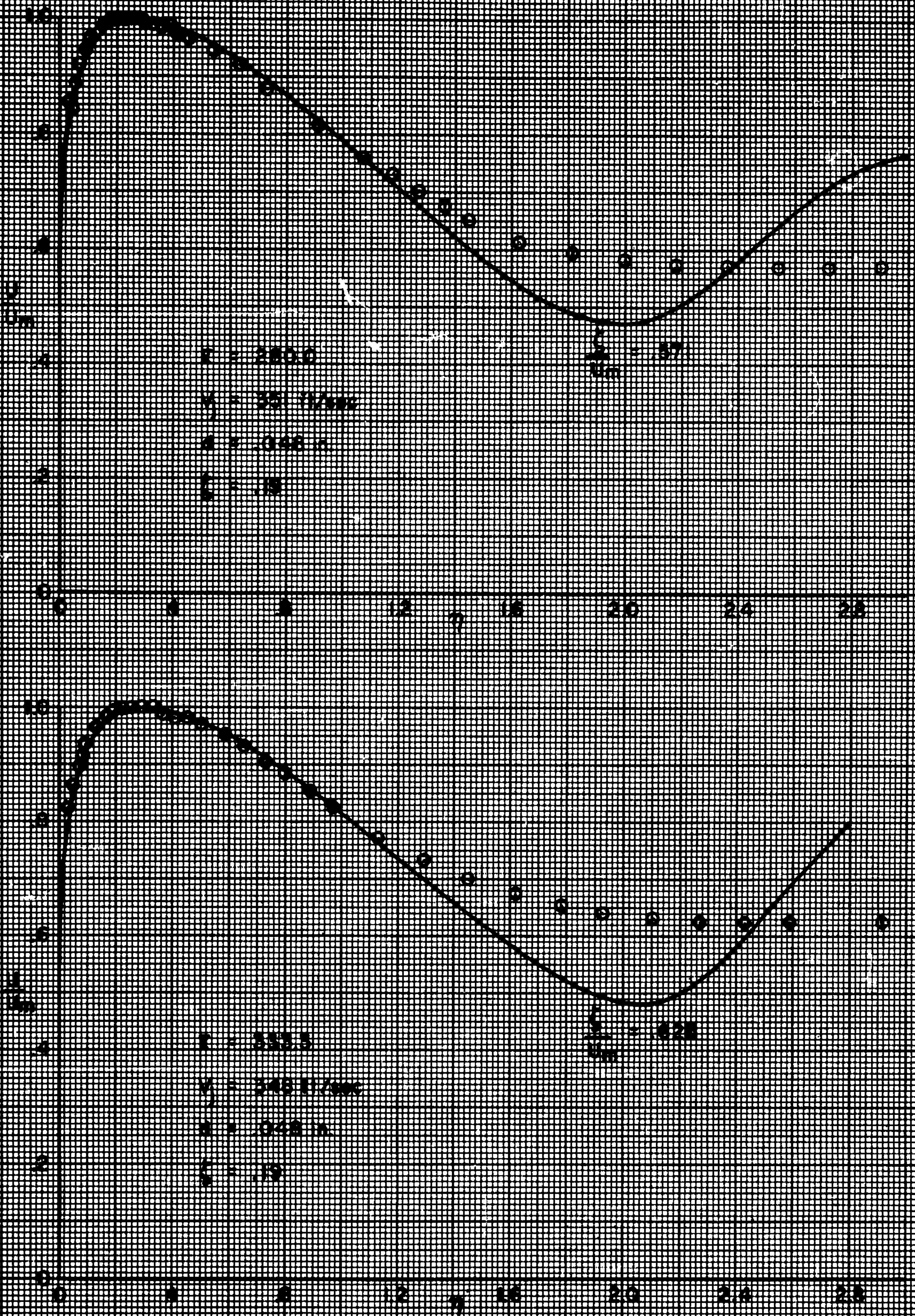

FIGURE 32. COMPARISON WITH EXPERIMENTAL DATA

Re_d = 2400

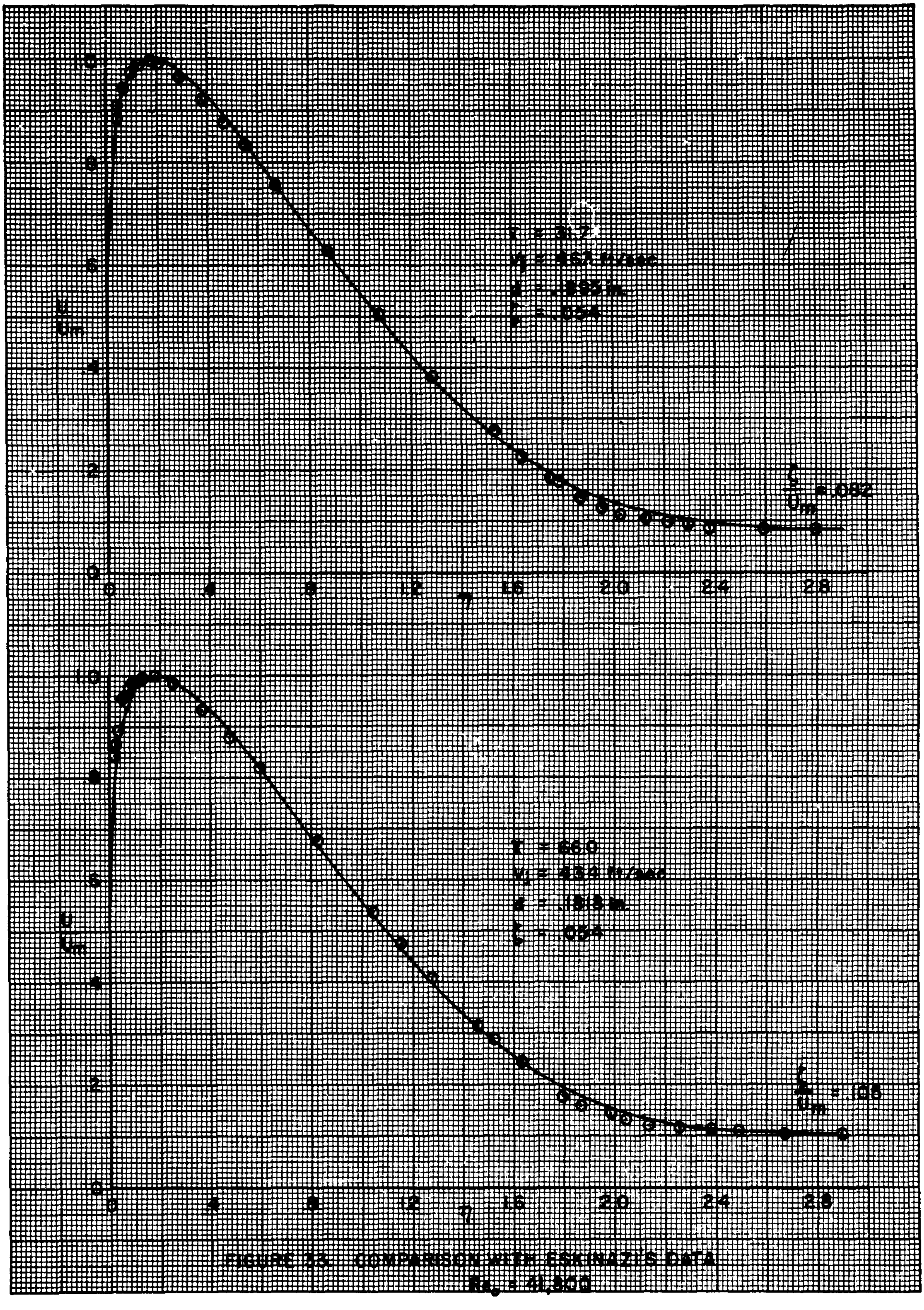

FIGURE 33. COMPARISON WITH ESKINAZI'S DATA
R_{e_o} = 41,800

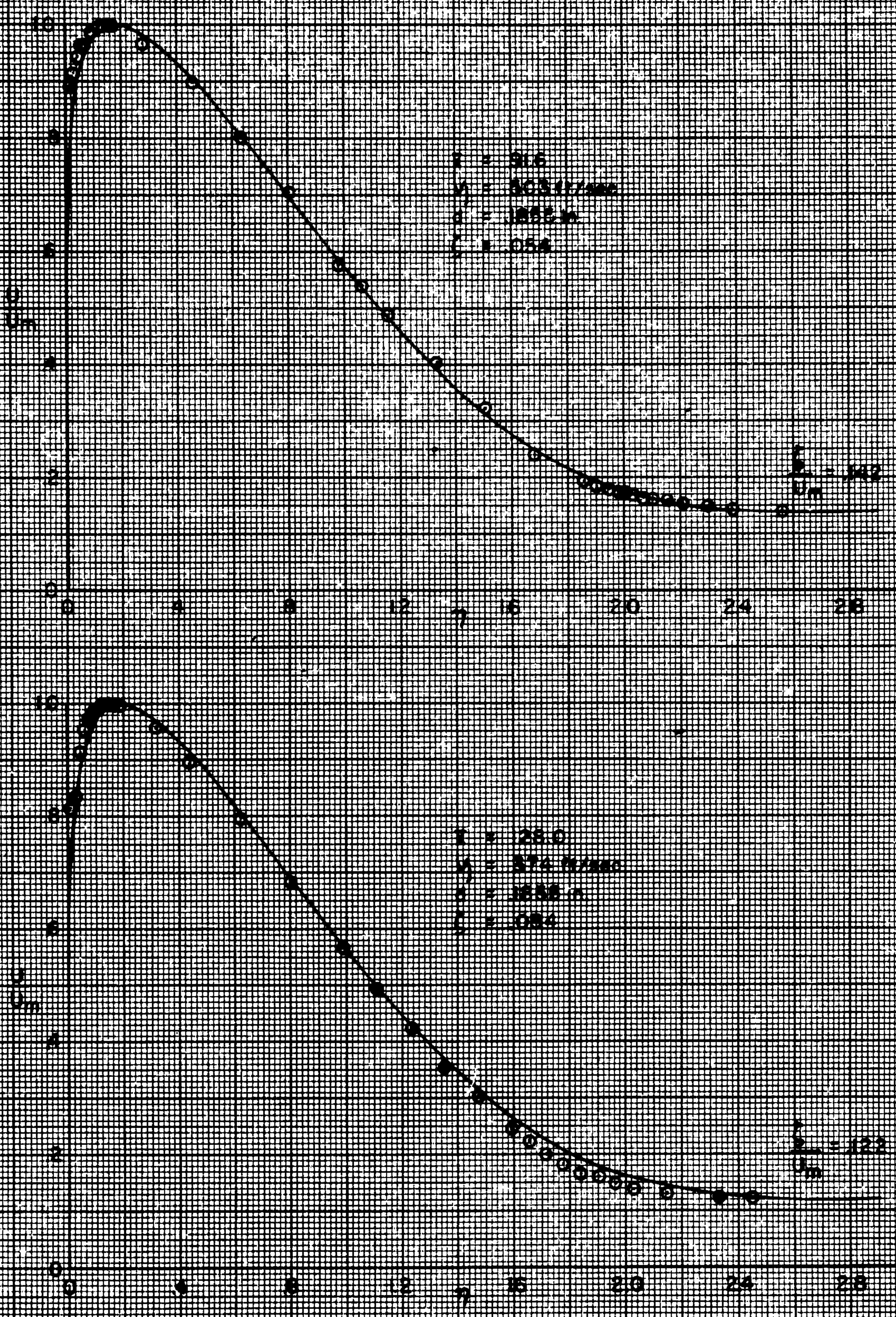

FIGURE 34. COMPARISON WITH ESKINAZI'S DATA
Re_0 = 41,800

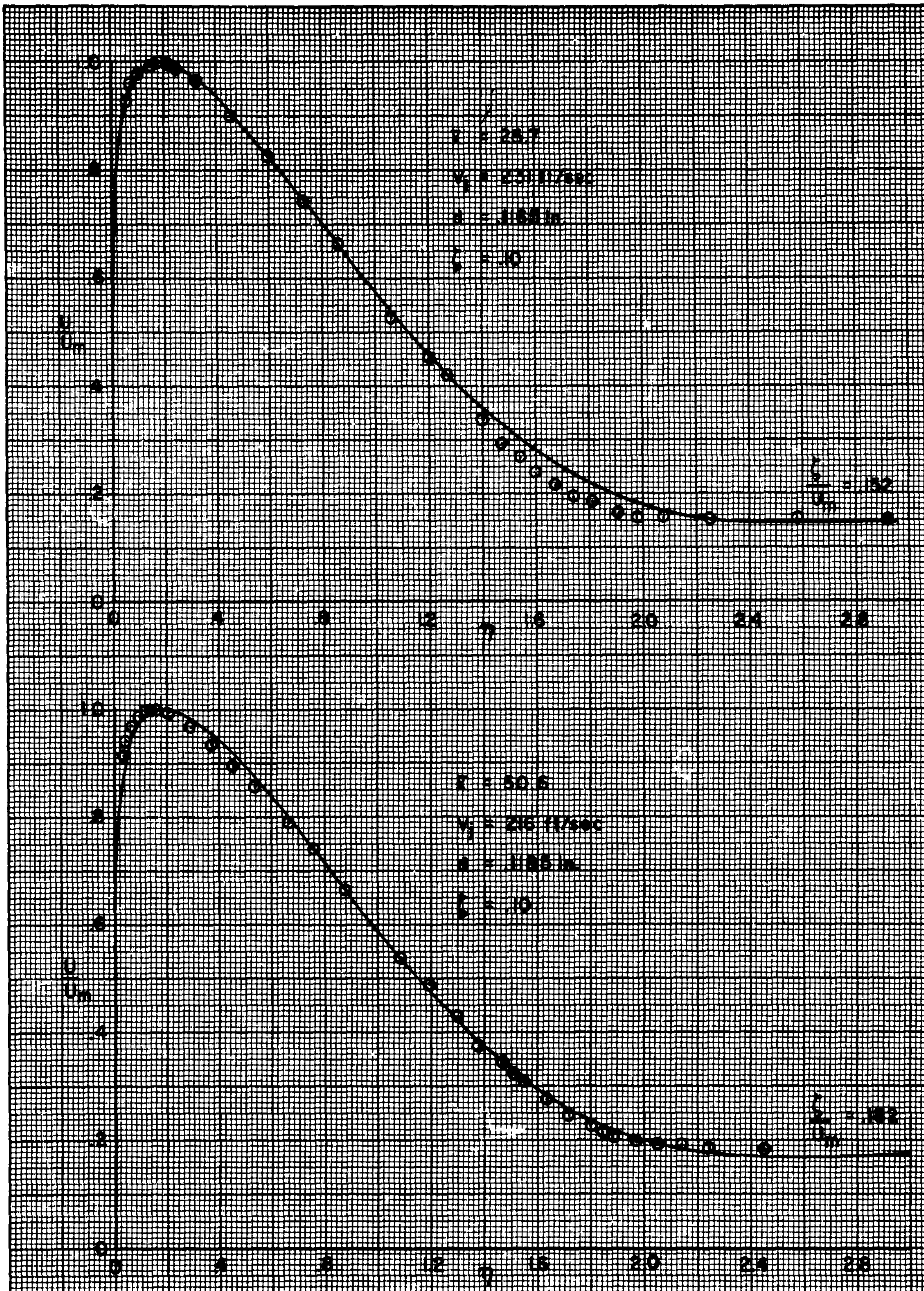

FIGURE 38. COMPARISON WITH ESKINAZI'S DATA
Re_o = 12,600

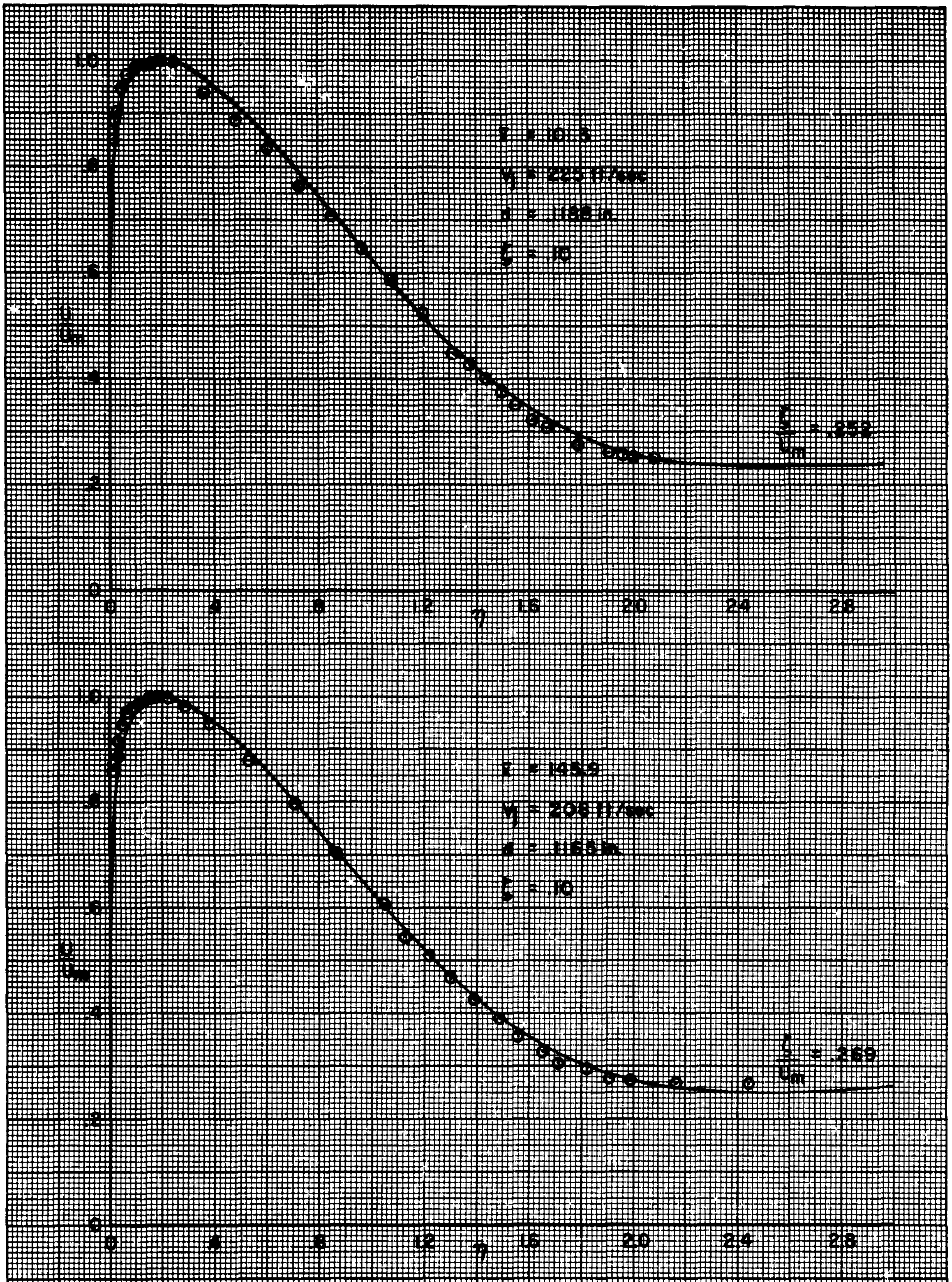

FIGURE 36. COMPARISON WITH ESKINAZI'S DATA

Re_δ = 12,600

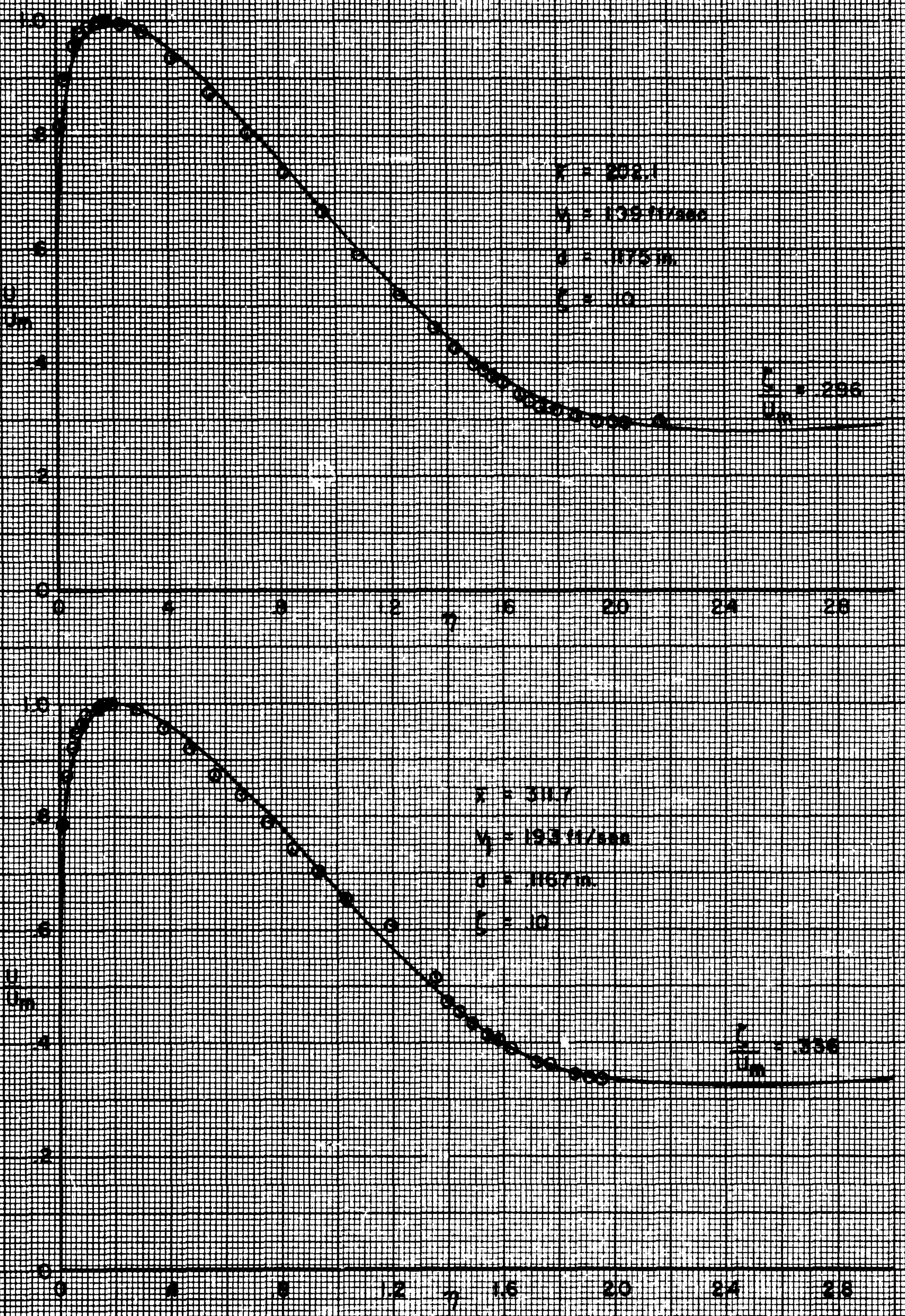

FIGURE 37. COMPARISON WITH ESKINAZI'S DATA
Re_o = 12,600

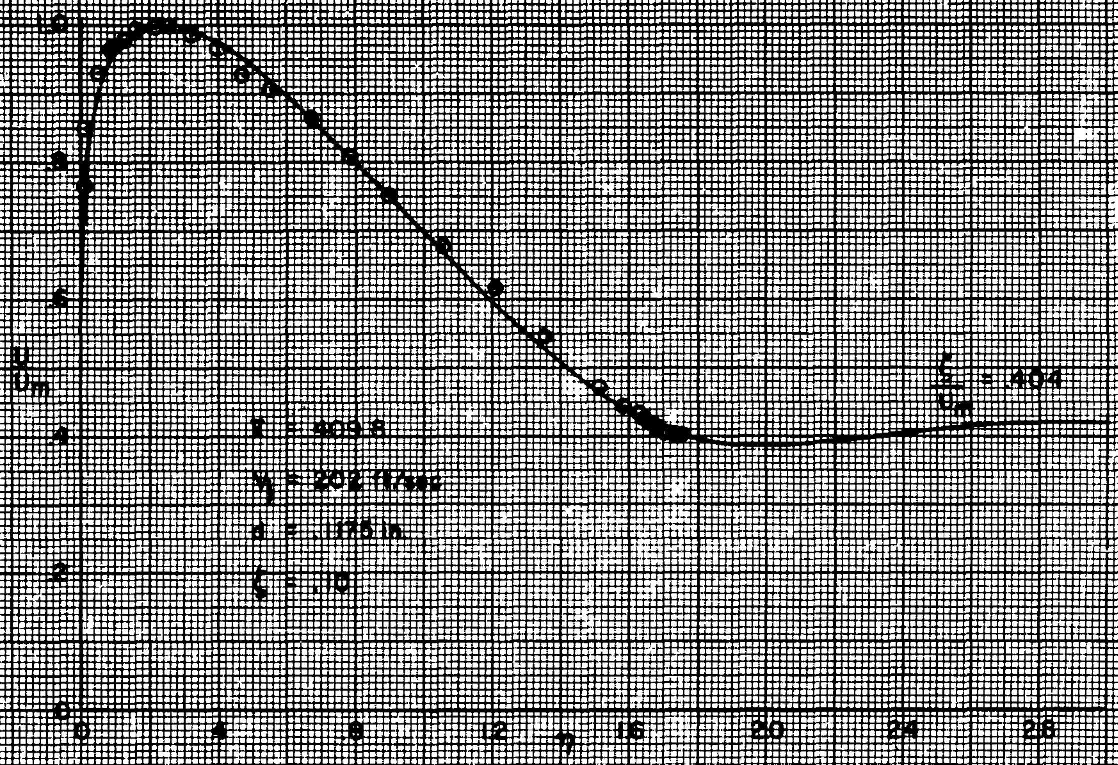

FIGURE 38. COMPARISON WITH ESKINAZI'S DATA
Re_o = 12,600

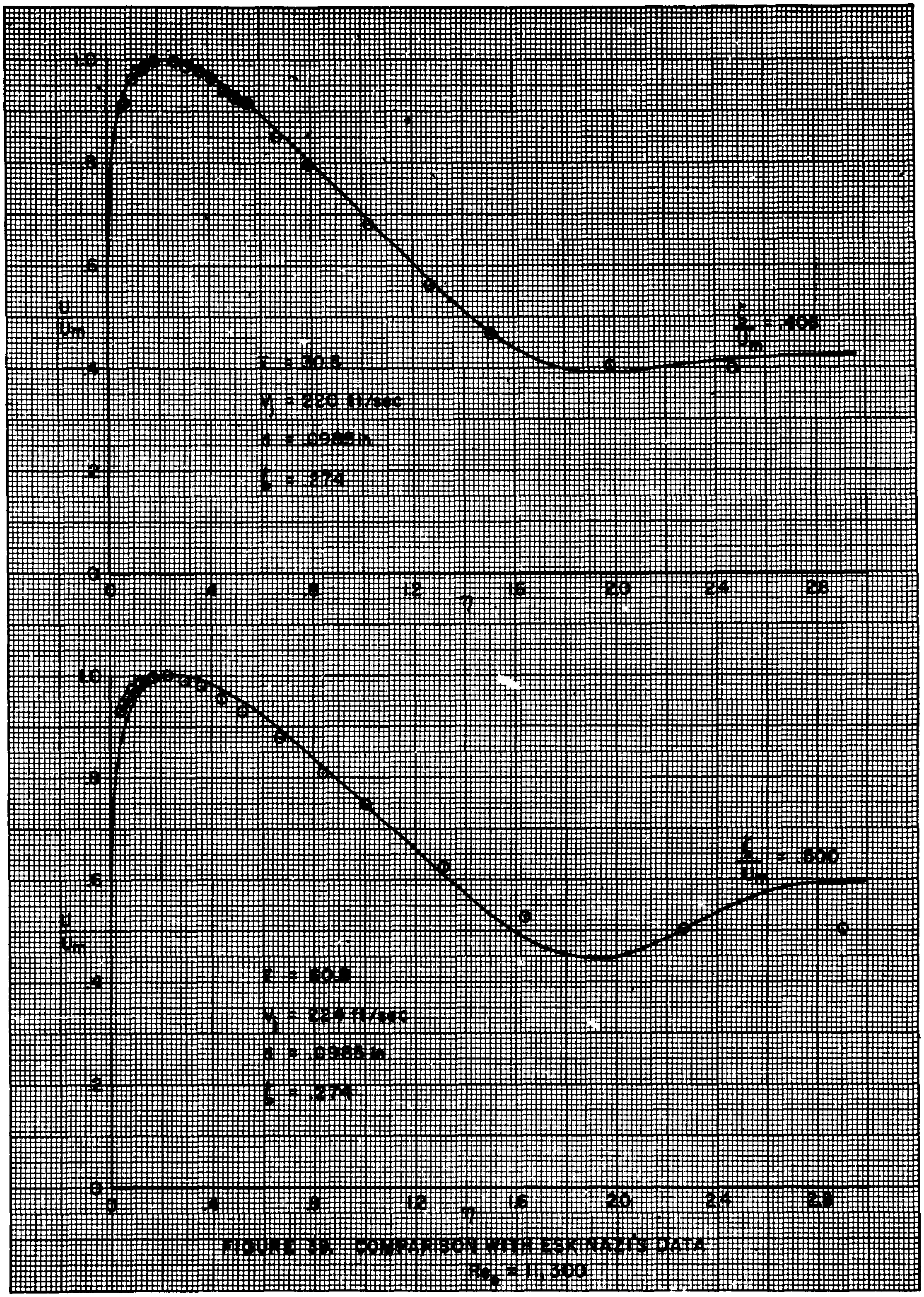

FIGURE 39. COMPARISON WITH ESKINAZI'S DATA
R_{e_s} = 11,300

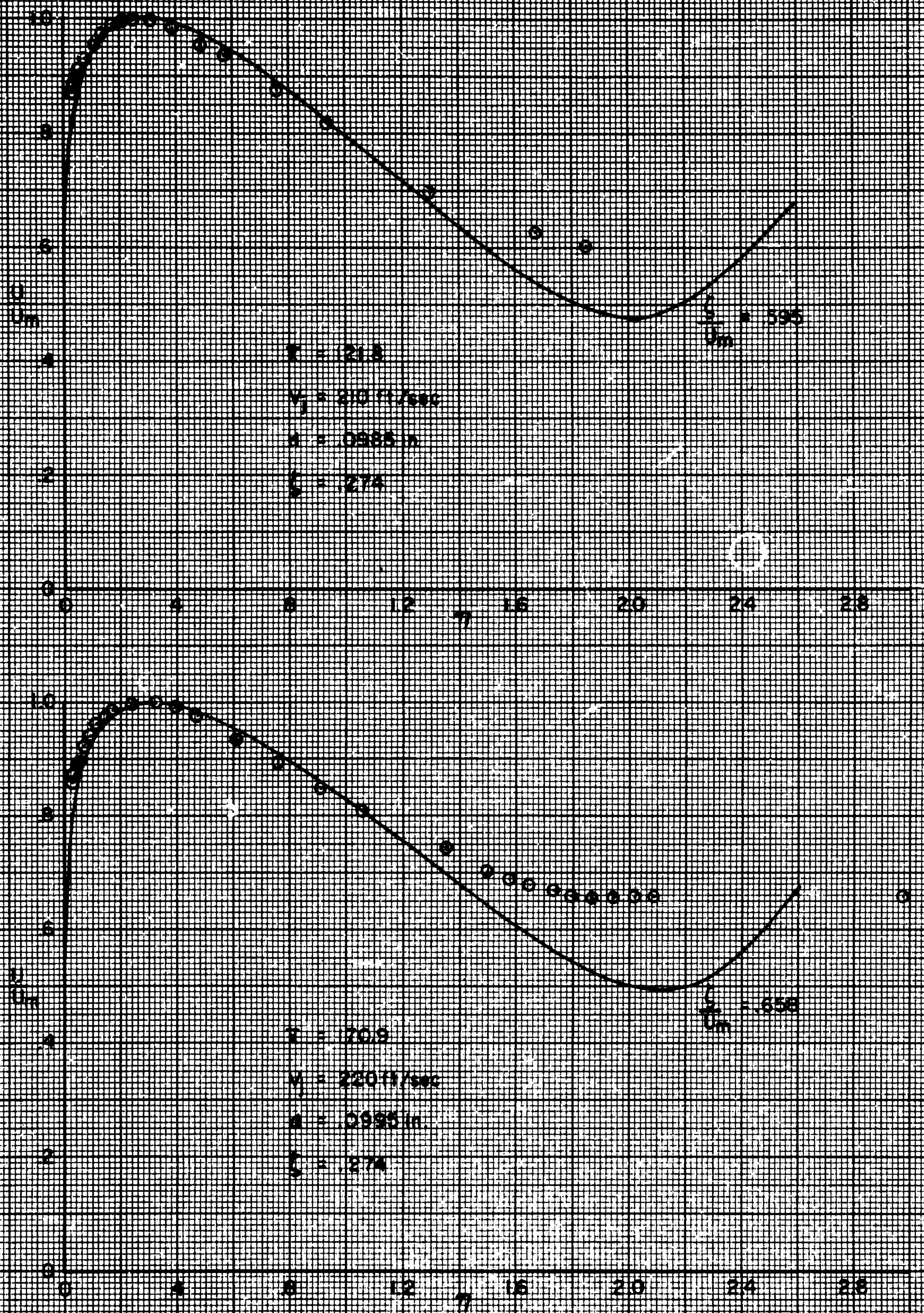

FIGURE 40 COMPARISON WITH ESKINAZI'S DATA
Re_o = 11,300

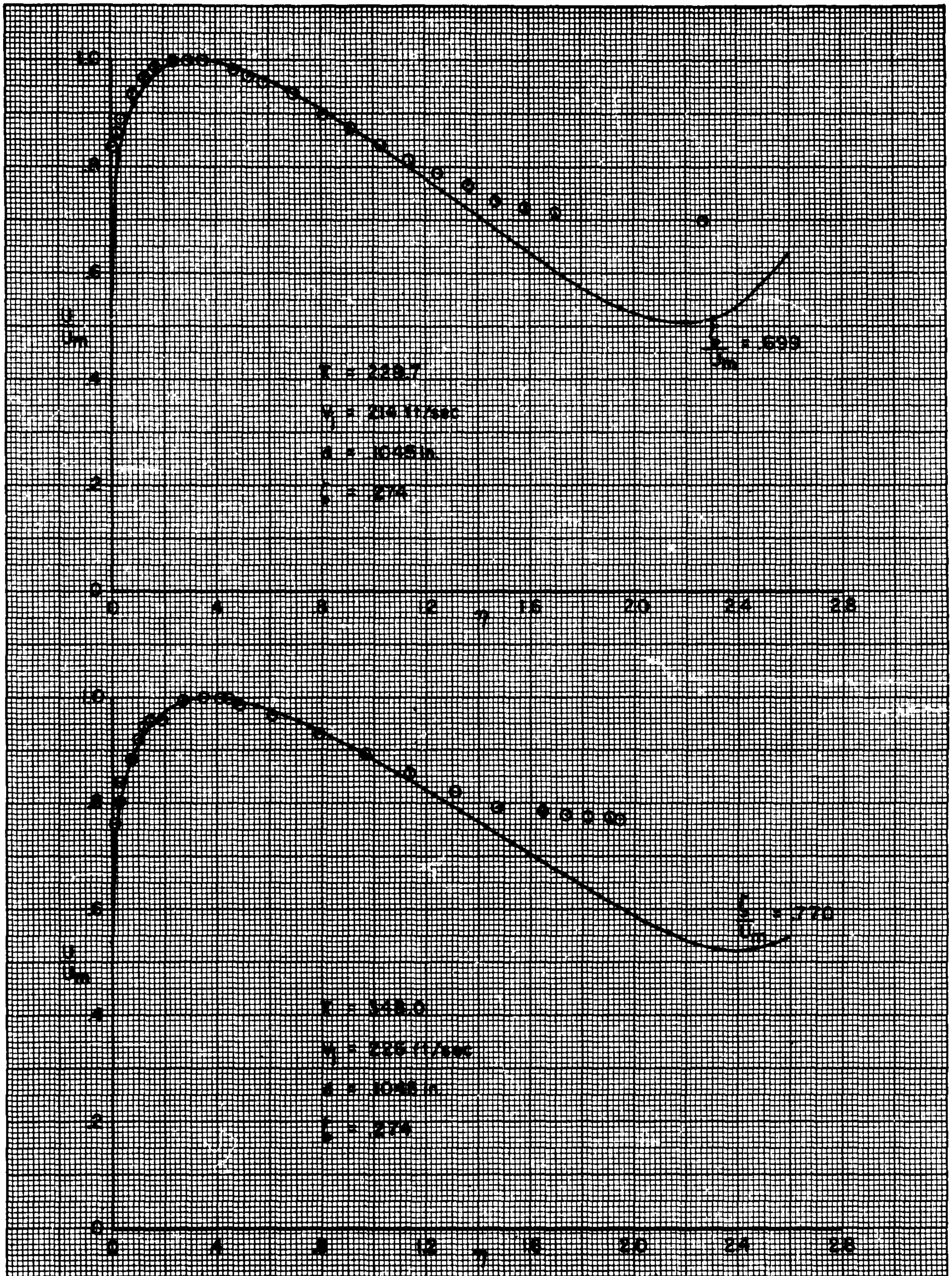

FIGURE 4. COMPARISON WITH ESKINAZI'S DATA
Re_0 = 11,300

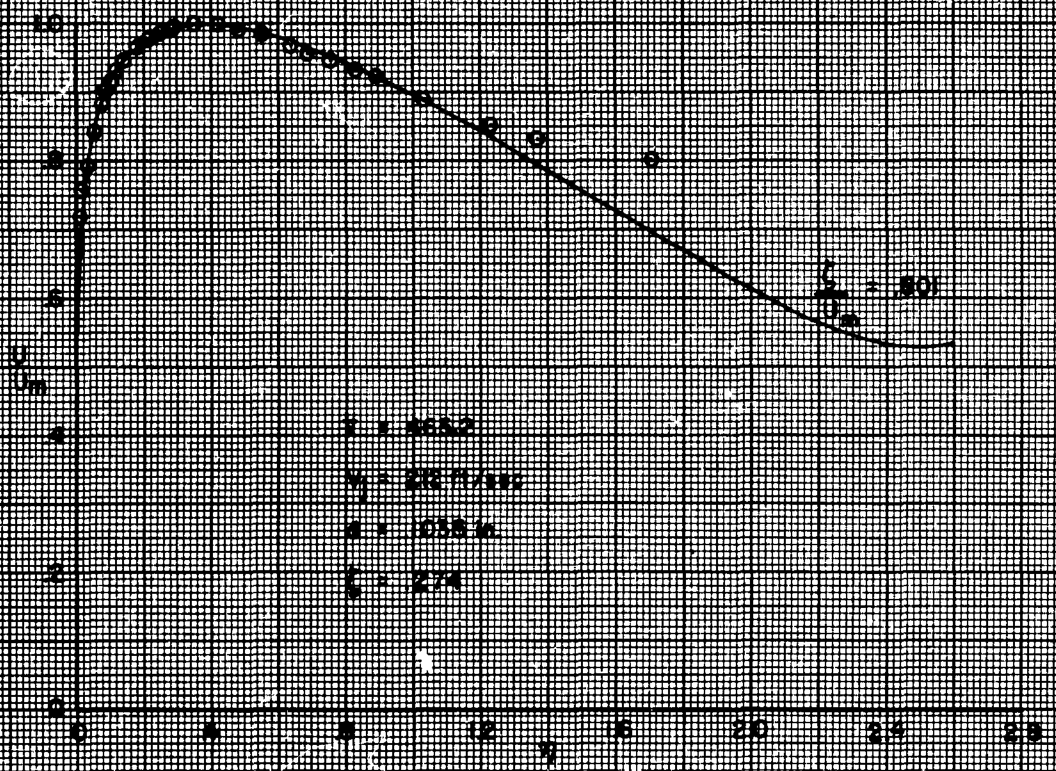

FIGURE 42. COMPARISON WITH ESKINAZI'S DATA
$Re_e = 11,300$

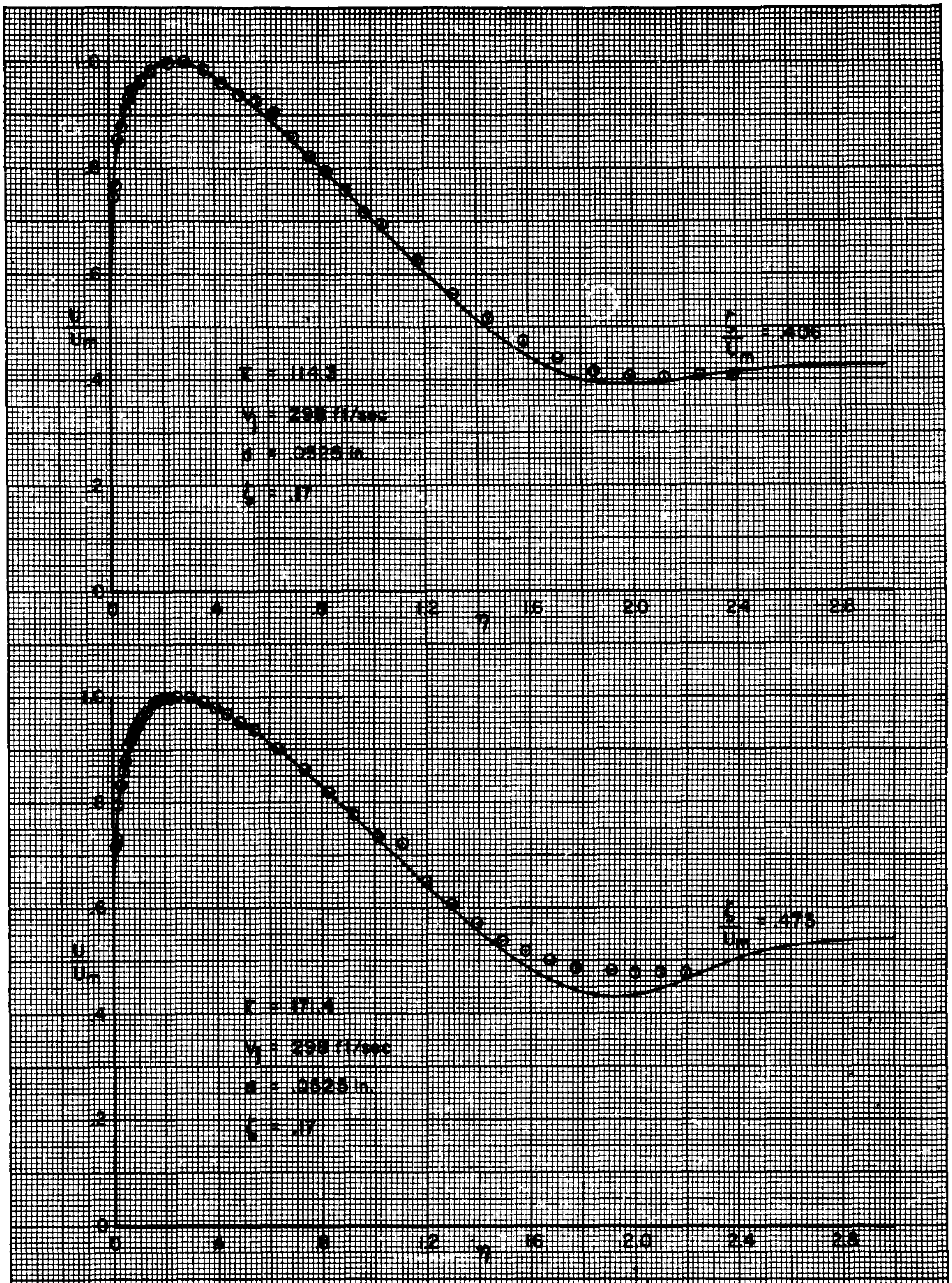

FIGURE 42. COMPARISON WITH GEORGE'S DATA
Re_0 = 7850

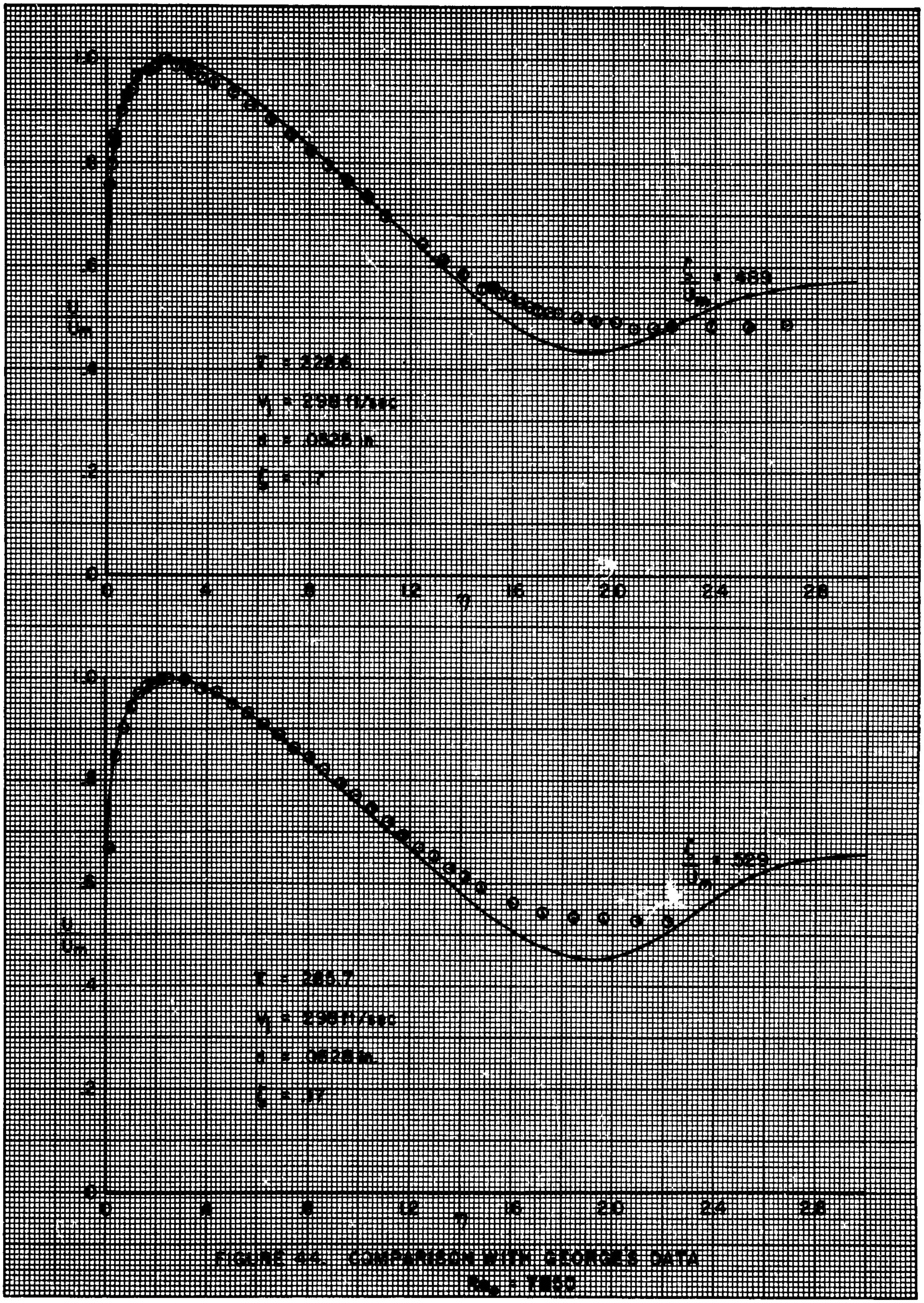

FIGURE 44. COMPARISON WITH GEORGE'S DATA
$Re_s = 7850$

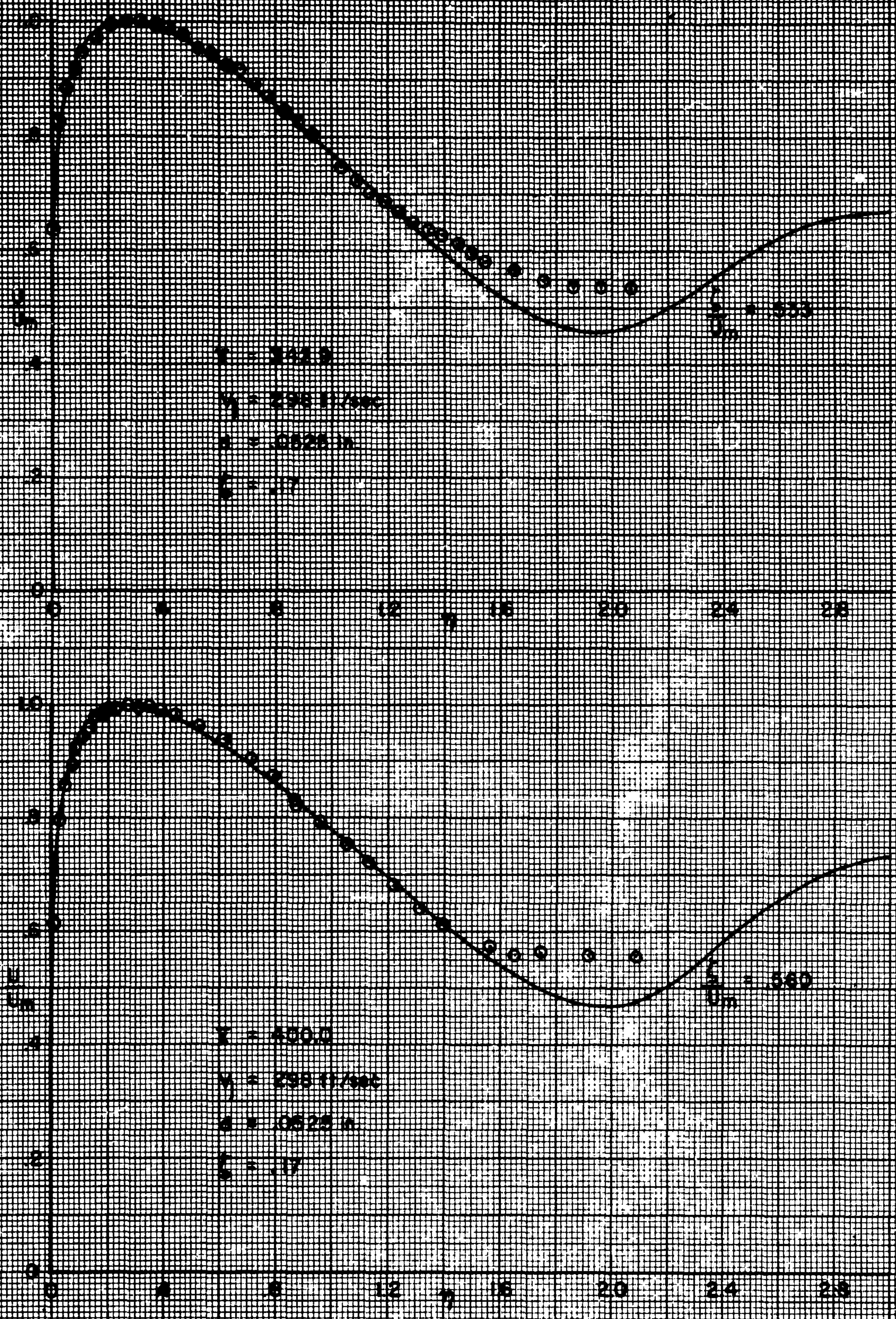

FIGURE 45. COMPARISON WITH GEORGE'S DATA
Re_o = 7850

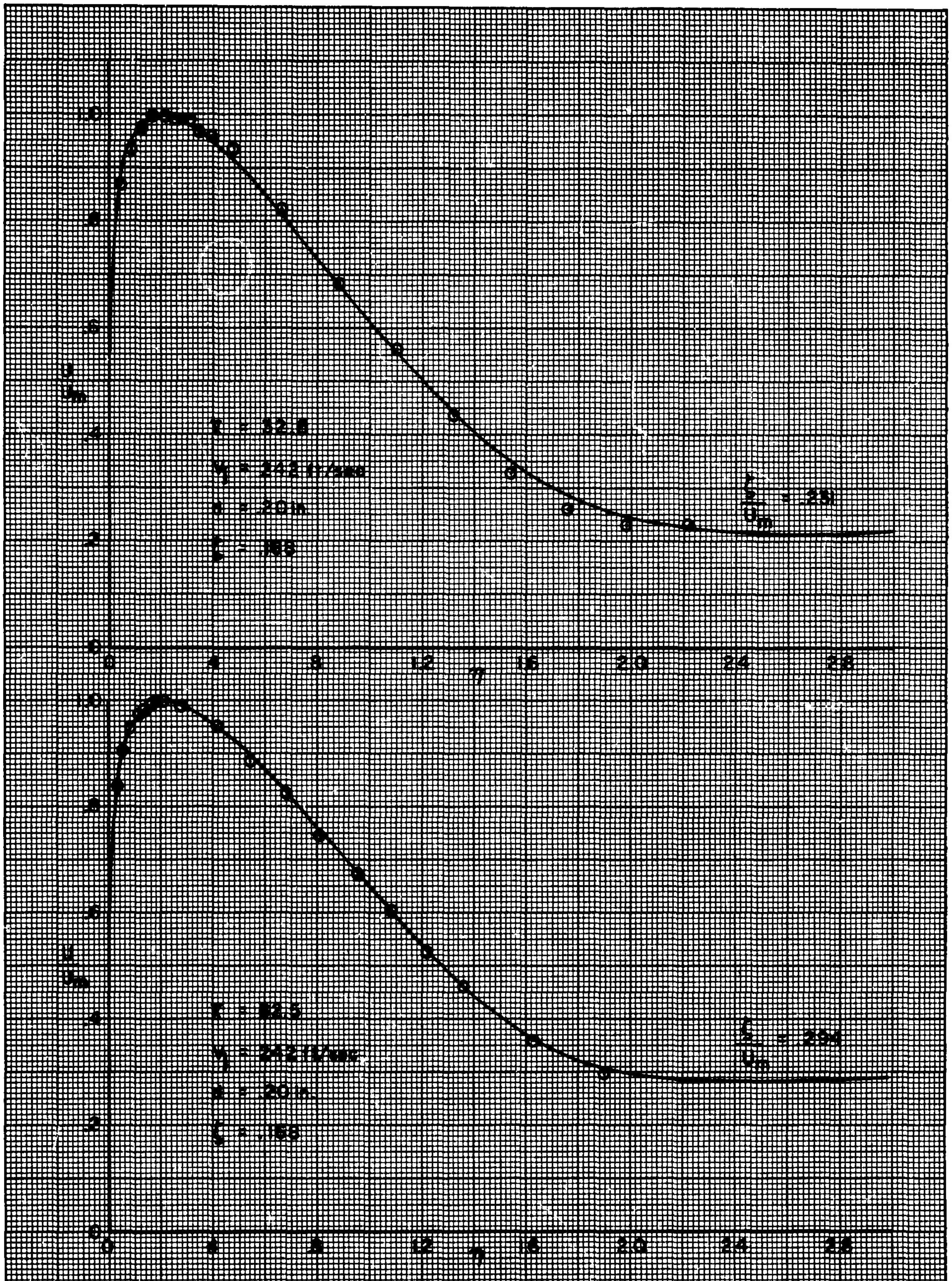

FIGURE 46. COMPARISON WITH PATEL'S DATA
Re_δ = 24,500

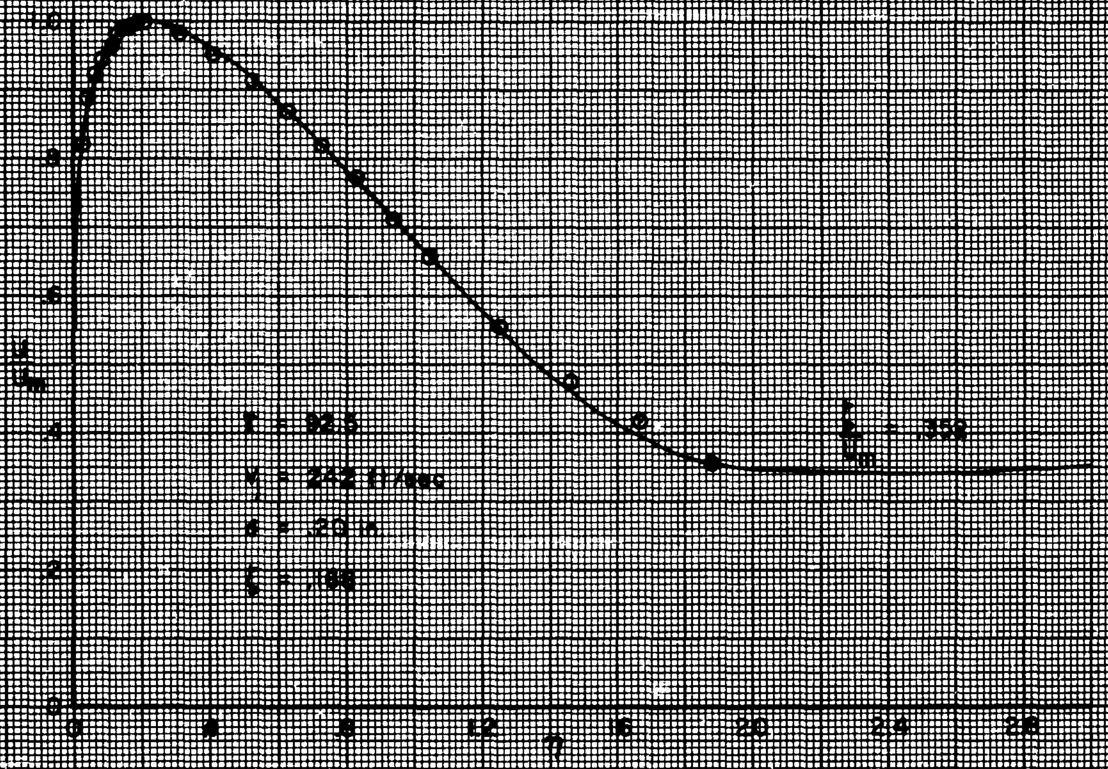

FIGURE 47. COMPARISON WITH PATEL'S DATA
Re_x = 24,500

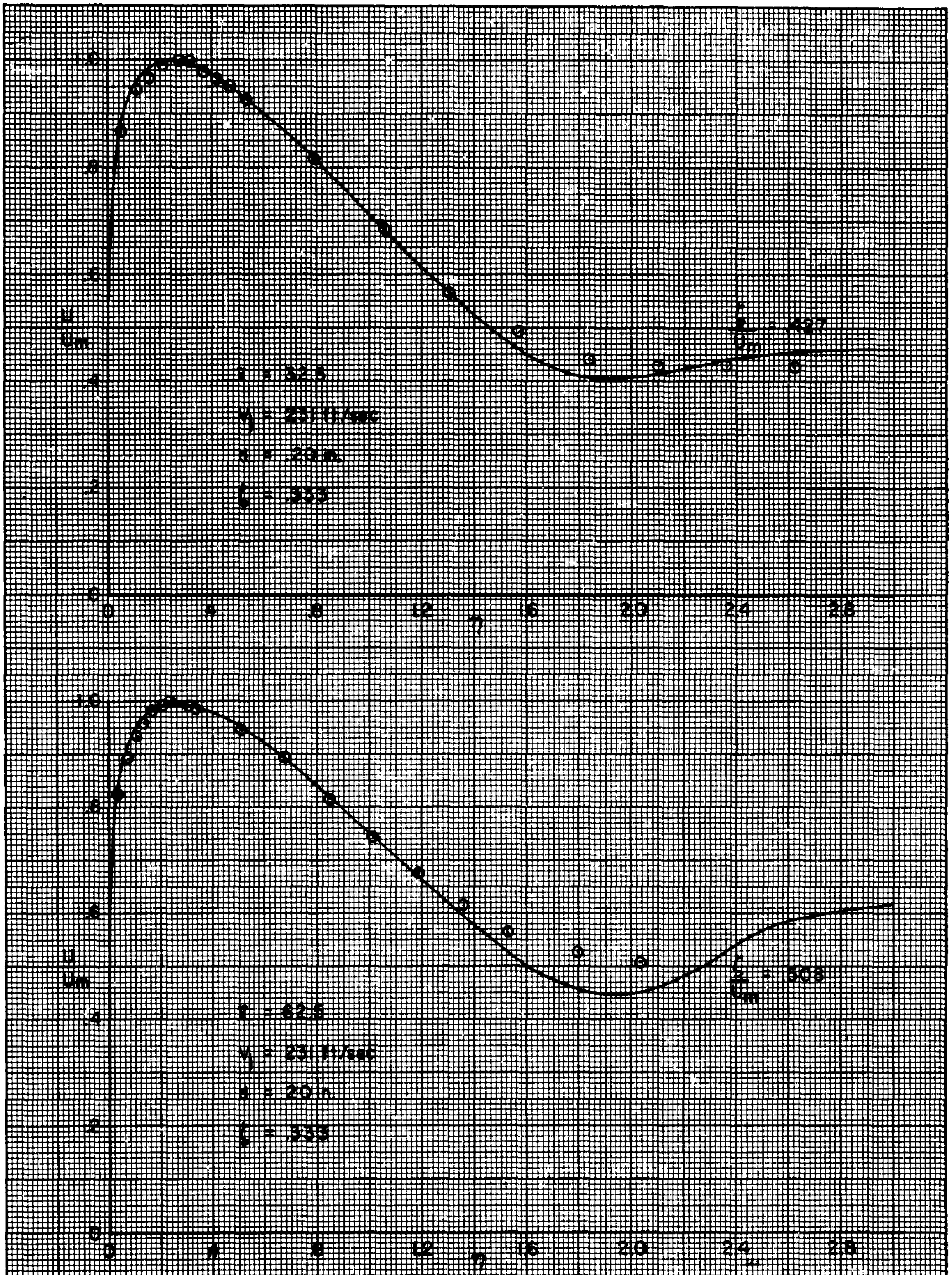

FIGURE 46. COMPARISON WITH PATEL'S DATA
Re_o = 23,400

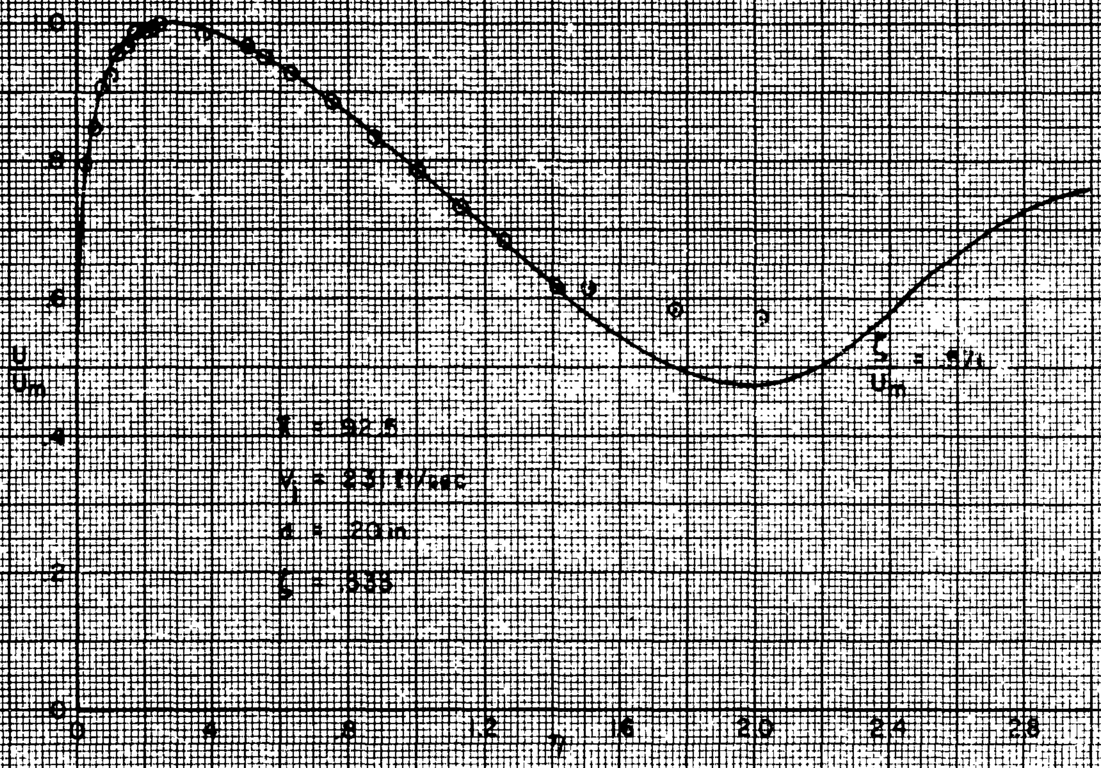

FIGURE 49. COMPARISON WITH PATEL'S DATA

Re_o = 23,400

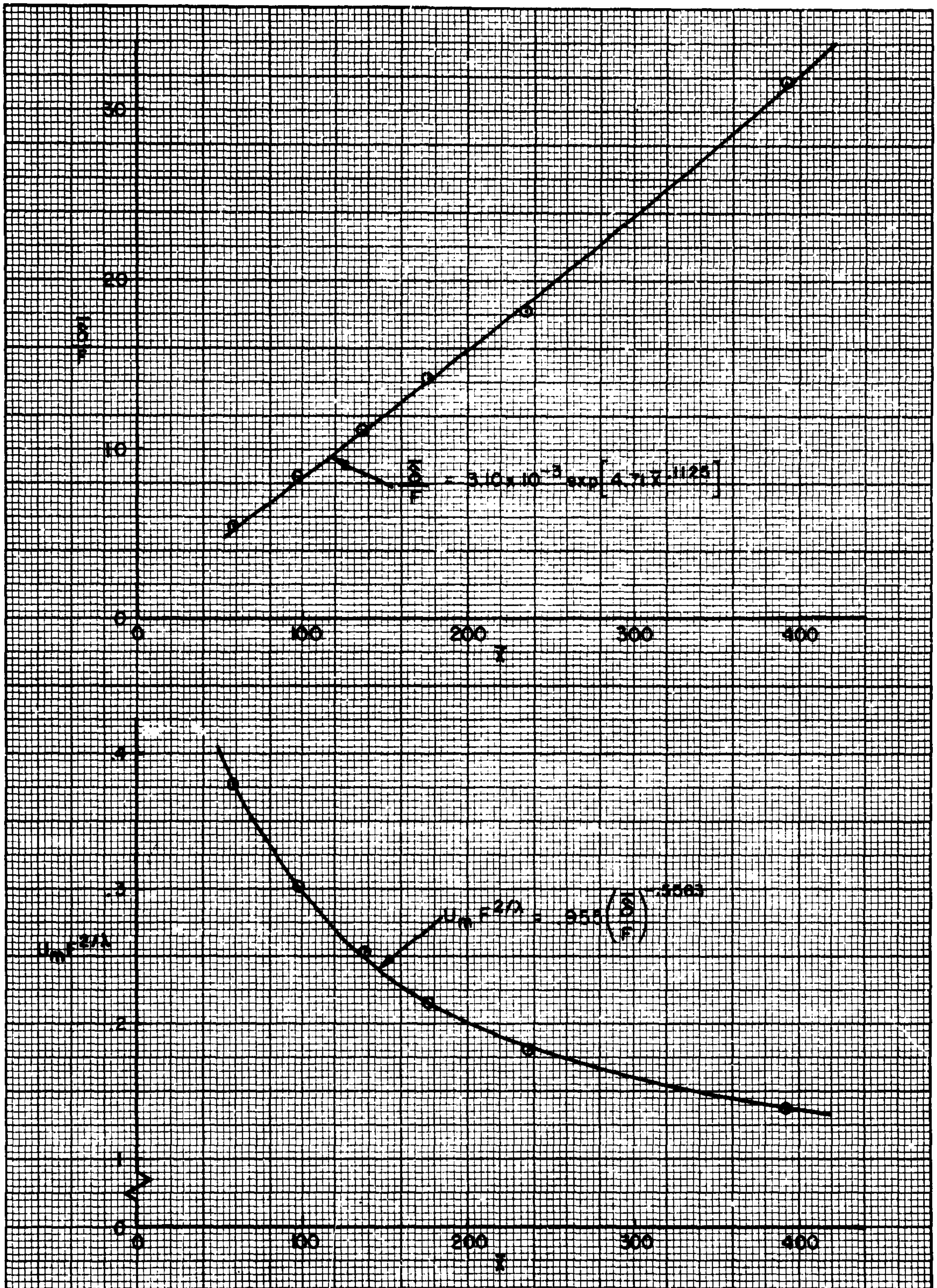

FIGURE 50. VARIATION OF VELOCITY AND LENGTH SCALES

$Re_o = 8900 \qquad \frac{l}{D} = .082$

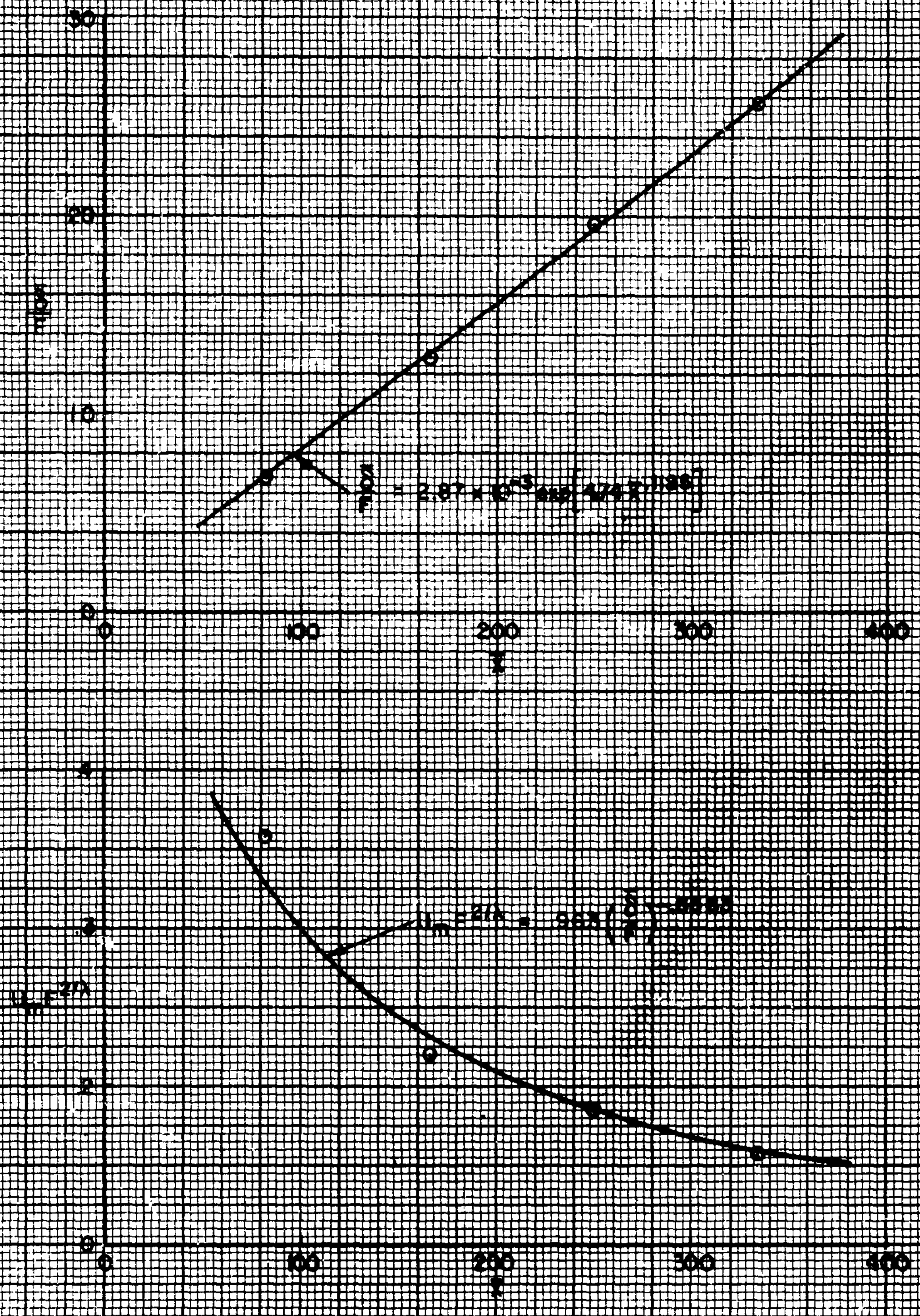

FIGURE 51 VARIATION OF VELOCITY AND LENGTH SCALES

Re_b = 9400 $\frac{P}{S}$ = .19

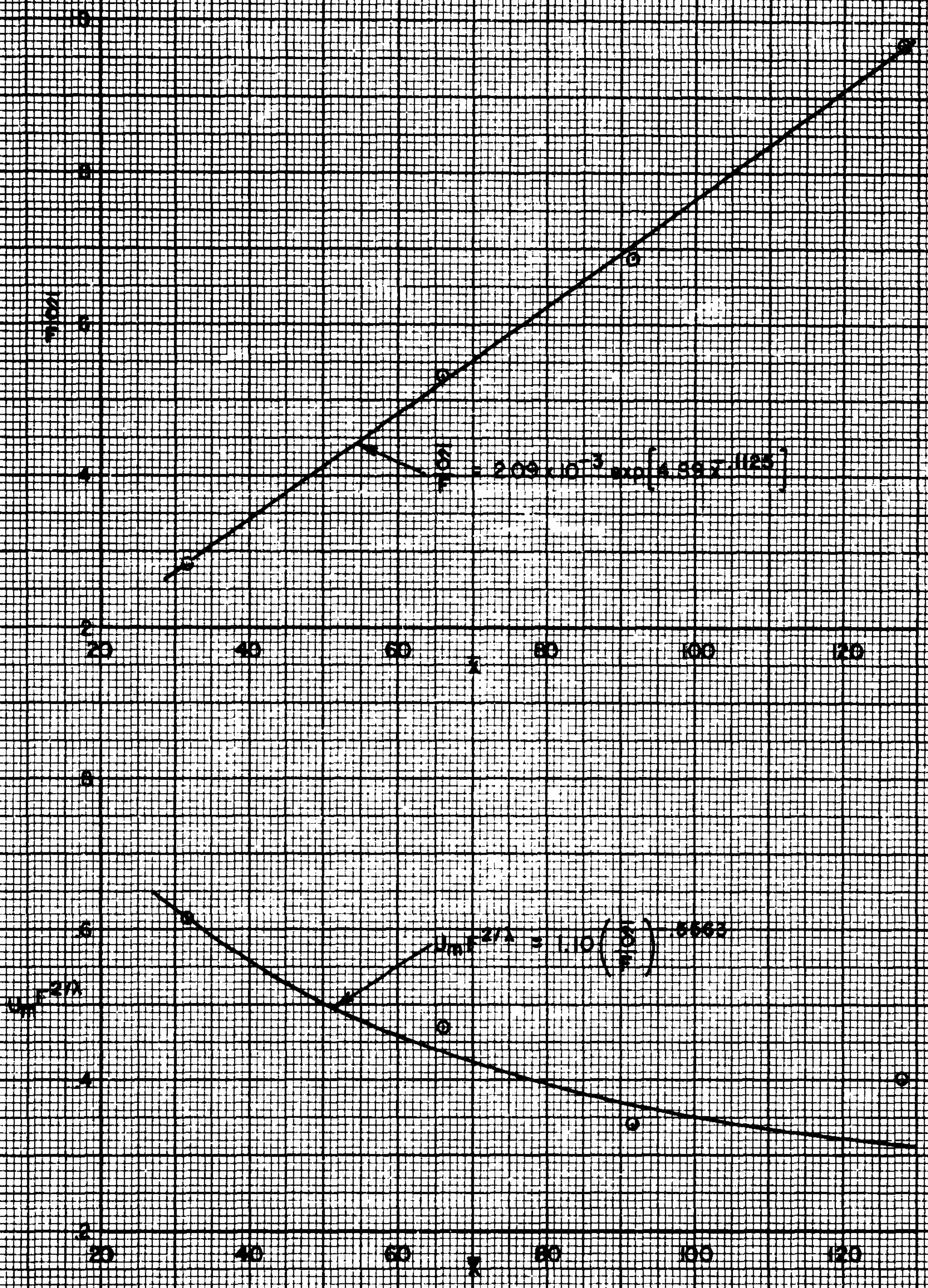

FIGURE 52. DATA OF ESKINAZI
Re = 41,800 ζ = .054

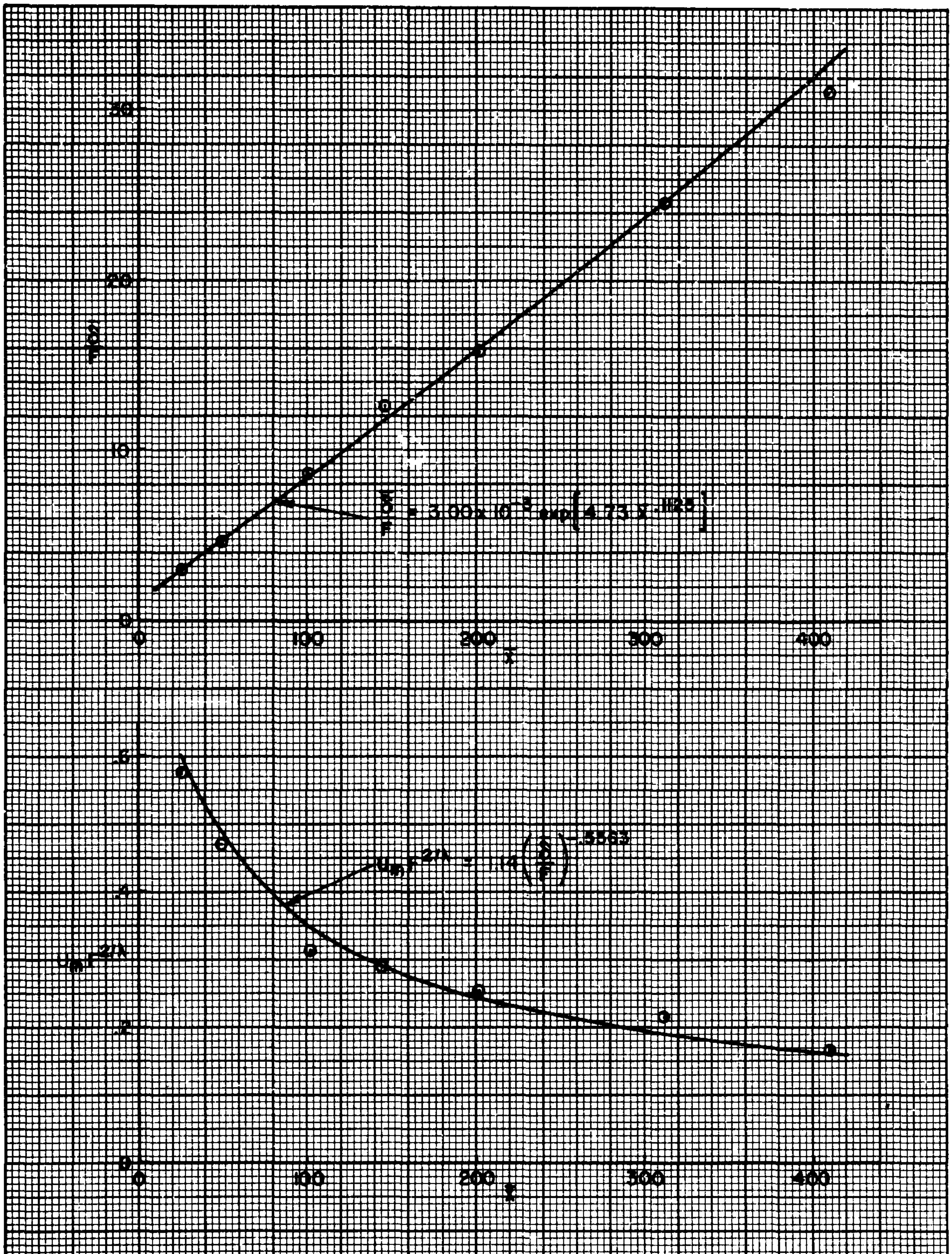

FIGURE 53. DATA OF ESKINAZI

$Re_0 = 12{,}600 \quad \zeta = .10$

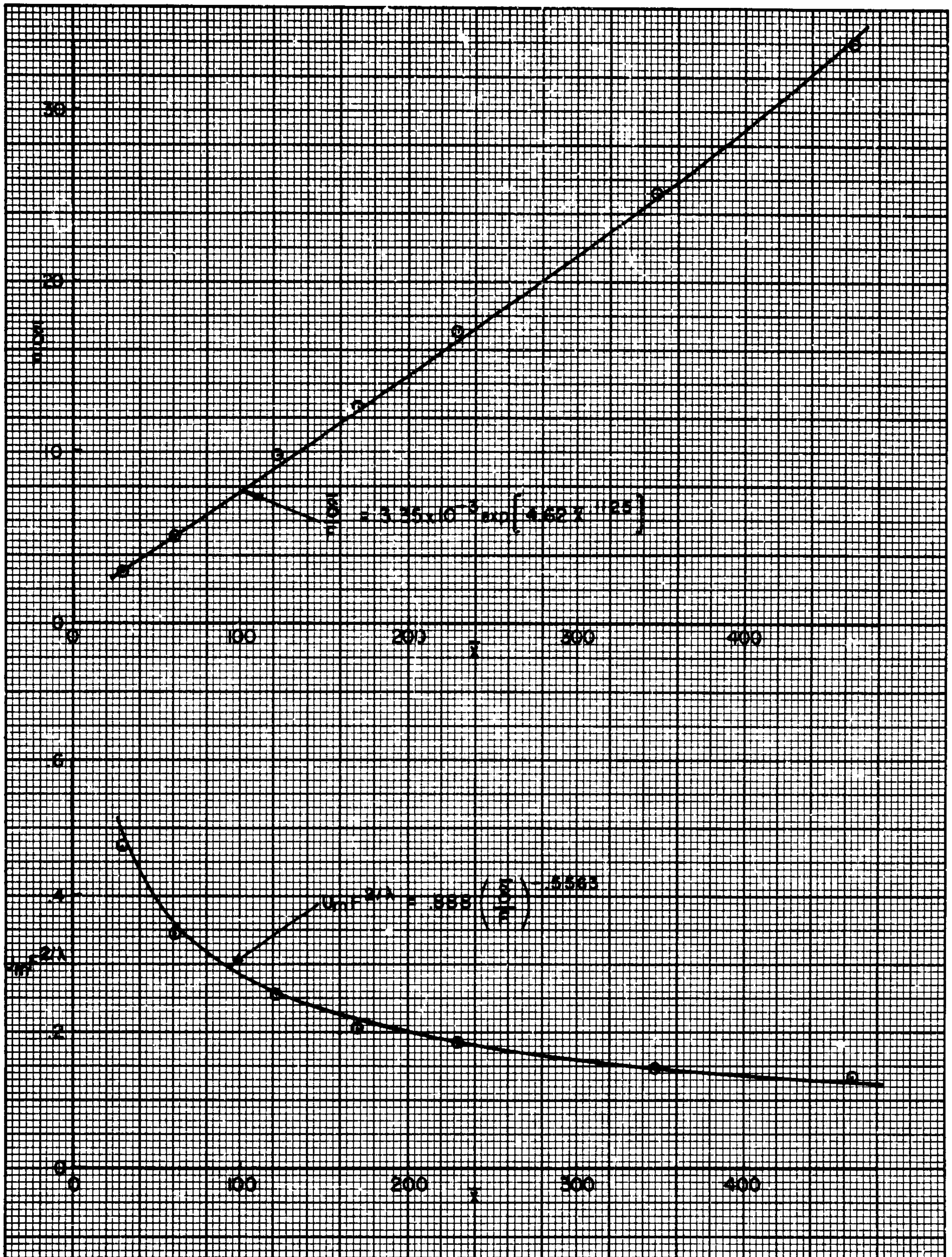

FIGURE 54 DATA OF ESKINAZI

$Re_c = 11{,}500 \quad \zeta = .274$

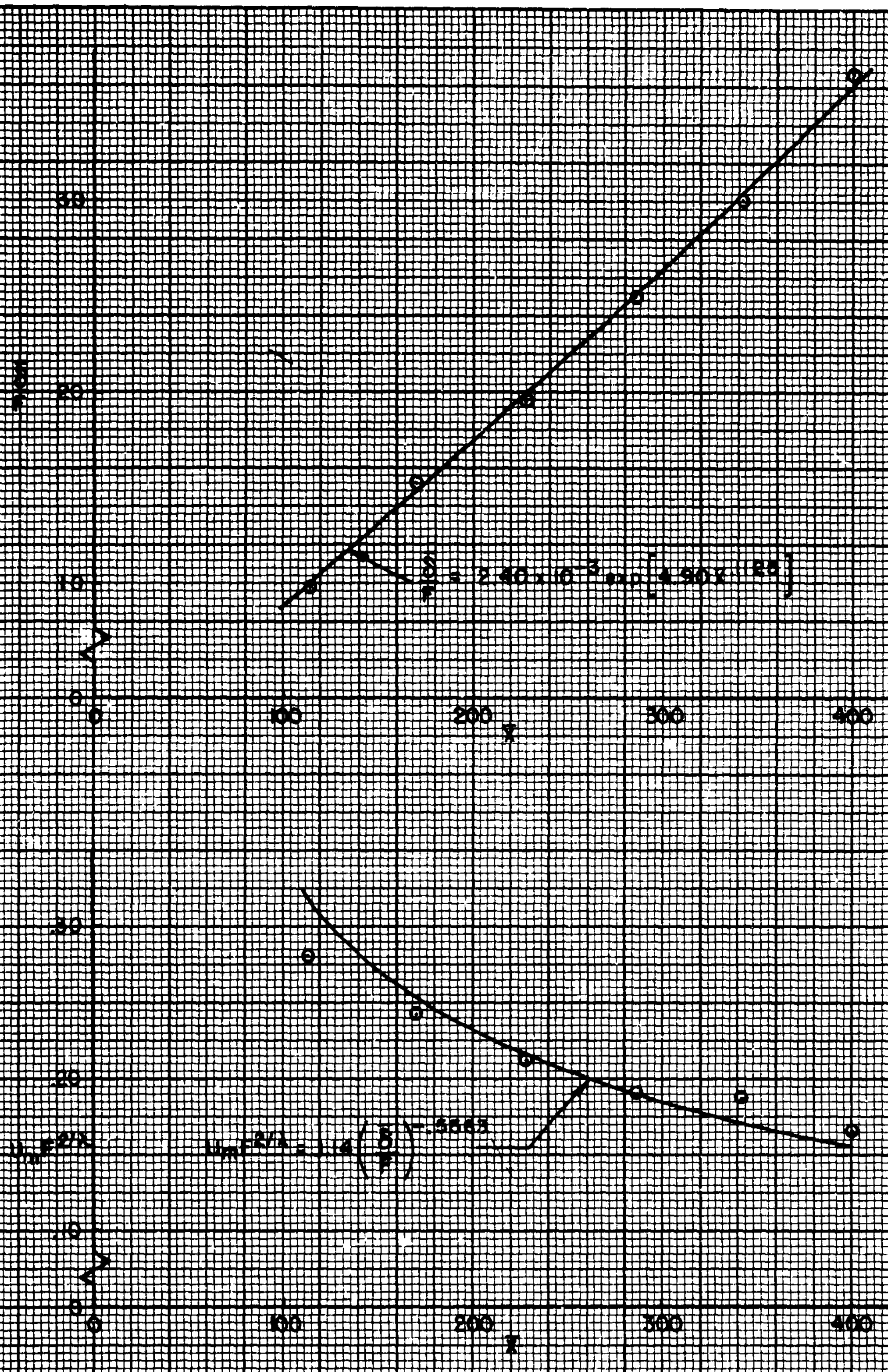

FIGURE 55. DATA OF GEORGE

$Re_x = 7850 \quad \zeta = .170$

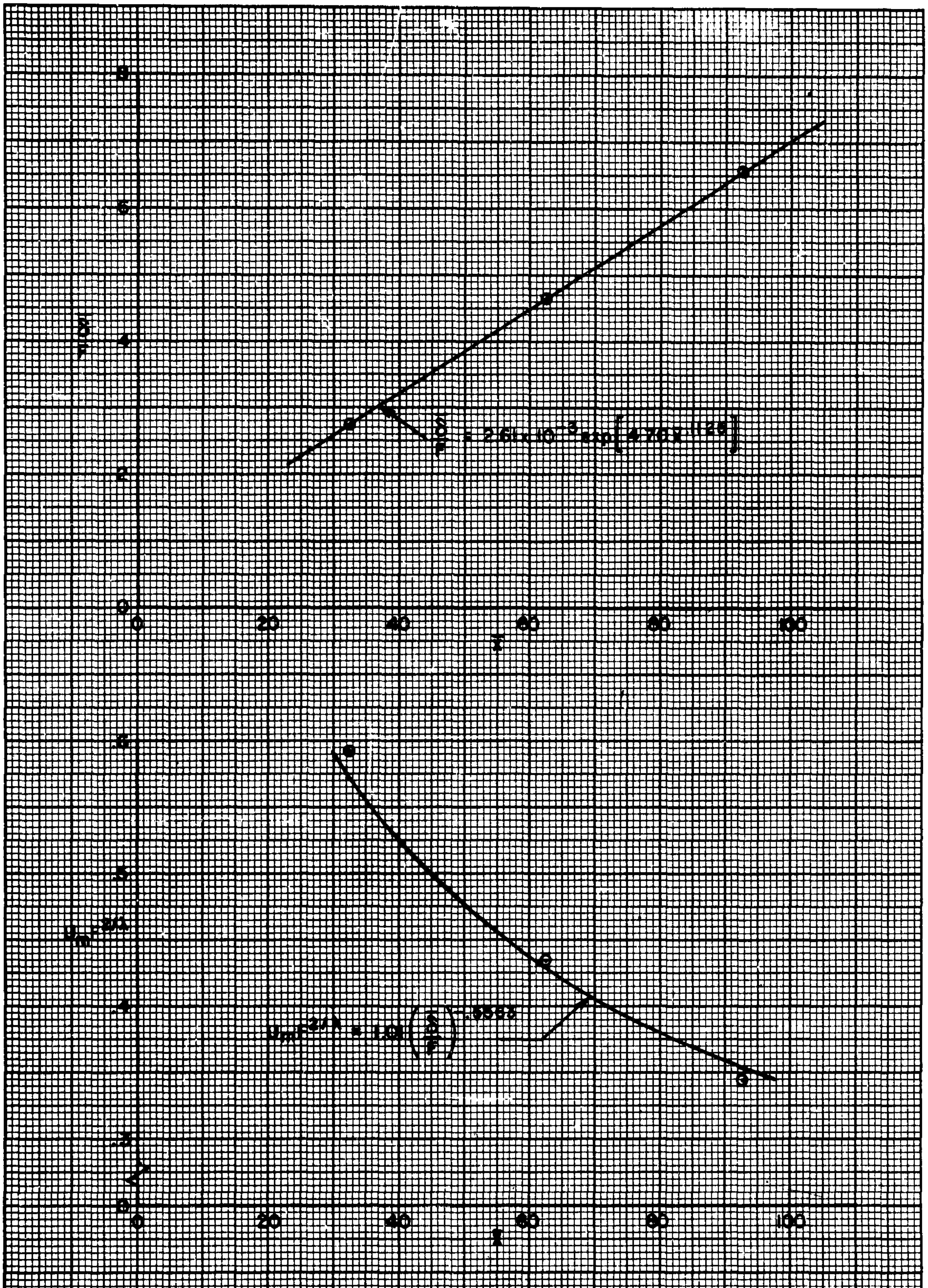

FIGURE 56. DATA OF PATEL

$Re_c = 24,500 \quad \zeta = 168$

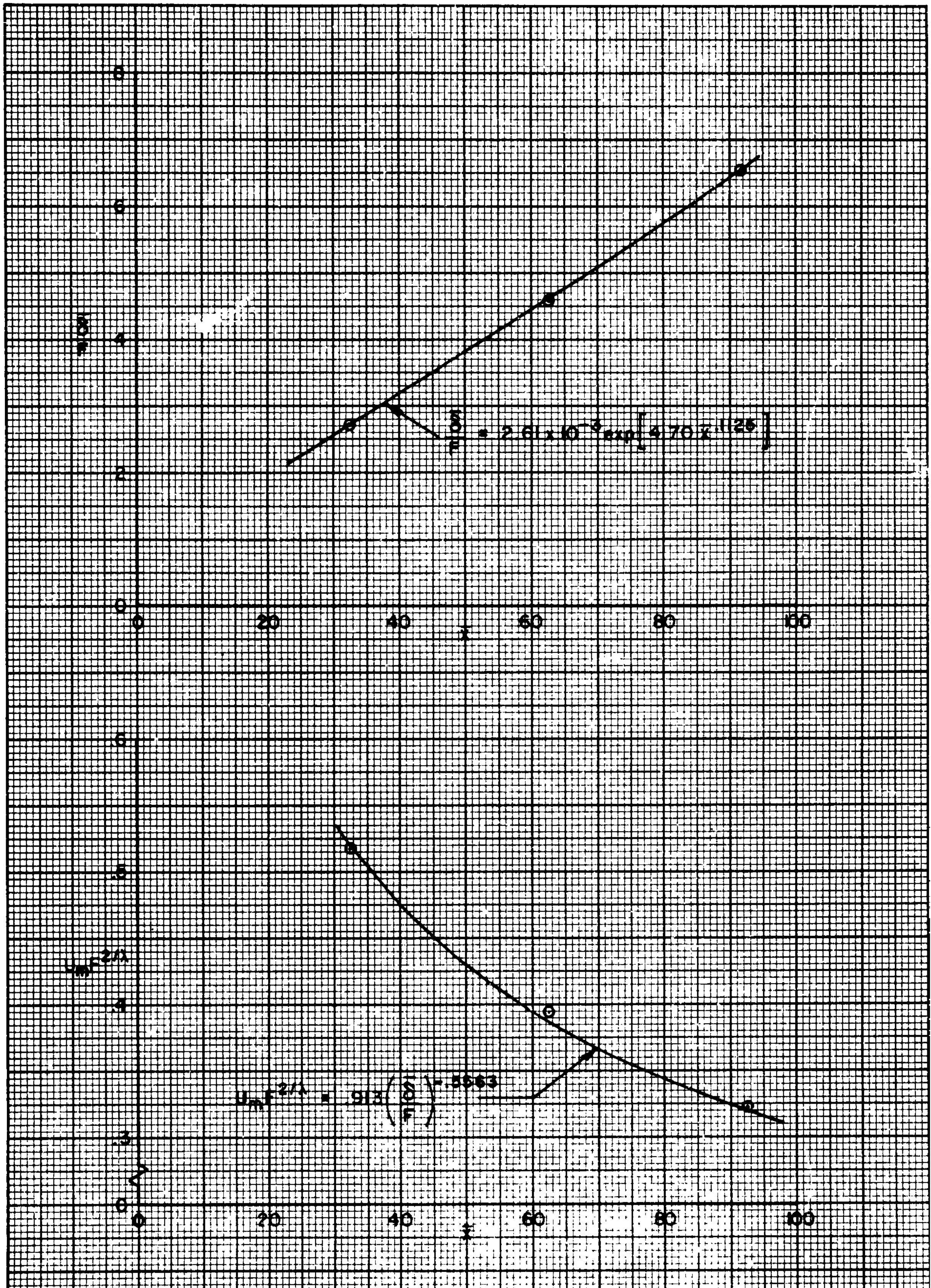

FIGURE 57. DATA OF PATEL
$Re_* = 23{,}400 \quad \bar{\zeta} = .333$

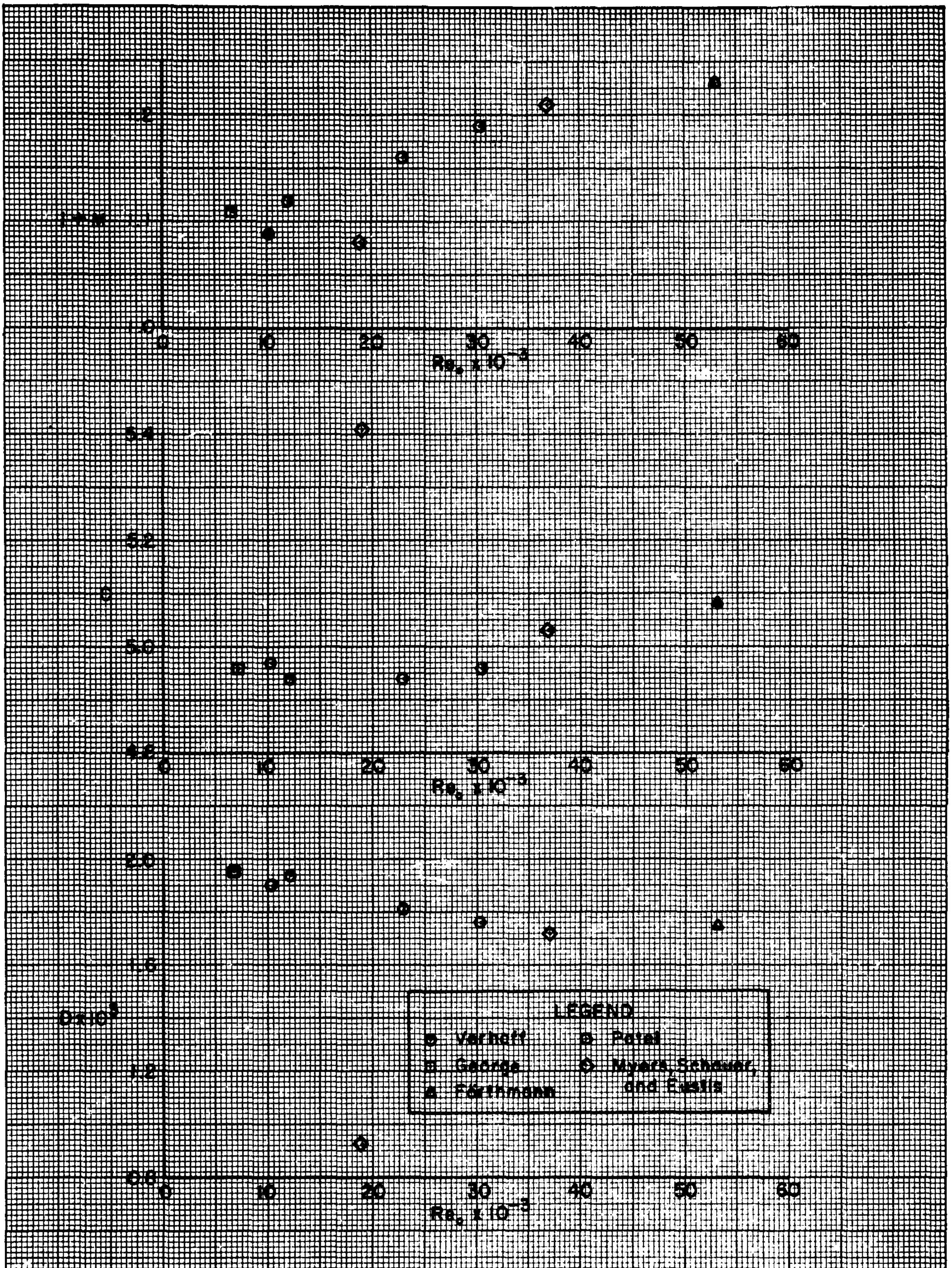

FIGURE 53. PROPORTIONALITY FACTORS FOR VELOCITY AND LENGTH SCALE VARIATION

λ = 1.7977 ζ = 0

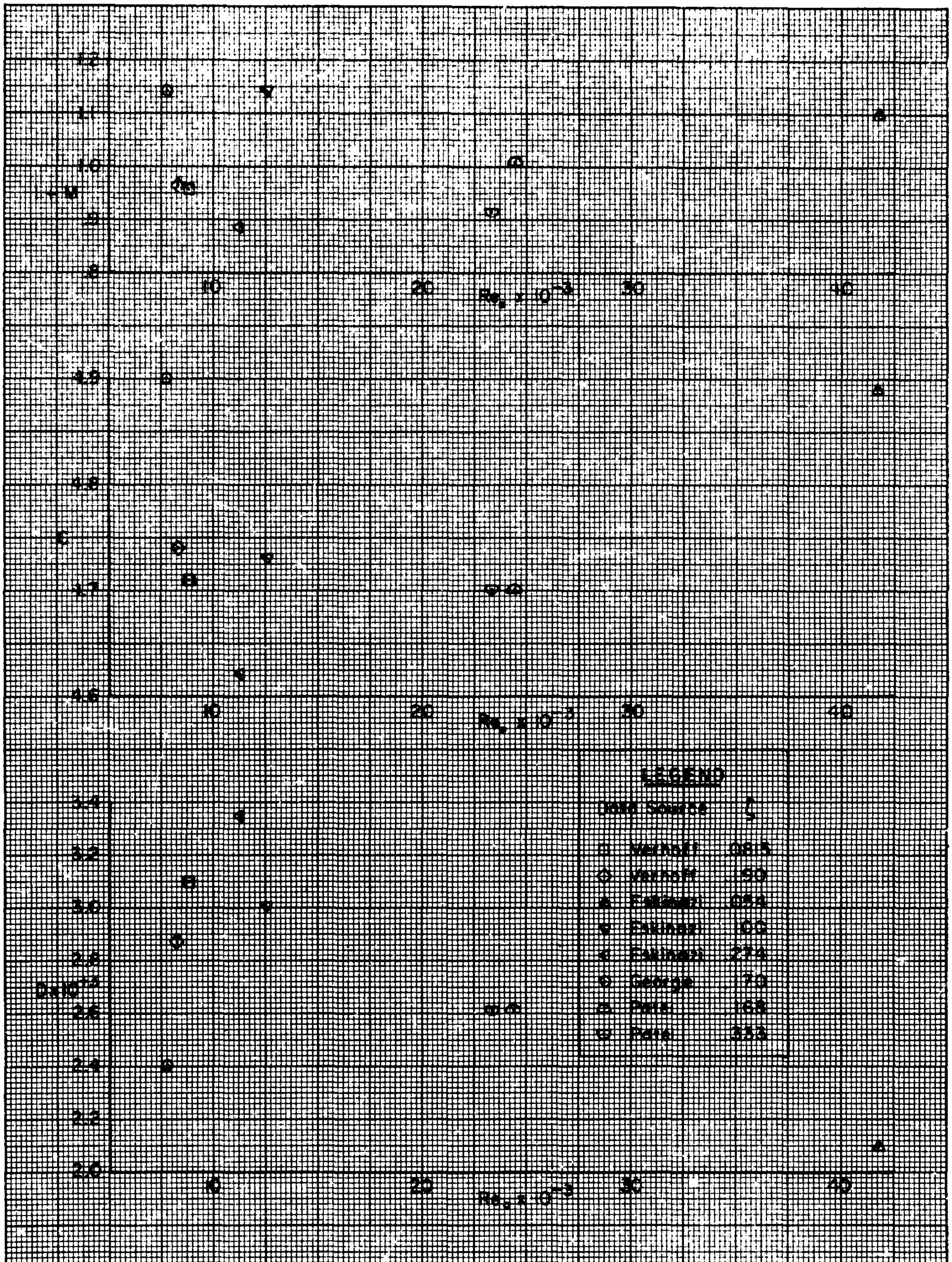

FIGURE 52. PROPORTIONALITY FACTORS FOR VELOCITY AND LENGTH SCALE VARIATION

$\lambda = 1.7977$

DISTRIBUTION LIST

Chief, Bureau of Naval Weapons
(RAAD-3)
Department of the Navy
Washington 25, D. C.

Chief, Bureau of Naval Weapons
(RAAD-32)
Department of the Navy
Washington 25, D. C.

Chief, Bureau of Naval Weapons
(RAAD-33)
Department of the Navy
Washington 25, D. C.

Chief, Bureau of Naval Weapons
(RAAD-34)
Department of the Navy
Washington 25, D. C.

Chief, Bureau of Naval Weapons
(RA-4)
Department of the Navy
Washington 25, D.C.

Chief, Bureau of Naval Weapons
(R-55)
Department of the Navy
Washington 25, D. C.

Chief, Bureau of Naval Weapons
(RR-25)
Department of the Navy
Washington 25, D. C.

Chief, Bureau of Naval Weapons
(RRRE-4)
Department of the Navy
Washington 25, D. C.

Commanding Officer and Director
David Taylor Model Basin
Aerodynamics Laboratory
Washington 25, D. C.

Commanding Officer and Director
David Taylor Model Basin
Aerodynamics Laboratory
Washington 7, D. C.
ATTN: Mr. H. Chaplin

Chief of Naval Research (Code 461)
Department of the Navy
Washington 25, D. C. (6 copies)

Chief of Naval Research (Code 438)
Department of the Navy
Washington 25, D. C.

Commanding Officer
Office of Naval Research Branch Office
Navy #100, Box 39, F.P.O.
New York, New York
ATTN: Head, Documents Section
(2 copies)

Commanding Officer
Office of Naval Research Branch Office
346 Broadway
New York 13, New York

Commanding Officer
Office of Naval Research Branch
86 E. Randolph Street
Chicago 1, Illinois

Commanding Officer
Office of Naval Research Branch Office
1030 East Green Street
Pasadena, California

Director
Naval Research Laboratory
Technical Information Office
Washington 25, D. C. (6 copies)

Commander
Army Material Command
ATTN: AMCRD-RS-PE-A
Department of the Army
Washington 25, D. C. (2 copies)

Commanding Officer
U. S. Army Transportation Research
Command
ATTN: SMOFE-TD (1 copy)
Fort Eustis, Virginia
and ATTN: Research Reference
Center (1 copy)

Army Research Center
Physical Sciences Division
ATTN: Mr. R. Ballard
3045 Columbia Pike
Arlington 4, Virginia

U. S. Air Force (SRGL)
Office of Scientific Research
Washington 25, D. C.

Aeronautical Systems Division
Deputy for Technology
ATTN: ASRSMS
Wright-Patterson AFB, Ohio

Aeronautical Systems Division
Deputy for Technology
ATTN: ASRSSC
Wright-Patterson AFB, Ohio

Aeronautical Systems Division
Deputy for Technology
ATTN: ASRMDF
Wright-Patterson AFB, Ohio

Aeronautical Systems Division
Deputy for Systems Management
Support Systems Programs Office
ATTN: ASZT
Wright-Patterson AFB, Ohio

Armed Services Technical Information
Agency
Document Service Center
Arlington Hall Station
Arlington 12, Virginia (20 copies)

National Aeronautics and Space
Administration
1512 H Street N. W.
Washington 25, D. C.
ATTN: Mr. J. Brewer, Code RA

National Aeronautics and Space
Administration
1512 H. Street N. W.
Washington 25, D. C.
ATTN: Mr. N. F. Rekos, Code RAP

National Aeronautics and Space
Administration
Langley Research Center
Langley AFB, Virginia
ATTN: Mr. Donnelly

National Aeronautics and Space
Administration
Ames Research Center
Moffett Field, California
ATTN: Mr. W. Cook, 40 x 80 tunnel

Office of Technical Services
Department of Commerce
Washington 25, D. C.

Library
American Institute of Aeronautics
and Astronautics
Two East 64 Street
New York 21, New York (2 copies)

Bell Helicopter Company
P. O. Box 482
Fort Worth 1, Texas
ATTN: Mr. Robert Lynn

Chance Vought Corp.
Dallas 22, Texas
ATTN: Mr. George T. Upton

Cornell Aeronautical Lab., Inc.
4455 Genesee Street
Buffalo 21, New York
ATTN: Mr. Frank duWaldt

Collins Radio Company
Cedar Rapids, Iowa
ATTN: Dr. A. Lippisch

Mr. A. M. O. Smith, Supervisor
Aerodynamics Research Group
Aircraft Division
Douglas Aircraft Co., Inc.
Long Beach, California

Georgia Institute of Technology
Guggenheim School of Aeronautics
Atlanta 13, Georgia
ATTN: Mr. D. W. Dutton

Advanced Research Division
Hiller Aircraft Corporation
1350 Willow Road
Palo Alto, California

Lockheed Georgia Company
86 S. Cobb Drive
Marietta, Georgia
ATTN: Dr. Frank Sutton

Massachusetts Institute of
Technology
Aeronautical Engineering Dept.
Cambridge 30, Massachusetts
ATTN: Professor R. H. Miller

McDonnell Aircraft Corporation
St. Louis, Missouri
ATTN: Dr. Kurt Hohenemser

Mississippi State University
Engineering and Industrial Research
Station
State College, Mississippi
ATTN: Dr. J. J. Cornish

North American Aviation, Inc.
Columbus Division
Columbus 16, Ohio
ATTN: Mr. S. F. Kwiatkowski

Syracuse University
Mechanical Engineering Department
Syracuse, New York
ATTN. Dr. S. Eskinazi

Therm Advanced Research Division
Therm, Inc.
Ithaca, New York
ATTN: Dr. Ritter

Vehicle Research Corporation
1661 Lombardy Road
Pasadena, California
ATTN: Dr. Scott Rethorst

University of Virginia
Aeronautical Engineering Dept.
Charlottesville, Virginia
ATTN: Dr. G. B. Matthews

Vertol Division
Boeing Airplane Company
Woodland Avenue
Morton, Pennsylvania
ATTN: Dr. W. Z. Stepniewski

Vidya, Incorporated
1450 Page Mill Road
Stanford Industrial Park
Palo Alto, California
ATTN: Dr. J. N. Nielsen

Naval Postgraduate School
Aeronautical Engineering Dept.
Monterey, California
ATTN: Dr. R. Head

Sikorsky Aircraft Division
United Aircraft Corporation
Stratford 1, Connecticut
ATTN: Mr. Philip Michel